



João Pedro Azevedo Santos

Bachelor of Sciences in Chemical and Biochemical Engineering

Biopolymers valorization using biocompatible ionic liquids for biomedical applications

Dissertation to obtain the Master of Science degree in Biochemistry

Supervisor Dr. Noémi Tamar do Carmo Jordão, Junior Researcher, FCT NOVA

Co-supervisor Dr. Luísa Alexandra Graça Neves, Assistant Researcher, FCT NOVA

Jury

President Prof. Dr. Pedro António de Brito Tavares, Assistant Professor, FCT NOVA

Arguer Dr. Hugo Gonçalo da Silva Cruz, Junior Researcher, FCT NOVA

Vowel Dr. Noémi Tamar do Carmo Jordão, Junior Researcher, FCT NOVA



FACULDADE DE
CIÊNCIAS E TECNOLOGIA
UNIVERSIDADE NOVA DE LISBOA

January 2021

João Pedro Azevedo Santos

BSc degree in Chemical and Biochemical Engineering



**Biopolymers valorization using biocompatible ionic liquids for
biomedical applications**

Dissertation to obtain the MSc degree in Biochemistry

Supervisor: Doctor Noémi Tamar do Carmo

Jordão, Junior Researcher, FCT NOVA

Co-supervisor: Doctor Luísa Alexandra Graça

Neves, Assistant Researcher, FCT NOVA

January 2021

Biopolymers valorization using biocompatible ionic liquids for biomedical applications



This master's thesis was conducted under the project "Development of biomaterials using innovative biocompatible ionic liquids for transdermal drug release" (InnovIL4SkinDrug) financed by national funding through the Foundation for Science and Technology I.P. (PTDC/CTM-CTM/29869/2017).

© João Pedro Azevedo Santos, Faculdade de Ciências e Tecnologia, Universidade Nova de Lisboa.

The Faculty of Sciences and Technology and the NOVA University of Lisbon have the right, perpetual and without geographical boundaries, to file and publish this dissertation through printed copies reproduced on paper or on digital form, or by any other means known or that may be invented, and to disseminate through scientific repositories and admit its copying and distribution for non-commercial, educational or research purposes, if credit is given to the author and editor.

Imagination is more important than knowledge. For knowledge is limited to all we now know and understand, while imagination embraces the entire world, and all there ever will be to know and understand.

Albert Einstein

Agradecimentos

O presente trabalho não existiria sem o contributo de várias pessoas, pelo que desta forma, presto aqui os meus agradecimentos.

Em primeiro lugar quero agradecer às minhas orientadoras pela oportunidade de realizar este projeto completamente ao encontro dos meus interesses.

À Dr.^a Noémi Jordão, por me ter acompanhado em todas as tarefas e ter sido das profissionais que mais contribuiu para a minha aprendizagem e formação durante esta fase final do meu percurso académico.

À Dr.^a Luísa Neves, por me ter ajudado a ultrapassar todas as dificuldades durante este projeto de dissertação e pela sua simpatia e excelente capacidade de delegação.

À Inês Ferreira e à Rita Nabais, que sempre se mostraram disponíveis para me ajudar no laboratório e na explicação de algumas técnicas.

À Dr.^a Ana Lopes, à Carla Rodrigues e Paula Chicau, e à Rita Craveiro, pela realização dos ensaios, fulcrais na caracterização dos líquidos iónicos.

Ao Prof. Vítor Alves e à Prof. Isabel Nogueira, pela realização e/ou supervisão dos ensaios de reologia e de microscopia no Instituto Superior de Agronomia e no Instituto Superior Técnico, onde fui sempre bem recebido.

Aos meus pais, irmã e familiares que sempre me apoiaram e garantiram as melhores condições para atingir os objetivos a que me proponho. Por último, mas não menos importantes, aos meus amigos cujo apoio e inspiração é crucial para me tornar na minha melhor versão.

Todas as minhas conquistas são vossas também!

A todos, muito obrigado!

Resumo

Nas últimas décadas, os biopolímeros receberam bastante atenção, especialmente devido às suas propriedades inerentes tais como biodegradabilidade, biocompatibilidade e propriedades biológicas. No entanto, eles apresentam algumas limitações numa ampla gama de aplicações, tais como na área da biomedicina, devido à sua baixa solubilidade em água e em solventes orgânicos biocompatíveis. Os líquidos iônicos (LIs) são considerados sais orgânicos com baixo ponto de fusão e surgiram como uma alternativa para superar esta limitação, devido essencialmente às suas propriedades peculiares. As propriedades dos LIs podem ser modeladas de acordo com a seleção adequada do catião e do anião.

Nesse contexto, o objetivo desta tese visa o desenvolvimento de estruturas poliméricas através da dissolução de biopolímeros usando líquidos iônicos biocompatíveis. De modo a realçar as propriedades terapêuticas das estruturas poliméricas desenvolvidas, LIs que contenham fármacos na sua estrutura, nomeadamente a lidocaína e a procaína bem como o ibuprofeno, com propriedades analgésicas e anti-inflamatórias, respetivamente, foram sintetizados.

Diferentes LIs parcialmente ionizados, designados usualmente como LIs próticos, foram sintetizados através de uma reação ácido-base, em que o catião selecionado apresenta um fármaco na sua estrutura (lidocaína e procaína) e estes foram combinados com aniões carboxilatos, nomeadamente acetato, propionato, hexanoato ou ibuprofenato (propriedades anti-inflamatórias). Os LIs foram caracterizados através de análises espectroscópicas (^1H RMN e FTIR) de modo a elucidar a sua estrutura, térmicas (TGA e DSC) para avaliação das suas propriedades térmicas e estudos de viscosidade. Posteriormente, os LIs foram testados como solventes para a dissolução de biopolímeros, nomeadamente o complexo quitina-glucanos (CGC) e quitosano. Em geral, os LIs preparados que contêm o anião acetato ou propionato na sua estrutura demonstraram capacidade para dissolver o biopolímero CGC (1 wt. %). As estruturas poliméricas obtidas foram caracterizadas usando métodos adequados de modo a elucidar a sua morfologia (SEM), composição (FTIR), propriedades térmicas (TGA e DSC) e mecânicas (ensaios de perfuração) dependendo da sua forma (filme ou gel). A análise dos espectros de FTIR das estruturas poliméricas na forma de filme sugere que estas são constituídas maioritariamente por lidocaína na sua forma básica e no caso do gel, por procaína na sua forma básica. Em geral, todas as estruturas poliméricas apresentam menor estabilidade térmica relativamente ao CGC. O gel obtido apresenta um comportamento viscoso, enquanto que o filme apresenta uma superfície hidrofílica e fracas propriedades mecânicas, que limitam a sua aplicação.

Palavras-chave

Biopolímeros, líquidos iônicos, complexo quitina-glucanos, libertação de fármacos

Abstract

In the last decades, biopolymers received much attention, especially due to its inherent properties, such as biodegradability, biocompatibility and biological properties. However, they showed some limitations in a wide range of applications, mainly in the biomedical field, due to their low solubility in water and in biocompatible organic solvents. To overcome this, ionic liquids (ILs) as low-melting organic salts appeared as an alternative dissolution agent, mainly due to their peculiar properties, which can be tuned according to the adequate selection of the cation and anion.

In this context, this thesis aims the development of polymeric structures *via* biopolymer dissolution using innovative biocompatible ILs. ILs containing pharmaceutically acceptable drugs – namely lidocaine, procaine, and ibuprofen with anaesthetic and anti-inflammatory effects, respectively – were synthesized to enhance the therapeutic properties of the produced biopolymeric structures. This way, the IL will have a double role, it will act as a solvent for the biopolymer dissolution as well as a therapeutic agent, for example for topical delivery of anaesthetic and anti-inflammatory drugs.

Different protic ionic liquids, which are ILs that are not fully ionized, have been successfully synthesized by acid-base reactions, using active pharmaceutical drugs as a cation (lidocaine or procaine) combined with carboxylate anions, namely acetate, propionate, hexanoate or ibuprofenate (anti-inflammatory properties). They have been characterized by spectroscopic techniques (^1H NMR, FTIR) to assess their structure, thermal analysis (TGA, DSC) to evaluate their thermal stability, and viscosity studies. The prepared ILs have been tested as dissolution agents for different biopolymers, namely chitin-glucan complex (CGC) and chitosan. In general, the prepared ILs containing acetate or propionate anions seemed to be capable to dissolve the CGC biopolymer (1 wt. %). The obtained polymeric structures have been characterized by adequate methods to study their morphology (SEM), composition (FTIR), thermal (TGA, DSC) and mechanical properties depending on their form (films or gels). FTIR studies suggested the obtained films were composed mainly by lidocaine free base and the obtained gel was composed mainly by procaine free base. In general, all prepared polymeric structures showed lower thermal stability than the CGC biopolymer. The obtained gel exhibited a viscous behaviour, whereas films exhibited hydrophilic surface and, poor mechanical properties which limits their potential for application.

Keywords

Biopolymers, ionic liquids, chitin-glucan complex, topical drug delivery

List of Contents

| | |
|---|----|
| 1. Introduction | 1 |
| 1.1. Biopolymers valorization | 1 |
| 1.2. Chitin and chitosan | 2 |
| 1.1.1. Chitin–glucan complex | 3 |
| 1.3. Ionic liquids | 4 |
| 1.1.2. Synthesis of ionic liquids | 5 |
| 1.4. Dissolution of chitin, chitosan and CGC in ILs | 6 |
| 1.5. Main goals of the thesis | 7 |
| 1.6. Thesis outline | 8 |
| 2. Materials and methods | 11 |
| 2.1. Chemicals | 11 |
| 2.2. Experimental synthesis | 11 |
| 2.2.1. Purification of APIs | 11 |
| 2.2.2. Synthesis of API-ILs | 12 |
| 2.3. Characterization of API-ILs | 13 |
| 2.3.1. Proton nuclear magnetic resonance spectroscopy | 13 |
| 2.3.2. Fourier-transform infrared spectroscopy | 14 |
| 2.3.3. Thermogravimetric analysis | 14 |
| 2.3.4. Differential scanning calorimetry | 14 |
| 2.3.5. Viscosity studies | 14 |
| 2.3.6. Water content determination | 15 |
| 2.4. Dissolution studies | 15 |
| 2.5. Preparation of biopolymeric structures | 15 |
| 2.6. Characterization of films | 16 |
| 2.6.1. Scanning electron microscopy | 16 |
| 2.6.2. Fourier-transform infrared spectroscopy | 16 |
| 2.6.3. Thermogravimetric analysis | 16 |
| 2.6.4. Differential scanning calorimetry | 16 |

| | | |
|--------|--|----|
| 2.6.5. | Contact angle measurements | 17 |
| 2.6.6. | Mechanical properties | 17 |
| 2.7. | Characterization of hydrogel..... | 17 |
| 2.7.1. | Fourier-transform infrared spectroscopy | 17 |
| 2.7.2. | Thermogravimetric analysis | 17 |
| 2.7.3. | Differential scanning calorimetry..... | 17 |
| 2.7.4. | Rheological studies..... | 18 |
| 3. | Results and discussion..... | 19 |
| 3.1. | Synthesis of API-ILs | 19 |
| 3.2. | Characterization of API-ILs..... | 20 |
| 3.2.1. | Proton nuclear magnetic resonance spectroscopy | 21 |
| 3.2.2. | Fourier-transform infrared spectroscopy | 22 |
| 3.2.3. | Thermogravimetric analysis | 24 |
| 3.2.4. | Differential scanning calorimetry..... | 26 |
| 3.2.5. | Viscosity measurements | 28 |
| 3.3. | Characterization of biopolymers | 30 |
| 3.3.1. | Fourier-transform infrared spectroscopy | 30 |
| 3.3.2. | Thermogravimetric analysis | 31 |
| 3.4. | Dissolution studies | 31 |
| 3.5. | Development of biopolymeric structures | 33 |
| 3.6. | Characterization of films..... | 34 |
| 3.6.1. | Scanning electron microscopy..... | 34 |
| 3.6.2. | Fourier-transform infrared spectroscopy | 34 |
| 3.6.3. | Differential scanning calorimetry..... | 37 |
| 3.6.4. | Thermogravimetric analysis | 38 |
| 3.6.5. | Contact angle analysis | 39 |
| 3.6.6. | Mechanical properties | 39 |
| 3.7. | Characterization of hydrogel..... | 41 |
| 3.7.1. | Fourier-transform infrared spectroscopy | 41 |
| 3.7.2. | Differential scanning calorimetry..... | 43 |

| | | |
|--------|---|----|
| 3.7.3. | Thermogravimetric analysis | 44 |
| 3.7.4. | Rheological studies..... | 44 |
| 4. | Conclusions | 47 |
| 5. | Future work | 49 |
| | References | 51 |
| | Appendices | 55 |
| | Appendix I – Synthesis of API-ILs | 55 |
| | Appendix II – Proton nuclear magnetic resonance spectroscopy..... | 56 |
| | Appendix III – Viscosity measurements (shear rate sweeps)..... | 60 |
| | Appendix IV – Viscosity measurements (temperature sweeps)..... | 63 |
| | Appendix V – Thermogravimetric analysis | 66 |
| | Appendix VI – Scanning electron microscopy..... | 67 |
| | Appendix VII – Fourier-transform infrared spectroscopy..... | 69 |

List of Figures

| | |
|---|----|
| Figure 1.1 Examples of naturally derived polysaccharides comprising their molecular structure and source. | 1 |
| Figure 1.2 (a) Haworth projection of chitin showing two of the GlcNAc units that repeat to form long chains linked through C1 and C4 of the next unit (numbered in blue). <i>n</i> is the number of GlcNAc repeated units. (b) Chemical structure of chitin (<i>n</i> >50%) and chitosan (<i>m</i> >50%), where <i>n</i> is the number of GlcNAc units and <i>m</i> is the number of GlcN units | 2 |
| Figure 1.3 (a) Schematic representation of the molecular structure of β -glucan and chitin in CGC-FCT. (b) Colored scanning electron micrograph of <i>K. pastoris</i> | 3 |
| Figure 1.4 Evolution of ILs according to Rogers and coworkers. Physical properties, chemical properties and biological activity of the cation and anion are depicted with matching colors..... | 5 |
| Figure 2.1 Illustration of the 3-step procedure for the preparation of polymeric structures..... | 16 |
| Figure 3.1 Chemical structures of the pharmaceutical local anesthetics and anions selected for API-IL synthesis. | 19 |
| Figure 3.2 ¹ H NMR spectrum of lidocainium ibuprofenate ([Lid][Ibu]) in DMSO- <i>d</i> ₆ solution and assignment of the proton signals to hydrogen-labeled chemical structure of [Lid][Ibu]..... | 21 |
| Figure 3.3 FTIR-ATR spectra of lidocaine and procaine as free bases, and ibuprofen as free acid. Critical wavenumbers are depicted with corresponding colors..... | 22 |
| Figure 3.4 Chemical structure of [Lid][Ibu] and expanded FTIR-ATR spectra (C=O region) of lidocaine free base and ibuprofen free acid and the prepared [Lid][Ibu]..... | 23 |
| Figure 3.5 Hydrogen bond formation between ibuprofen (top) and procaine (bottom). | 24 |
| Figure 3.6 Thermogravimetric curves of lidocaine based-ILs (left) and procaine based-ILs (right) at 10 °C min ⁻¹ | 25 |
| Figure 3.7 Thermogravimetric curves (left Y-axis) and associated derivative curves (right Y-axis) of lidocainium acetate ([Lid][AcO]) (left) and procainium ibuprofenate ([Pro][Ibu] (right) at 10 °C/min, under argon. | 26 |
| Figure 3.8 Heat flow thermograms for [Lid][OAc] obtained at 10 °C min ⁻¹ (left) and at 20 °C min ⁻¹ (right) heating (1 st cycle) and cooling (2 nd cycle) scans..... | 27 |
| Figure 3.9 Shear stress as a function of shear rate for [Lid][OPr] at 20 °C..... | 28 |
| Figure 3.10 Profile of the dependence of viscosity with temperature for lidocaine based-ILs (left) and procaine based-ILs (right) at a heating rate of 5 °C/min. | 29 |
| Figure 3.12 Biopolymeric structures based on CGC-FCT (medium BSM). | 33 |
| Figure 3.13 Surface images of [Lid][OAc] based CGC films obtained from (a) a 1-day oil bath dissolution at 100 °C and prepared using water as nonsolvent, and (b) a 3-day oil bath dissolution at 70 °C and prepared using water as nonsolvent..... | 34 |

| | |
|--|----|
| Figure 3.14 FTIR-ATR spectra of CGC-FCT (medium BSM), lidocaine free base, lidocainium propionate ([Lid][OPr]) and respective films (A-D). | 35 |
| Figure 3.15 Expanded 2000 – 1500 cm^{-1} region of the FTIR-ATR spectra of lidocaine free base, lidocainium propionate ([Lid][OPr]) and respective films (A-D). | 36 |
| Figure 3.16 (a) Heat flow thermograms for lidocaine free base (Lidocaine, $T_m = 69\text{ }^\circ\text{C}$), lidocainium acetate ([Lid][OAc], $T_m = 64\text{ }^\circ\text{C}$), and respective films (A1-D1). (b) Heat flow thermograms for free lidocaine (Lidocaine, $T_m = 69\text{ }^\circ\text{C}$), lidocainium propionate ([Lid][OPr], $T_g = -52\text{ }^\circ\text{C}$), and respective films (A2-D2). | 37 |
| Figure 3.17 Thermogravimetric curves for [Lid][OAc] based CGC films (left) and for [Lid][OPr] based CGC films (right) at $10\text{ }^\circ\text{C}/\text{min}$ | 38 |
| Figure 3.18 FTIR-ATR spectra of CGC-FCT (medium BSM), procaine free base, procainium propionate ([Pro][OPr]), and respective hydrogel (A) obtained from a 1-day oil bath dissolution at $100\text{ }^\circ\text{C}$ and prepared using water as nonsolvent. | 41 |
| Figure 3.19 Expanded 1800 – 1300 cm^{-1} region of the FTIR-ATR spectra of procaine free base, procainium propionate ([Pro][OPr]), and respective hydrogel (A) obtained from a 1-day oil bath dissolution at $100\text{ }^\circ\text{C}$ and prepared using water as nonsolvent. | 42 |
| Figure 3.20 Heat flow thermograms for procaine free base (Procaine, $T_g = -38\text{ }^\circ\text{C}$), procainium propionate ([Pro][OPr], $T_g = -26\text{ }^\circ\text{C}$), and respective hydrogel (A, $T_g = -33\text{ }^\circ\text{C}$) obtained from a 1-day oil bath dissolution at $100\text{ }^\circ\text{C}$ and prepared using water as nonsolvent. | 43 |
| Figure 3.21 Thermogravimetric curve (left) and derivative curve (right) associated with mass loss of the obtained hydrogel. | 44 |
| Figure 3.22 Mechanical spectrum of the hydrogel obtained from a 1-day oil bath dissolution at $100\text{ }^\circ\text{C}$ and prepared using water as nonsolvent. | 45 |

List of Tables

| | |
|---|----|
| Table 3.1 Melting points (T_m) of APIs and the correspondent acid-base reaction yields performed to obtain the basic or acidic form of the desired API. | 20 |
| Table 3.2 Abbreviations and appearance of the synthesized API-ILs. | 20 |
| Table 3.3 Cation to anion ratio determined by quantitative integration of ^1H peaks. | 22 |
| Table 3.4 Decomposition temperatures associated with mass loss of the synthesized API-ILs. | 24 |
| Table 3.5 Thermal properties of the synthesized APIs and API-ILs. | 27 |
| Table 3.6 Viscosities and activation energies of the synthesized API-ILs. | 29 |
| Table 3.7 Decomposition temperatures associated with mass loss of the studied biopolymers. | 31 |
| Table 3.8 Dissolution results obtained at 70 °C (3-day oil bath) and at 100 °C (1-day oil bath). | 31 |
| Table 3.9 CGCs β -glucan:chitin molar ratio. | 32 |
| Table 3.10 Decomposition temperatures associated with mass loss of the obtained films. | 38 |
| Table 3.11 Contact angles of the obtained films. | 39 |
| Table 3.12 Mechanical properties of the obtained films. | 40 |

Abbreviations

| | |
|--------------------|---|
| ATR | Attenuated total reflection |
| API | Active pharmaceutical ingredient |
| API-IL | Active pharmaceutical ingredient - ionic liquid |
| BSM | Basal salts medium |
| CGC | Chitin-glucan complex |
| [Chol][OAc] | Cholinium acetate |
| [Chol][OPr] | Cholinium propionate |
| [Chol][OHex] | Cholinium hexanoate |
| Com | Commercial |
| DA | Degree of acetylation |
| DSC | Differential scanning calorimetry |
| DMSO | Dimethyl sulfoxide |
| FCT | Faculdade de Ciências e Tecnologia |
| FTIR | Fourier-transform infrared |
| G' | Storage modulus |
| G'' | Loss modulus |
| GlcN | 2-amino-2-deoxy-D-glucan |
| GlcNAc | 2-acetamido-2-deoxy-D-glucan |
| ¹ H NMR | Proton nuclear magnetic resonance |
| IL | Ionic liquid |
| KF | Karl Fischer |
| LAQV | Associated Laboratory for Green Chemistry |
| [Lid][OAc] | Lidocainium acetate |
| [Lid][OPr] | Lidocainium propionate |
| [Lid][OHex] | Lidocainium hexanoate |
| [Lid][Ibu] | Lidocainium ibuprofenate |

| | |
|-------------|-----------------------------------|
| [Pro][OAc] | Procainium acetate |
| [Pro][OPr] | Procainium propionate |
| [Pro][OHex] | Procainium hexanoate |
| [Pro][Ibu] | Procainium ibuprofenate |
| SEM | Scanning electron microscopy |
| $T_{5\%}$ | Onset temperature to 5% mass loss |
| T_c | Crystallization temperature |
| T_{dec} | Decomposition temperature |
| T_g | Glass transition temperature |
| TGA | Thermogravimetric analysis |
| T_m | Melting temperature |
| wt. % | Percentage by weight |

Symbols

| Symbol | Description | Units |
|----------------|------------------|----------|
| τ | Shear stress | Pa |
| $\dot{\gamma}$ | Shear rate | s^{-1} |
| η | Viscosity | Pa·s |
| σ | Tensile strength | Pa |

1. Introduction

1.1. Biopolymers valorization

Biopolymers are polymeric materials derived from biological sources. Polysaccharides integrate one of the three classes of biopolymers and are linear or branched polymeric carbohydrates. Polysaccharide-based biomaterials have huge importance in the field of various biomedical applications such as tissue regeneration, controlled drug delivery devices and gel-entrapment systems for the immobilization of cells^{1,2}. Important properties of the polysaccharides include controllable biological activity, biodegradability, and their ability to form hydrogels³. Most of the polysaccharides used derive from natural sources (Figure 1.1) and they can be neutral, cationic or anionic, depending on the presence of hydroxyl, amide or carboxyl groups in their structure, respectively. These polysaccharides can be easily extracted from plant fibers such as cotton, crustacean shells of crab for example and brown seaweeds like kelp, respectively. Cellulose is the most common biopolymer on Earth (about 33% of all plant matter is cellulose⁴).

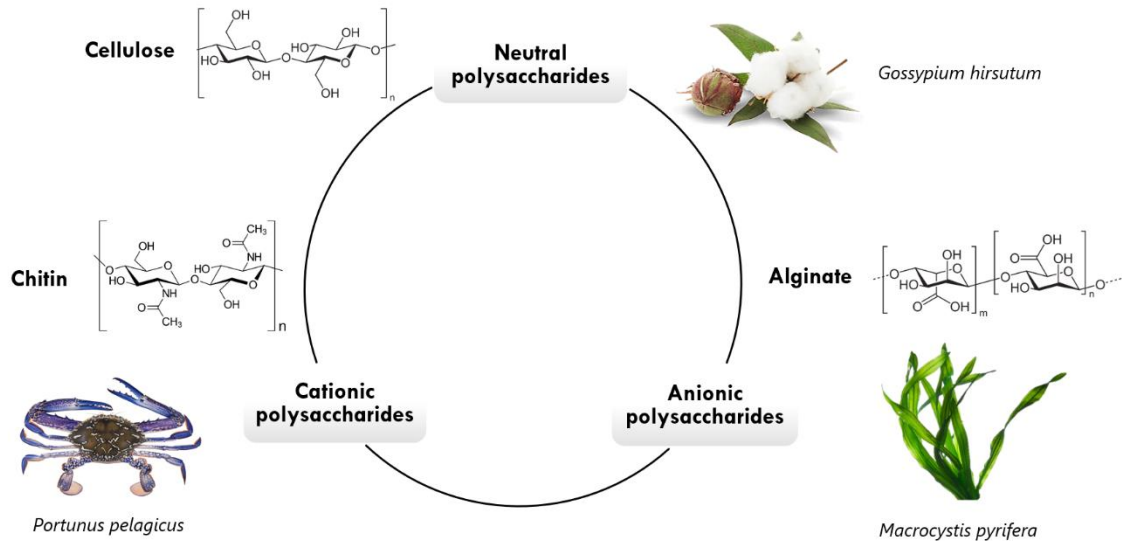


Figure 1.1 Examples of naturally derived polysaccharides comprising their molecular structure and source. Adapted from Xiong *et al.*⁵.

Extensive research has been conducted on biodegradable polymeric materials, mainly because they are, in a huge majority, obtained from renewable sources³. Some of them present wide availability in nature and can be obtained at low price^{2,4}. Frequently, they exhibit characteristics such as controlled reactivity, low toxicity, biocompatibility, biodegradability, and filmogenic properties⁵. These properties may find applications in a variety of fields, particularly in the fields of pharmacy, biomedicine and food packaging⁶.

1.2. Chitin and chitosan

Chitin and its derivative, chitosan, are biodegradable polymers obtained from natural sources. Both biopolymers are linear polysaccharides composed by monomeric repeating units linked through β -(1 \rightarrow 4) glycosidic bonds⁷ (Figure 1.2. a). Chitin, which consists of 2-acetamido-2-deoxy-D-glucan (GlcNAc) repeating units, is the second most abundant polysaccharide after cellulose and is insoluble in most organic solvents. Chitosan, which is composed of randomly distributed GlcNAc and 2-amino-2-deoxy-D-glucan (GlcN) units (Figure 1.2. b), is obtained as a partially or completely deacetylated form of chitin, leading to an improvement of its solubility depending on the proportion of GlcNAc units relative to the total number of units, known as degree of acetylation (DA)⁸. Generally, a lower DA in chitosan enhances its solubility in organic solvents. The applications of these biopolymers obtained from marine waste (*e.g.*, crustacean shells and shellfish waste) into high-value biomaterials has both economic and environmental benefits⁹.

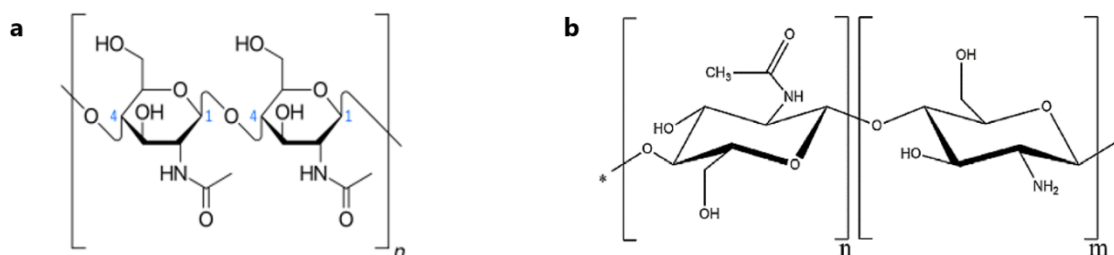


Figure 1.2 (a) Haworth projection of chitin showing two of the GlcNAc units that repeat to form long chains linked through C1 and C4 of the next unit (numbered in blue). n is the number of GlcNAc repeated units. (b) Chemical structure of chitin ($n > 50\%$) and chitosan ($m > 50\%$), where n is the number of GlcNAc units and m is the number of GlcN units.¹⁰

Chitin itself has appealing properties for biomedical applications, namely the acceleration of wound healing and tumor cell growth suppression⁹. The mentioned key properties of chitin have stimulated the development of many chitin-based products such as dressings for burns, vascular implants, artificial blood vessels and tumor inhibitors¹⁰. On the other hand, chitosan possesses film-forming ability and bacteriostatic action¹¹. Moreover, chitosan is a strong base owing to the presence of primary amino groups and becomes a polyelectrolyte when such amino groups get protonated¹⁰, and as an example, chitosan can be dissolved in a 0.10 M acetic acid solution¹⁰.

These polymers are formed by strong inter- and intramolecular hydrogen bonds between the polymer chains, which results in a low solubility in conventional solvents. Therefore, only a limited number of solvents have been found for chitin dissolution such as dimethylacetamide–lithium chloride (DMAc–LiCl), NaOH/urea and hexafluoroacetone⁸. Although dissolution of chitin is possible by these solvents, many of them are toxic, hardly degradable, corrosive, or mutagenic⁸. Therefore, the selection of a suitable solvent for chitin solubilization is an important and primary issue for laboratorial scale research and further scaling up for industrial practices¹².

1.1.1. Chitin–glucan complex

Chitin–glucan complex (CGC) is a copolymer vastly found on the cell wall of yeasts and fungi, conferring stability and rigidity to the cells¹³. Two of the CGCs studied in this master's thesis were produced by the Biochemical Engineering (BIOENG) group at UCIBIO/REQUIMTE within the facilities of FCT NOVA (Lisbon, PT), and will be designed throughout this thesis as CGC-FCT. CGC-FCT is a copolymer (Figure 1.3 a) composed by two types of polysaccharides, chitin, and glucans (repeating glucose units)¹³. CGC-FCT is the main component from the cell wall of *Komagataella pastoris*, formerly known as *Pichia pastoris* (Figure 1.3 b), a methylotrophic yeast commonly used in the pharmaceutical industry as a host to produce various recombinant heterologous proteins¹³ due to its capacity to reach high cell densities¹⁴.

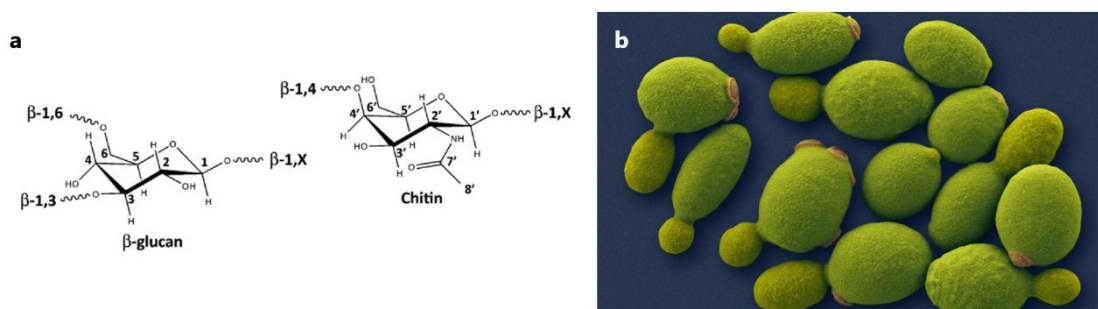


Figure 1.3 (a) Schematic representation of the molecular structure of β -glucan and chitin in CGC-FCT.¹³ (b) Colored scanning electron micrograph of *K. pastoris*¹⁶. © Dennis Kunkel (Science Photo Library, London, UK).

In this work, CGC-FCT inoculated in two different mediums, namely K and BSM, were used. Basal salts medium (BSM), developed by Invitrogen Co. (Carlsbad, USA), is the most used for cultivation of *K. pastoris*¹⁵. However, the utilization of BSM suffers from some operational problems and comprises some toxic compounds such as boric acid and sodium iodide¹⁶. In order to reduce or eliminate these problems, a novel cultivation medium, K, was reported in 2019 by Freitas *et al.*¹⁵. Medium K has considerably lower salts content, thus representing a simplification of the bioprocess with no precipitation problems, without impacting on the polymers' composition¹⁵. Depending on the cultivation conditions (such as the pH, temperature or medium composition), and the extraction procedures, the content of CGC in *K. pastoris* biomass ranges within 11–20 wt.%^{13,15}.

As it is a non-animal chitin source, CGC avoids any allergen risk of crustacean sources¹⁴ and contains no heavy metals. CGC has also demonstrated to combine antioxidant, antibacterial and anti-inflammatory properties which make it attractive for high-added value applications, such as in cosmetics or in biomedicine (*e.g.*, wound dressing and surgical adhesives).¹⁴ Similarly to chitin, biomedical applications of CGC have some limitations due to their insolubility in water and in most of the conventional organic solvents^{14,17}.

Another non-animal chitin source, obtained from the mycelium of non-genetically

modified strains of *Aspergillus niger* derived from a fermentation process¹⁷, was also used in this master's thesis for comparison purposes, and is designed here as CGC-Com. CGC-Com is sold under the trade name KiOnutrime[®]-CG by KitoZyme, the global leader in manufacturing chitosan and chitin–glucan from fungal origin. This product has a content of more than 90% chitin–glucan and was marketed in different food supplement formats to enhance the daily intake of fiber¹⁷. The European Food Safety Authority Panel stated that KiOnutrime[®]-CG is safe as a food ingredient at the proposed conditions of use and the proposed intake levels¹⁷.

Within this scenario, the dissolution of biopolymers such as CGC and chitosan in biocompatible ionic liquids was pointed out as an alternative approach. Hence, this approach combines two Green Chemistry principles, namely the use of environmentally benign solvents and biopolymers obtained from renewable resources (*i.e.*, the yeast *K. pastoris*).

1.3. Ionic liquids

In a search for more efficient and at the same time more environmentally benign processes, chemists have turned their attention to a class of alternative solvents – ionic liquids (ILs). ILs are currently defined as organic salts with low melting points, conventionally below 100 °C (some are liquid at room temperature – RTILs), and are composed only by ions^{18,19}. *Via* an appropriate selection of the anion and the cation it is possible to tailor ILs with completely different properties. Although ILs are not as environmentally safe as they were previously thought, they can be regenerated and reused several times, which would decrease their ecological impact significantly.

This class of organic salts has several properties of interest, such as its low vapor pressure and flammability, high thermal and chemical stability, tunable density and viscosity depending on cation and anion selection, as well as solubility in water and in common organic solvents¹⁸. Extensive research into ILs has led to a fast development of this area in recent decades, leading to distinct classifications of ILs by generations based on their properties.

The earliest examples of ILs have been classified according to their chemical structure and properties into 3 different generations: (1) chloroaluminates, (2) non-chloroaluminates and (3) task specific ILs. Later, Rogers and coworkers proposed to classify ILs into other 3 different generations according to their properties and applications (Figure 1.4). Generation 1 includes compounds with adjustable physical properties, such as density, viscosity, conductivity and solubility depending on the nature of the cation and anion and/or their ratio. Unlike the first generation, Generation 2 comprises ILs with targeted chemical properties. Lastly, Generation 3 consists of ions with known biological activities such as active pharmaceutical ingredients (APIs) in their cation, anion, or both, resulting in biologically active ILs, also known as API-ILs. Since the third generation of ILs employs biodegradable and biological ions, they usually have low toxicity^{20,21}.

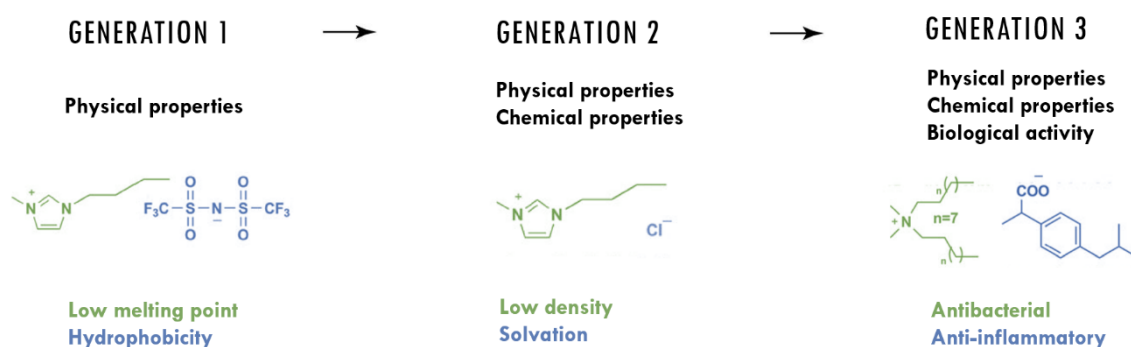


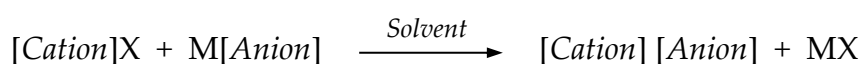
Figure 1.4 Evolution of ILs according to Rogers and coworkers. Physical properties, chemical properties and biological activity of the cation and anion are depicted with matching colors. Adapted from Rogers *et al.*²²

Researchers have attempted to overcome the obstacles in the synthesis of APIs and crystallization, which have recurrent problems related to their reduced solubility and consequently bioavailability^{19,20}, by performing the synthesis of API-ILs. Even though favorable results were obtained, the pharmaceutical industry does not yet use ILs as solvents for industrial practices due to doubts regarding cost, purity, toxicity, and regulatory approval¹⁹.

Still, ILs have different physicochemical properties which have been widely studied for industrial applications outside the pharmaceutical industry. Large companies such as Merck KGaA have developed hundreds of specialty IL products and several companies have been founded to synthesize ILs in small to large scale quantities for novel applications (*e.g.*, 525 Solutions, Solvent Innovation, Iolitec, Solvionic, Bioniqs, among others)¹⁹. Some examples of product lines are BASIONIC™ (a range of ILs) and CELLIONIC™ (5 wt.% cellulose dissolved in the IL 1-ethyl-3-methylimidazolium acetate) launched by BASF¹⁹ (Ludwigshafen, Germany).

1.1.2. Synthesis of ionic liquids

There are two basic methods for the preparation of ILs: ion-exchange or acid-base neutralization reactions²³. Ion-exchange reactions (Scheme 1.1) can be employed if the desired anion and cation are available as salts themselves, commonly paired with an alkali metal and halogen, respectively. Unfortunately, this reaction generates a halide salt as byproduct that usually cannot be completely extracted from the IL²⁴, leading to undesired effects on its physical and chemical properties²⁵. On the other hand, the acid-base reaction avoids the inorganic salt formation, making it preferable over the ion-exchange reaction.



Scheme 1.1. Generalized ion-exchange reaction for exchanging anions, where X is a halogen, M is an alkali metal and MX is the halide salt byproduct (inorganic salt).

The main challenge in synthesizing ILs *via* ion-exchange reaction often lies in the purification step, since separating byproducts by traditional methods such as distillation is not

possible with ILs because of their low vapor pressure and high thermal stability. Alternatively, the ion-exchange reaction can be carried out in an organic solvent that allows for precipitation of the inorganic salt (*i.e.*, a solvent in which the byproduct is insoluble) for subsequent separation via filtration. Another problem related with IL purity lies with their hygroscopicity. ILs are hygroscopic salts, *i.e.*, they uptake water during synthesis and it is difficult to remove the water completely. In any case, the presence of water in residual amounts changes the ILs physicochemical properties. This includes an increase in the electrical conductivity and a decrease in viscosity, a narrowing of the electrochemical window, hydrolysis, thermal decomposition and a change of reactivity and solvating ability^{26,27}.

In the case of an API-IL, the API can be either the cation, anion, or both.²⁷ Several advantages are expected by eliminating the need to dissolve the API in a solvent including (1) high API concentration; (2) low IL vapor pressure, which essentially eliminates problems associated with evaporation; and (3) increased API stability due to lack of interactions with a solvent^{22,27}. The molar ratio between the API and counterion and the degree of ionicity are critical for the IL properties, since these influence bioavailability (including solubility, absorption, distribution, metabolism, and excretion)²⁷.

1.4. Dissolution of chitin, chitosan and CGC in ILs

Recent works have shown the potential of ILs as solvents for the dissolution and processing of biopolymers, such as cellulose, chitin²⁸, chitosan¹⁰ and CGC. One of the most remarkable properties of ILs is their ability to dissolve cellulose, which has structural resemblance to chitin (*i.e.*, cellulose with one hydroxyl group on each monomer replaced with an acetyl amine group resembles chitin).

Several studies reported in the literature have proved that the solubilization of chitin is possible in ILs and differs upon distinct factors, comprising: (1) the crystallinity, *i.e.*, β -chitin has a parallel arrangement with weak intermolecular forces leading to higher reactivity and affinity for solvent compared to α -chitin; (2) the mineral contents, practical grade chitin with higher mineral contents is considerably harder to dissolve than pure chitin; (3) the DA and the molecular weight (MW), where typically for lower DA and MW, chitin is more soluble; (4) the nature of the cation of the IL, where a short alkyl chain on the IL may improve chitin solubility; and (5) the nature of the anion of the IL, as chitin needs a more basic anion due to the higher number of H-bond donors and acceptors compared to cellulose²⁸.

In 2002, 1-butyl-3-methylimidazolium chloride ([C₄mim]Cl) and 1-butyl-3-methylimidazolium acetate ([C₄mim][OAc]) ILs were reported to be capable to dissolve chitin²⁹. According to Swatloski *et al.*²⁹, dissolution studies were performed in a 100 °C-oil bath, yet, neither detailed conditions such as chitin grade, solubility values nor dissolution time in these ILs were provided at that time. A few years later, Xie *et al.*³⁰ reported that [C₄mim]Cl can dissolve

pure grade chitin (*i.e.*, commercial chitin conventionally with chitin content above 80%) and chitosan with solubilities of approximately 10 wt.% for 5 hours at 110 °C. However, chitin origin was not mentioned. Qin *et al.*³¹ reported that using 1-ethyl-3-methylimidazolium acetate ([C₂mim][OAc]) was capable to dissolve pure chitin from crab shells with 16.7 wt.% solubility (this value was calculated from a 80% load mass dissolved) at 100 °C for 19 h.

Given the large variety of chitin and chitosan grades, ILs, and dissolution conditions reported or misreported in the literature as above-mentioned, it becomes difficult to understand which IL and dissolution conditions are more effective. Recent studies using molecular dynamics simulations and then, experimental confirmation about the mechanism of dissolution of chitin in imidazolium based-ILs have been reported^{32,33}. These studies showed that the predominant interaction between ILs and chitin appears to be H-bonding between the anion and the polymer, and that anions, namely bromide and acetate, interact with the polar domains of chitin. Chen *et al.*³⁴ studied the solubilities of chitosan, with temperatures ranging from 50 °C to 150 °C, in [C₄mim]-based ILs combined with basic anions and suggested that H-bonds in the polymer have also been disrupted partially by the increase of temperature (*e.g.*, the solubility in [C₄mim][OAc] at 150 °C was nearly 9-fold higher than at 70 °C).

Recently, in the Bio(chemical) Process Engineering research group at the Associated Laboratory for Green Chemistry (LAQV) in collaboration with the BIOENG group, several works regarding the preparation of biopolymeric structures based on CGC biopolymer dissolution using ILs have been conducted. The selected ILs were based on the cholinium cation and short alkyl chain carboxylate anions (acetate, propionate and hexanoate) using different dissolution conditions depending on the CGC origin: 24 h at 80 °C^{35,36} and 24 h at 110 °C^{35,36} for CGC-FCT and CGC-Com, respectively. In 2020, Ferreira *et al.*³⁷ reported CGC dissolution values above 5 wt% using choline based-ILs, namely, cholinium acetate ([Chol][OAc]), cholinium propionate ([Chol][OPr]) and choline hexanoate ([Chol][OHex]), which were the same carboxylate anions selected to be tested in this master's thesis.

1.5. Main goals of the thesis

Biomedical applications of CGC biopolymers have been hindered due to their insolubility in water and in most of the conventional organic nontoxic solvents. As an alternative to these conventional organic nontoxic solvents, the above-mentioned studies have shown the potential of using ILs as solvents for the dissolution of chitin, chitosan, and CGCs³⁵⁻³⁷. In this context, this thesis aims the development of polymeric structures *via* biopolymer dissolution using innovative biocompatible ILs, containing pharmaceutically acceptable drugs, and further evaluate their potential application in the biomedical field.

Further characterization of the polymeric structures developed in our group at LAQV proved that some IL remained in the biopolymeric structure after phase inversion in water, which was

supposed to remove the IL completely³⁵⁻³⁷. Since it was not possible to remove the IL from the prepared biopolymeric structures, ILs containing active pharmaceutical ingredients (APIs) – namely lidocaine, procaine, and ibuprofen with anesthetic and anti-inflammatory effects – were synthesized to enhance the therapeutic properties of the produced biopolymeric structures. This way, the API-IL plays a double role, in one hand act as a dissolution agent for the biopolymer and on the other hand acts as a therapeutic agent for potential topical delivery of anesthetic and anti-inflammatory drugs when present in the biopolymeric structure.

In order to obtain polymeric structures, several tasks were accomplished, including: (1) synthesis of API-ILs composed of short alkyl chain carboxylate anions and/or pharmaceutically acceptable drugs; (2) characterization of API-ILs by rheological studies, spectroscopic (¹H NMR and FTIR) and thermal analysis (DSC and TGA) techniques to assess their viscosity, purity, functional groups and thermal stability, respectively; (3) characterization of biopolymers by spectroscopic (FTIR) and thermal analysis (DSC and TGA) techniques to assess their functional groups (composition) and thermal stability, respectively; (4) dissolution studies of the biopolymers chitosan, CGC-FCT (inoculated in two different mediums) and CGC-Com using the synthesized API-ILs, where biopolymer concentration, oil-bath temperature, operation time and stirring rate were changed and optimized; (5) phase inversion method in water and in glycerol 10% (v/v), after visually assessing dissolution and casting the mixture, to partially remove the IL and promote a biopolymeric structure formation after drying at room temperature; (6) characterization of the obtained biopolymeric structures *via* adequate methods to study their morphology, composition, thermal stability, and mechanical and viscoelastic properties depending on their form (films or hydrogels).

1.6. Thesis outline

Firstly, ILs containing in their structure APIs as cations and/or anions were synthesized and purified. Given the studies for acetate based ILs in chitin, chitosan and CGC dissolution, the anion acetate (conjugate base of acetic acid) and similar short alkyl chain carboxylate anions (propionate and hexanoate) were selected as anions due to their low steric hindrance to tune the design of the API-ILs.

Secondly, characterization of the prepared API-ILs was performed to assess the cation to anion ratio, elucidate the cation and anion functional groups and evaluate physicochemical properties such as viscosity and thermal stability. After confirming that the cation to anion ratio was approximately 1:1, dissolution studies using 4 different biopolymers in 8 different API-ILs were performed. Then, for those where a successful dissolution was visually observed, a biopolymeric structure was developed.

Thirdly, characterization of the obtained biopolymeric structures and respective biopolymers

was performed *via* adequate methods to study their morphology, composition, thermal stability and, mechanical and viscoelastic properties depending on their form (films or hydrogels).

2. Materials and methods

2.1. Chemicals

All acquired reagents and solvents for IL synthesis were used without further purification. Ibuprofen sodium salt (99.9 %), hydrochloric acid (37.0%), lidocaine hydrochloride monohydrate (99.0 %), propionic acid for synthesis (99.0 %) and hexanoic acid for synthesis (98.0%) were purchased from Sigma-Aldrich (Missouri, USA). Lidocaine free base (99.9%) was purchased from Biosynth Carbosynth (Berkshire, UK). Procaine hydrochloride (99.4%) was purchased from Tokyo Chemical Industry (Tokyo, Japan) and Alfa Aesar (Massachusetts, USA). Glacial acetic acid (99.8%) was purchased from Carlo Erba Reagents (Paris, France). Sodium hydroxide (99.0%) was purchased from LaborSpirit (Lisbon, Portugal). Deuterated dimethyl sulfoxide (DMSO- d_6) was purchased from Eurisotop (Saint-Aubin, France). Hydranal Coulomat AG was purchased from Riedel-de Haën (Seelze, Germany).

All tested biopolymers were used without further purification. Chitosan (practical grade, from shrimp shells, SLBX7456) was purchased from Sigma-Aldrich (Missouri, USA). CGCs-FCT (mediums K and BSM) were supplied and produced by the BIOENG group (FCT NOVA, Lisbon). CGC-Com was purchased from KitoZyme (Herstal, Belgium) under the trade name KiOnutrim[®]-CG.

2.2. Experimental synthesis

2.2.1. Purification of APIs

Prior to the synthesis of lidocaine- or procaine-based ILs with an equimolar of a suitable organic acid, lidocaine, procaine free base as well as ibuprofen free acid, were previously prepared through an acid-base titration reaction against an equimolar aqueous solution of sodium hydroxide or hydrochloric acid solution, respectively. These procedures were generally adapted from previous literature reports²⁷. The experimental procedures are described below.

Lidocaine free base: Lidocaine hydrochloride monohydrate (19.60 g, 0.70 mol) was dissolved in distilled water at room temperature using a magnetic stirrer (Velp Scientifica, Italy). A 4.7 M of sodium hydroxide solution was added dropwise to the previous solution under vigorous stirring at room temperature. A white, crystalline precipitate was formed after approximately 30 minutes and subsequently, it was filtered and washed with water to remove any traces of sodium chloride (by-product). The isolated product was dried in a vacuum line for one hour and then, lyophilized for approx. 24 hours using a LyoQuest benchtop freeze dryer (Telstar, Japan). A white solid (14.89 g, 93.4%) was obtained, and the chemical structure was checked by FTIR-ATR spectroscopy.

Procaine free base: Procaine hydrochloride (34.41 g, 0.13 mol) was dissolved in distilled water at room temperature using a magnetic stirrer (Velp Scientifica, Italy). A 5.1 M sodium hydroxide aqueous solution was added dropwise to the previous solution and the solution was stirred at room temperature. A white precipitate was formed but rapidly became a colorless oil. To promote the crystallization of the desired product, the previous solution was placed into an ice bath during 2 hours. Then, the precipitated was isolated by vacuum filtration as well as washed with distilled water to remove any traces of sodium chloride (by-product). The desired product was lyophilized for approx. 24 h using a LyoQuest benchtop freeze dryer (Telstar, Japan) and then, dried in vacuum line to give a light-yellow oil (31.15 g, 97.2 %), and the chemical structure was checked by FTIR-ATR spectroscopy.

Ibuprofen free acid: Ibuprofen sodium salt (30.15 g, 0.13 mol) was placed into a 250 mL glass beaker. The salt was dissolved at 40 °C into 150 mL of distilled water using a magnetic stirrer (Velp Scientifica, Italy) until a clear solution was observed. Following the dissolution, 19 mL of a 7.0 M hydrochloric acid aqueous solution was added dropwise to the previous solution with mild stirring for the neutralization reaction to occur at room temperature. The mixture continued to be stirred at room temperature until ibuprofen free acid precipitated completely (after approx. 3 h). The precipitate was separated by vacuum filtration as well as washed with distilled water to remove any traces of sodium chloride (by-product). The final product was then collected into a 50 mL round-bottomed flask and dried under vacuum line for approx. 6 h for 3 days yielding a white powder (23.34 g, 85.7%). The chemical structure was checked by FTIR-ATR spectroscopy.

2.2.2. Synthesis of API-ILs

These procedures were generally adapted from previous literature reports²⁷. The experimental procedures are described below.

Lidocainium acetate: Glacial acetic acid (11.0 mL, 0.18 mol) was added dropwise to an equimolar amount of lidocaine free base previously prepared and melted (43.11 g, 0.18 mol) in a square-bottomed Schott flask. The mixture was warmed with mild stirring at 80 °C (water bath temperature) using a magnetic stirrer (Velp Scientifica, Italy) for one hour and a free-flowing clear liquid was observed. After the solution was cooled, a clear, viscous liquid was obtained, until starting to crystallize.

Lidocainium propionate: Propionic acid (12.9 mL, 0.17 mol) was added dropwise to an equimolar amount of lidocaine free base previously melted (41.24 g, 0.17 mol) in a square-bottomed Schott flask. The mixture was warmed with mild stirring at 80 °C (water bath temperature) using a magnetic stirrer (Velp Scientifica, Italy) for one hour and a free-flowing clear liquid was observed. After the solution was cooled, a clear, yellowish liquid was obtained.

Lidocainium hexanoate: Hexanoic acid (18.1 mL, 0.16 mol) was added dropwise to an equimolar amount of lidocaine free base previously melted (36.33 g, 0.16 mol) in a square-bottomed Schott flask. The mixture was warmed with mild stirring at 80 °C (water bath temperature) using a magnetic stirrer (Velp Scientifica, Italy) for one hour and a free-flowing clear liquid was observed. After the solution was cooled, a clear and colorless liquid was obtained.

Procainium acetate: Glacial acetic acid (4.5 mL, 0.82 mol) was added dropwise to procaine free base previously melted (19.00 g, 0.80 mol) in a square-bottomed flask. The mixture was warmed with stirring at 80 °C (oil bath temperature) for one hour and a free-flowing clear liquid was observed. After the solution was cooled, a clear and dark yellow liquid was obtained.

Procainium propionate: Propionic acid (4.2 mL, 0.57 mol) was added dropwise to an equimolar amount of procaine free base previously melted (13.40 g, 0.57 mol) in a square-bottomed Schott flask. The mixture was warmed with mild stirring at 80 °C (oil bath temperature) for one hour and a free-flowing liquid was observed. After the solution was cooled, a pale waxy liquid was obtained.

Procainium hexanoate: Hexanoic acid (7.2 mL, 0.62 mol) was added dropwise to an equimolar amount of procaine free base previously melted (14.62 g, 0.62 mol) in a square-bottomed Schott flask. The mixture was warmed with mild stirring at 80 °C (oil bath temperature) for one hour and a free-flowing liquid was observed. After the solution was cooled, a pale liquid was observed.

Lidocainium ibuprofenate: Ibuprofen free acid (16.59 g, 0.80 mol) and lidocaine free base (18.84 g, 0.80 mol) were melted with stirring at 80 °C (water bath temperature) in a square-bottomed Schott flask for one hour, and a free-flowing clear liquid was observed. After the solution was cooled, a colorless viscous liquid was obtained.

Procainium ibuprofenate: Ibuprofen free acid (24.82 g, 0.12 mol) was previously melted with stirring at 80 °C using a magnetic stirrer (Velp Scientifica, Italy) and procaine free base (28.99 g, 0.12 mol) was added, and the mixture was warmed with stirring at 80 °C (water bath temperature), for one hour and a free-flowing clear liquid was observed. After the solution was cooled, a yellowish waxy liquid was obtained.

2.3. Characterization of API-ILs

2.3.1. Proton nuclear magnetic resonance spectroscopy

Proton nuclear magnetic resonance (¹H NMR) spectra were collected by Dr. Ana Lopes using a Bruker Avance III 400 MHz spectrometer operating at 400.13 MHz. Samples were dissolved at various concentrations in deuterated dimethyl sulfoxide (approx. 25 mg of IL in 0.5

mL of DMSO- d_6) and placed in capillary tubes. ^1H chemical shifts (δ) are reported as parts per million (ppm) relative to the quintet signal of DMSO- d_6 solvent at 2.50 ppm. These solvent peaks were used as external reference during assignment and integration of proton peaks using MestReNova v. 6.0 (Mestrelab Research S.L., Spain).

2.3.2. Fourier-transform infrared spectroscopy

Fourier-transform infrared (FTIR) spectra were collected at room temperature using a Perkin Elmer Spectrum Two spectrometer featuring an attenuated total reflection (ATR) by placing neat samples over a diamond crystal. Spectra were recorded with 14 scan accumulations at 1.0 cm^{-1} resolution and were obtained in the range of $400 - 4000\text{ cm}^{-1}$.

2.3.3. Thermogravimetric analysis

Thermogravimetric analysis (TGA) was performed by Carla Rodrigues from chemical analysis laboratory at LAQV (FCT NOVA) on a Setaram LABSYS evo from analysis laboratory from LAQV (FCT NOVA). Samples were placed into aluminum crucibles and were heated at a constant rate of $10\text{ }^\circ\text{C}/\text{min}$, from $25\text{ }^\circ\text{C}$ to $500\text{ }^\circ\text{C}$, under an argon flow of $50\text{ mL}/\text{min}$.

2.3.4. Differential scanning calorimetry

Differential scanning calorimetry (DSC) was performed using a TA Instruments Discovery DSC 25 with a refrigerated cooling system. Samples were placed in closed aluminum pans. To allow any residual water to escape and to avoid the risk of the pans bursting under pressure, a small pinhole was made on the pan lid. An empty closed pan was used as reference. Heating and cooling were conducted at a constant rate of $10\text{ }^\circ\text{C}/\text{min}$, except where mentioned, under a nitrogen atmosphere using a purge flow rate of $50\text{ mL}/\text{min}$.

A typical experiment was run as follows: after equilibration at $20\text{ }^\circ\text{C}$ the sample was cooled to $-90\text{ }^\circ\text{C}$ followed by a 1-minute isotherm and then, heated to $100\text{ }^\circ\text{C}$ followed by a 1-minute isotherm. This cycle was repeated three times. Besides the experiments with all synthesized API-ILs, experiments with the reagent APIs were also employed using a slightly wider temperature range. In general, the second and third cycles proved to be identical, hence transition temperatures were acquired in the last cycle, except where mentioned.

2.3.5. Viscosity studies

Viscosity studies were performed by Dr. Rita Craveiro from Des.solve Group at FCT-NOVA (Lisbon, PT). Viscosity measurements were executed on an Anton Paar MCR 102 modular compact rheometer. Two different experiments were performed: (1) shear rate sweep from 0.1 to 100 s^{-1} at $20\text{ }^\circ\text{C}$, and (2) temperature sweep from room temperature to $80\text{ }^\circ\text{C}$ at a

heating rate of 5 °C/min and a constant shear stress of 20 Pa.

2.3.6. Water content determination

Coulometric Karl Fischer (KF) titration was performed using a Metrohm AG 831 KF coulometer. Droplets of fluid IL samples were injected into the titration vessel of the KF apparatus using a syringe. The sample mass (obtained by posteriorly weighing of the syringe) was set to produce results (water content in parts per million). The measurements were made in triplicate. The residual or penetrating water that the KF apparatus removed per minute was in the range from 8 to 14 µg/min. The reagent (analyte solution) used was Hydranal Coulomat AG.

2.4. Dissolution studies

Dissolution studies of the biopolymer's chitosan, CGCs-FCT (inoculated in mediums K and BSM) and CGC-Com using the prepared API-ILs were performed. The biopolymers mass was calculated as a percentage by weight (wt%) relative to the used API-IL mass. Dissolution studies were performed using two different dissolution conditions: (1) 70 °C for 3 days and, (2) 100 °C for 1 day.

All the experiments were carried out in the same fashion, according to the following procedure: (1) 5 to 9 g of API-IL were weighed into a glass vial; (2) the vial was then immersed in a silicone oil bath (Baysilone M350), and the API-IL was heated with stirring until the dissolution temperature is reached; (3) 1 wt% of biopolymer was slowly added; (4) the mixture was stirred at 1000 rpm and heated in a thermostatic oil bath at 70 °C for 3 days or at 100 °C for 1 day; (5) after that period, dissolution was assessed visually. After assessing a partial or successful dissolution (*i.e.*, no biopolymer's particles were observed in suspension), the previous experiment was scaled up to 10 g API-IL and the correspondent amount of biopolymer (1 wt%).

2.5. Preparation of biopolymeric structures

A 3-step procedure, as illustrated in Figure 2.1, was followed to prepare biopolymeric structures. These steps comprise: (1) 10 g API-IL and 1 wt% biopolymer mixture casting into a metal disc (the mixture covers the surface of the disc with 6.5 cm diameter); (2) metal disc immersion on a coagulation bath – phase inversion in distilled water or aqueous solution containing 10% (v/v) of glycerol – for 24 h at room temperature; (3) drying for 24 h at room temperature.

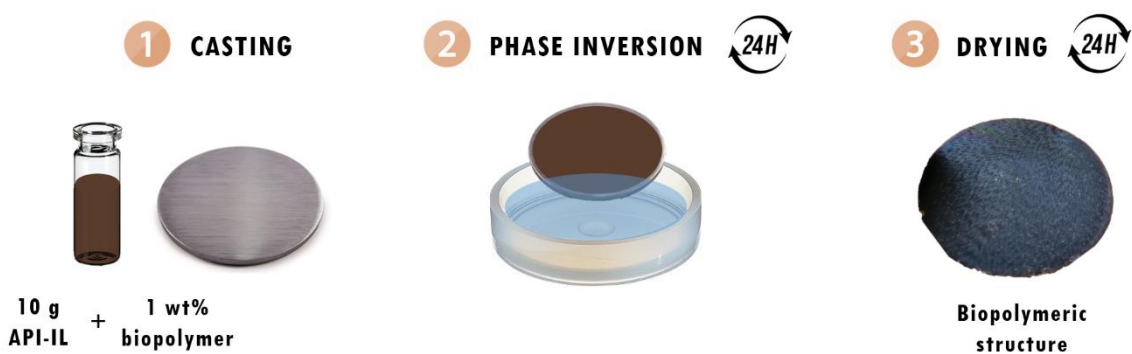


Figure 2.1 Illustration of the 3-step procedure for the preparation of polymeric structures.

2.6. Characterization of films

2.6.1. Scanning electron microscopy

Scanning electron microscopy (SEM) was performed by Isabel Nogueira from MicroLab at Instituto Superior Técnico (Lisbon, PT). Micrographs of the cross section and surface of the samples were obtained at magnifications of 40 \times and 100 \times for the cross section and at 100 \times , 500 \times and 1000 \times for the surface, using a SEM Hitachi model S2400 with an accelerating voltage of 20 kV. The samples were placed on an Al sample holder using double-sided carbon tape and sputter coated with a gold/palladium (Au/Pd) thin film on a Quorum Technologies Q150T ES. Micrographs were acquired using Esprit 1.9 software (Bruker, Massachusetts).

2.6.2. Fourier-transform infrared spectroscopy

Fourier-transform infrared (FTIR) spectra were collected at room temperature using a Perkin Elmer Spectrum Two spectrometer featuring an attenuated total reflection (ATR) by placing neat samples over a diamond crystal. Spectra were recorded with 14 scan accumulations at 1.0 cm^{-1} resolution and were obtained in the range of 400 – 4000 cm^{-1} .

2.6.3. Thermogravimetric analysis

Thermogravimetric analysis (TGA) was performed by Carla Rodrigues from chemical analysis laboratory at LAQV (FCT NOVA) on a Setaram LABSYS EVO. Samples were placed into aluminum crucibles and were heated at a constant rate of 10 $^{\circ}\text{C}/\text{min}$, from 25 $^{\circ}\text{C}$ to 600 $^{\circ}\text{C}$, under an argon flow of 50 mL/min .

2.6.4. Differential scanning calorimetry

Differential scanning calorimetry (DSC) was performed using a TA Instruments DSC Q2000 with a refrigerated cooling system. Samples of approximately 5 mg were placed in closed aluminum pans. To allow any residual water to escape and to avoid the risk of the pans bursting under pressure, a small pinhole was made on the pan lid. An empty closed pan was used as

reference. Heating and cooling were conducted at a constant rate of 10 °C/min, under a nitrogen atmosphere using a purge flow rate of 50 mL/min.

A typical experiment was run as follows: after equilibration at 20 °C from the set point (40 °C), the sample was cooled to -90 °C followed by a 1-minute isotherm and then heated to 120 °C followed by a 1-minute isotherm. This cycle was generally repeated three times. The drying procedure employed to remove any residual water from the samples consisted of the first heating scan, where the sample was heated to 100 °C followed by a 1-minute isotherm. For this reason, the thermal transitions were determined from the last heating or cooling scan, except where mentioned.

2.6.5. Contact angle measurements

Contact angle measurements were made using a goniometer. A drop of distilled water was placed at the film surface using a syringe (sessile drop method). The measurements were performed in triplicate at room temperature. Programming of the experiments and data collection was done using CAM2008 software (KSV Instruments, Finland).

2.6.6. Mechanical properties

The mechanical properties were determined using a Stable Micro Systems TA.XTplus Texture Analyzer. Samples of approximately 25×25 mm size were immobilized on a flat platform with a 5 mm diameter hole. The maximum force at break was estimated using a needle probe of 2 mm in diameter at a test speed of 0.5 mm/s. The measurements were performed in triplicate and the maximum values obtained were averaged. The thickness of the films was determined using a micrometer (Elcometer Ltd., UK) averaging measurement at three random positions of the film (avoiding edges) to calculate the mean thickness.

2.7. Characterization of hydrogel

2.7.1. Fourier-transform infrared spectroscopy

Same method described at 2.6.1 was done for the characterization of hydrogels.

2.7.2. Thermogravimetric analysis

Same method described at 2.6.3 was done for the characterization of hydrogels.

2.7.3. Differential scanning calorimetry

Same method described at 2.6.4 was done for the characterization of hydrogels.

2.7.4. Rheological studies

Rheological studies were performed at 25 °C on a Thermo Scientific Haake Mars III controlled stress rheometer equipped with a cone-plate geometry (diameter 35 mm) with a gap of 0.105 mm. A stress sweep was performed in the range of 0.1 to 1000 Pa at a constant frequency of 1 Hz. From this measurement, a tension of 0.5 Pa was selected to perform the frequency sweep in the range of 0.01 to 100 Hz. The mechanical spectrum was obtained using HAAKE RheoWin Job Manager software (Thermo Scientific, Germany) where the storage (G') and loss (G'') moduli were plotted as a function of frequency to assess the viscoelastic properties of the sample.

3. Results and discussion

3.1. Synthesis of API-ILs

Bearing in mind the potential topical drug delivery application, pharmaceutically acceptable APIs with anesthetic and anti-inflammatory response were selected as base or acid to for IL synthesis. Herein, lidocaine and procaine, which are members of the Caine family of pharmaceutical local anesthetics, and ibuprofen, which is member of the nonsteroidal anti-inflammatory drugs (NSAIDs) class, have been selected as APIs to prepare API-ILs. In this context, lidocaine and procaine were combined with different organic acids, including ibuprofen (in its acidic form) as shown in Figure 3.1. The anion acetate (conjugate base of acetic acid) and similar short alkyl chain carboxylate anions (propionate and hexanoate) were chosen due to their low steric hindrance and hydrogen-bond basicity, which are important parameters for biopolymer dissolution as reported in previously mentioned studies for acetate based ILs in cellulose, chitin, chitosan and CGC dissolution³⁵⁻³⁷.

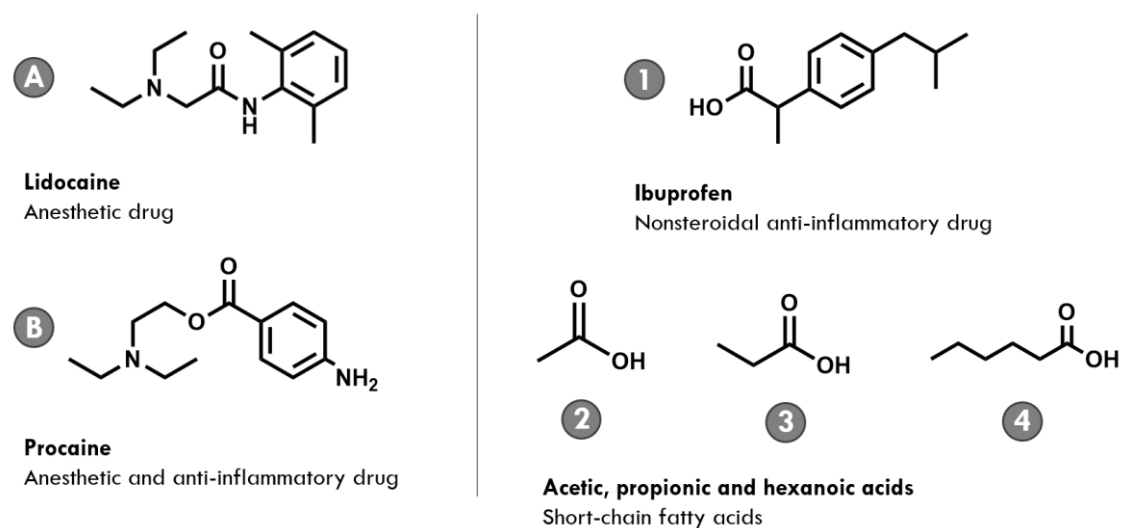


Figure 3.1 Chemical structures of the pharmaceutical local anesthetics and anions selected for API-IL synthesis. Each base, A and B, was combined with a carboxylic acid from 1 to 4.

All the above-mentioned acids and bases were combined *via* acid-base reactions to produce the desired API-ILs. The acid-base reaction avoids the formation of inorganic salts, making it preferable over the conventional ion-exchange reaction. Prior to the synthesis of the API-ILs, the salt form of the three selected APIs were converted to their basic or acidic form *via* acid-base reactions using water as solvent.

Table 3.1 Melting points (T_m) of APIs and the correspondent acid-base reaction yields performed to obtain the basic or acidic form of the desired API.

| API salt form | API | T_m^a [°C] | Yield [%] |
|----------------------|---------------------|------------------------|-----------|
| HCl·H ₂ O | Lidocaine free base | 68–69 ^{52,53} | 93.4 |
| HCl | Procaine free base | 61 ⁵⁴ | 97.2 |
| Na | Ibuprofen free acid | 76 ⁵⁵ | 85.7 |

^a Melting temperature reported in the literature.

A total of eight API-ILs were synthesized by mixing equimolar amounts of lidocaine or procaine in its basic form with the selected acid at room temperature. The appearance and the abbreviations chosen for the API-ILs are presented in Table 3.2. A picture of the synthesized API-ILs is provided in Appendix I.

Table 3.2 Abbreviations and appearance of the synthesized API-ILs.

| API-ILs | Abbreviation | Appearance ^a |
|--------------------------|--------------|--------------------------|
| Lidocainium acetate | [Lid][OAc] | Pale crystalline solid |
| Lidocainium propionate | [Lid][OPr] | Yellowish viscous liquid |
| Lidocainium hexanoate | [Lid][OHex] | Colorless liquid |
| Lidocainium ibuprofenate | [Lid][Ibu] | Colorless viscous liquid |
| Procainium acetate | [Pro][OAc] | Dark yellow liquid |
| Procainium propionate | [Pro][OPr] | Pale waxy liquid |
| Procainium hexanoate | [Pro][OHex] | Pale liquid |
| Procainium ibuprofenate | [Pro][Ibu] | Yellowish waxy liquid |

^a Appearance observed at room temperature after 2–3 weeks after the synthesis.

3.2. Characterization of API-ILs

The main aim of the performed characterization techniques was to assess the structure, viscosity, and thermal stability of the synthesized API-ILs prior to performing dissolution studies. As the water content in ILs affects all the properties mentioned above, it will consequently influence their reactivity and solvating ability³⁸, and thus it is relevant to determine API-ILs water content.

Although water content determination *via* coulometric Karl Fischer (KF) titration of the prepared API-ILs was attempted, the synthesized procaine based ILs were too viscous to be injected through a needle across the sample injection cap of the KF apparatus. The water content determined for the assessed fluid lidocaine based ILs was in the range of 0.15% to 0.25% ± 0.05 (w/w). These low values can be attributed to the lack of water uptake by lidocaine free base, which is slightly hygroscopic comparing to the procaine free base, making it an attractive base to tune the design of water free ILs for anesthetic drug delivery. On the other hand, in the case of [Pro][OAc] and possibly in all procaine based ILs, according to Rogers and coworkers³⁹, the presence of water leads directly to crystallization of a dihydrate form that cannot be dehydrated without decomposition.

As unintended crystallization of APIs in API-ILs can dramatically alter its solubility and bioavailability^{27,39}, it is important to study mainly their thermal stability by TGA and DSC, so that

we can assure no decomposition during dissolution and anticipate API-IL crystallization over time.

3.2.1. Proton nuclear magnetic resonance spectroscopy

Following API-IL synthesis and before performing further characterization techniques, proton nuclear magnetic resonance (^1H NMR) spectroscopy was performed to elucidate the chemical structure of the prepared API-ILs. Since both cation and anion have protons, we can determine the cation to anion ratio and assess if an equimolar ratio was attained.

An example of a ^1H NMR spectra of a prepared API-IL is presented in Figure 3.2, where the protons of the cation and anion are labeled alphabetically to check its chemical structure.

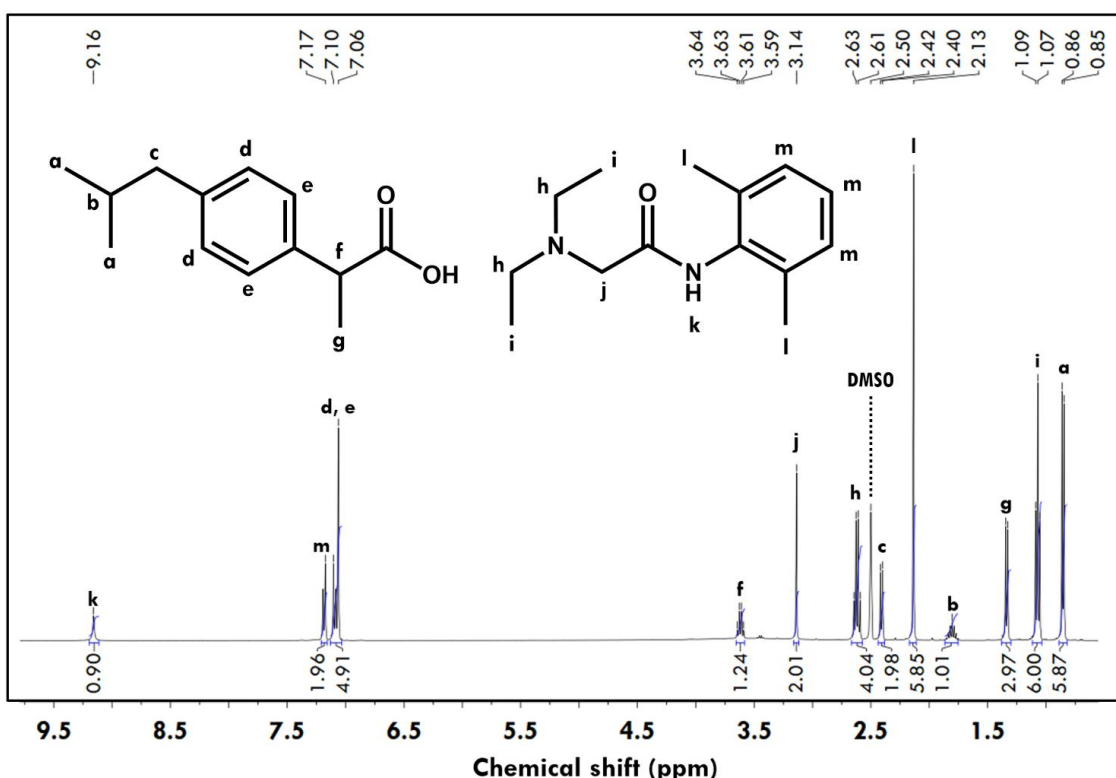


Figure 3.2 ^1H NMR spectrum of lidocainium ibuprofenate ([Lid][Ibu]) in $\text{DMSO}-d_6$ solution and assignment of the proton signals to hydrogen-labeled chemical structure of [Lid][Ibu].

The ^1H NMR analysis of [Lid][Ibu] showed signals in aliphatic and aromatic regions that can be attributed to the protons from both cation and anion structures, which agrees with the estimated integration values that correspond to the relative areas under the different attributed signals. Taking this into account, it is possible to conclude the sample contains both cation and anion structures as expected with high relative purity levels. Once, both cation and anion have protons in their structures it is possible estimate the proportion between them. The proton signals selected for cation to anion ratio determination were the ones associated to the six protons on the terminal methyl groups indicated with the letters “a” and “i” in Figure 3.2. Thus, the correlation used to determine the cation to anion ratio in [Lid][Ibu] was $H_i/6 : H_a/6$, where H_i is 6.00 (the

expected value for the six protons on the methyl groups indicated with the letter “i”; used as proton reference value) and H_a is the obtained value for the quantitative integration of the protons indicated with “a”(5.87) leading to a cation to anion ratio of 1:0.98.

The ^1H NMR spectra of the remaining API-ILs are provided in Appendix II. In general, the cation to anion ratio was determined by quantitative integration of the preferred proton peaks, usually protons on lidocainium or procainium aromatic ring and the obtained ratios had to be within the range of 0.95–1.05 on the anion, so that the desired IL equimolar proportion was confirmed as shown in Table 3.3. The range of 0.95–1.05 on the anion was established from the estimated values are affected by a 10–20% error⁴⁰ resulting from the integration of the proton signal areas in the ^1H NMR spectra.

Table 3.3 Cation to anion ratio determined by quantitative integration of ^1H peaks.

| API-ILs | Cation to anion ratio |
|-------------|-----------------------|
| [Lid][OAc] | 1: 0.97 |
| [Lid][OPr] | 1: 0.95 |
| [Lid][OHex] | 1: 1.03 |
| [Lid][Ibu] | 1: 0.98 |
| [Pro][OAc] | 1: 0.97 |
| [Pro][OPr] | 1: 0.97 |
| [Pro][OHex] | 1: 0.99 |
| [Pro][Ibu] | 1: 1.00 |

3.2.2. Fourier-transform infrared spectroscopy

Fourier-transform infrared (FTIR) spectroscopy was used to elucidate the functional groups of the prepared APIs and API-ILs by analysis of the infrared stretching vibrations. The FTIR-ATR spectra of lidocaine and procaine free bases, and ibuprofen free acid, which were used in the synthesis of API-ILs, is shown in Figure 3.3.

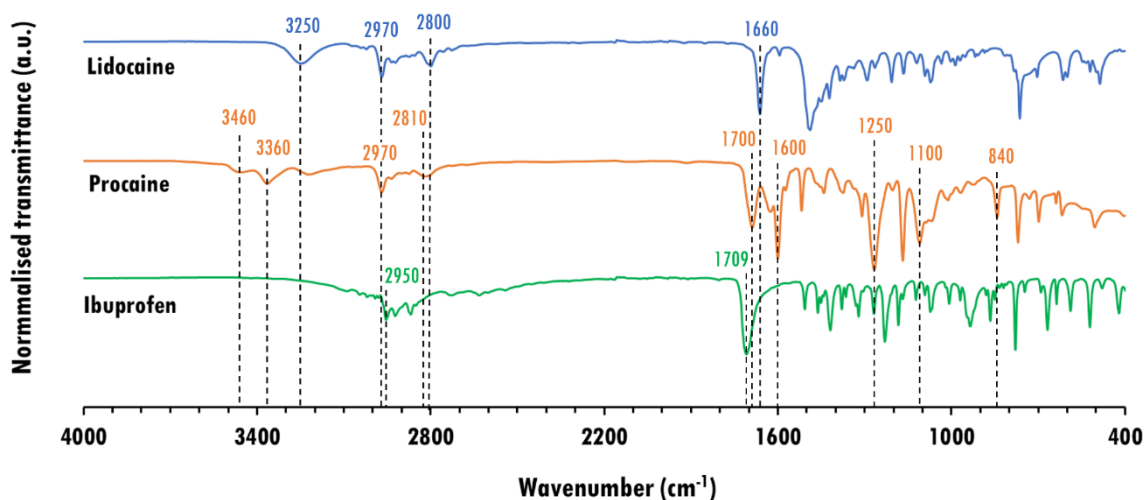


Figure 3.3 FTIR-ATR spectra of lidocaine and procaine as free bases, and ibuprofen as free acid. Critical wavenumbers are depicted with corresponding colors.

The spectrum of lidocaine free base showed several bands, namely at *ca.* 3250 cm^{-1} associated with the N–H stretch of secondary amide (broad band), at *ca.* 2970 cm^{-1} , at *ca.* 2800 cm^{-1} and at *ca.* 1660 cm^{-1} associated with the C=O bonds of the amide group. The spectrum of procaine free base showed several bands, namely at *ca.* 3460 cm^{-1} and *ca.* 3360 cm^{-1} associated with the N–H stretches of primary amine (two bands), at *ca.* 2970 cm^{-1} (alkene C–H stretches), at *ca.* 1700 cm^{-1} and at *ca.* 1600 cm^{-1} associated with the C=O stretches of the ester group, at *ca.* 1270 cm^{-1} and at *ca.* 1170 cm^{-1} related with the C–O stretches of the ester group and at *ca.* 840 cm^{-1} associated with aromatic C–H bending vibrations (outside the aromatic ring plane). The spectrum of ibuprofen free acid showed several bands, namely at *ca.* 2950 cm^{-1} associated with the O–H stretch of the carboxyl group and at *ca.* 1709 cm^{-1} related with the C=O stretch of the carboxyl group²⁷.

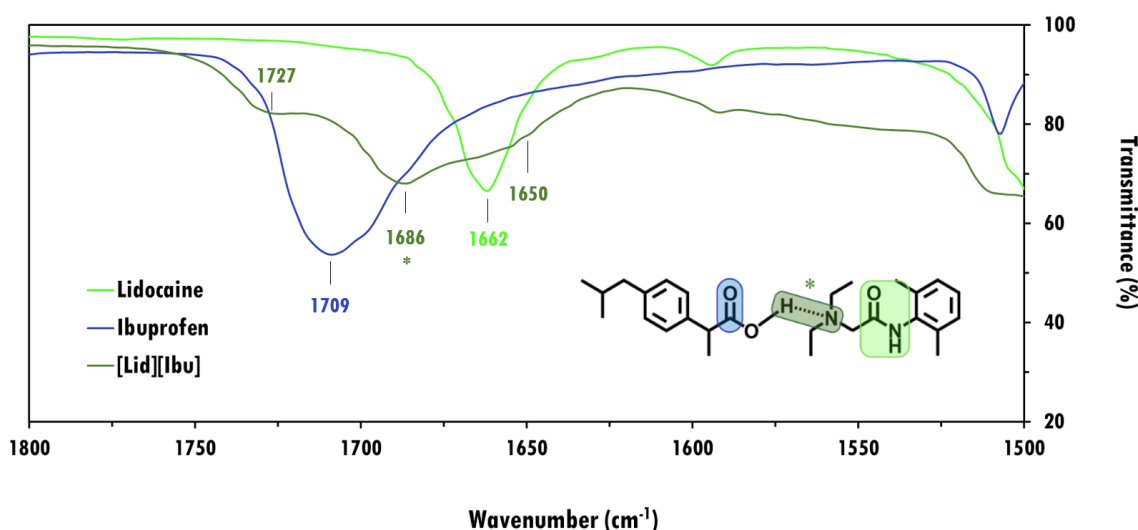


Figure 3.4 Chemical structure of [Lid][Ibu] and expanded FTIR-ATR spectra (C=O region) of lidocaine free base, ibuprofen free acid and the prepared [Lid][Ibu]. Critical wavenumbers, moieties and H-bonds (*), are depicted with matching colors.

Of all the synthesized API-ILs, the FTIR analysis of [Lid][Ibu] is already well established in literature²⁷. Indeed, the carbonyl stretch (C=O) is one of the most important bands, and in this case results from the combination of three peaks as indicated in dark green in Figure 3.4. According to the most recent literature²⁷, the peaks positioned at (1) *ca.* 1727 cm^{-1} can be assigned to carbonyl group of ibuprofen moiety, which showed a slightly shift to higher frequencies when compared with ibuprofen free acid (1709 cm^{-1}), suggesting that the ibuprofen is partially ionized; (2) *ca.* 1686 cm^{-1} as a minimum of the band, that is “*indicative of a dynamic equilibrium between acid, base and H-bonded eutectics*” as reported by Rogers and co-workers²⁷; and (3) *ca.* 1650 cm^{-1} that can be assigned to the carbonyl stretch (C=O) of lidocaine’s amide group, which showed a slightly shift to lower frequency when compared to the lidocaine free base (*ca.* 1660 cm^{-1}) as expected²⁷.

Additionally, the reported literature on the C=O stretch of [Pro][Ibu] also suggests that

the hydrogen-bonding occurs between the carboxyl group of ibuprofen and procaine⁴⁸ as illustrated in Figure 3.5. Indeed, the carboxylic acid shared the proton with the base to form an ionic specie, which is in dynamic equilibrium with the neutral species.

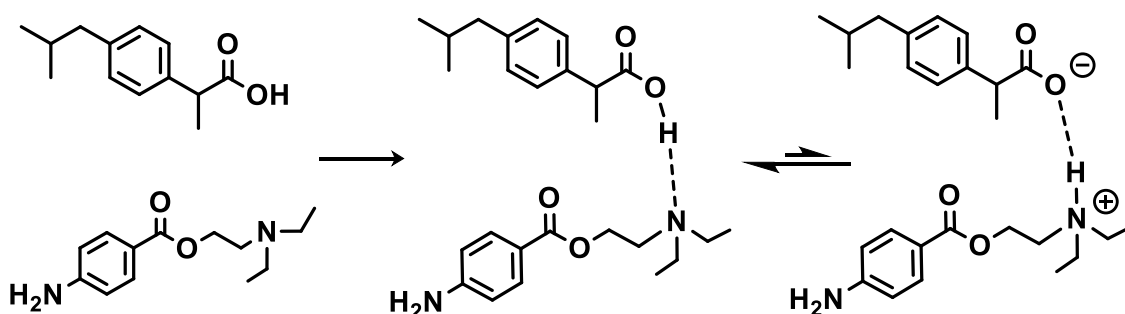


Figure 3.5 Hydrogen bond formation between ibuprofen (top) and procaine (bottom). The interaction represented in the center is more stable as indicated by the staggered equilibrium arrows. Adapted from Rogers *et al.*³⁰.

In general, a slight deviation of the C=O stretching absorption associated with the carboxyl group of the acid was observed in the prepared API-ILs, suggesting that the acid is partially ionized (if the carboxylic acid was fully ionized, the C=O stretch would appear at *ca.* 1560 cm⁻¹ instead of at *ca.* 1760 cm⁻¹). In summary, the synthesized API-ILs can be considered protic ILs because the acid and base both shared the carboxylic acid proton *via* strong hydrogen bonds or interactions between partially ionized species²⁷.

3.2.3. Thermogravimetric analysis

The thermal stability of the synthesized API-ILs was assessed *via* thermogravimetric analysis (TGA). The decomposition temperature values were obtained using the onset temperature, where the sample lost 5 % of its initial mass ($T_{5\%, \text{onset}}$) and the inflection point of the first step and second step of the mass loss process (T_{step1} and T_{step2}), which were taken as the minimum of the derivative of thermogravimetric curves (DTG). These temperatures are summarized in Table 3.4.

Table 3.4 Decomposition temperatures associated with mass loss of the synthesized API-ILs.

| API-ILs | $T_{5\%, \text{onset}}^a$ [°C] | T_{step1}^b [°C] | T_{step2}^b [°C] |
|-------------|--------------------------------|---------------------------|---------------------------|
| [Lid][OAc] | 213.2 | 275.2 | 341.1 |
| [Lid][OPr] | 135.4 | 272.6 | 331.1 |
| [Lid][OHex] | 151.8 (100.0 ⁶⁰) | 156.7 | 254.3 |
| [Lid][Ibu] | 221.5 (165.2 ⁵⁹) | 278.0 | 404.8 |
| [Pro][OAc] | 152.7 | 188.6 | 283.9 |
| [Pro][OPr] | 153.7 | 200.0 | 288.4 |
| [Pro][OHex] | 181.4 | 215.5 | 279.1 |
| [Pro][Ibu] | 216.8 (176.7 ⁴⁸) | 264.0 | 399.1 |

^a Onset temperature, where the sample lost 5% of its initial mass ($T_{5\%, \text{onset}}$) and. ^b Decomposition temperatures associated with the first and second step of the mass loss process (T_{step1} and T_{step2} , minimum of the peak of the mass loss derivative) were acquired at a heating rate of $10\text{ }^{\circ}\text{C min}^{-1}$ from $25\text{ }^{\circ}\text{C}$ to $500\text{ }^{\circ}\text{C}$, under continuous argon flow. The onset temperatures to 5% mass loss reported in the literature are also depicted enclosed in parentheses.

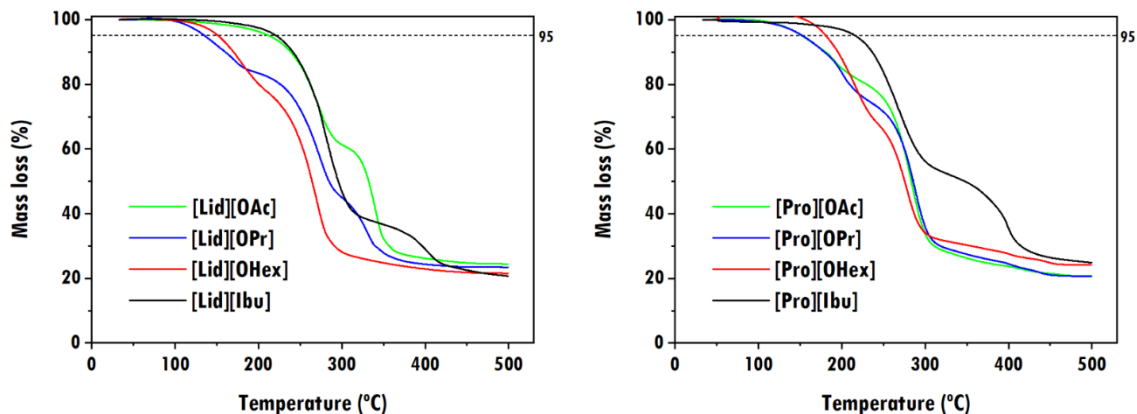


Figure 3.6 Thermogravimetric curves of lidocaine based-ILs (left) and procaine based-ILs (right) at $10\text{ }^{\circ}\text{C min}^{-1}$. The $T_{5\%, \text{onset}}$ were taken as the value corresponding to 95% mass loss represented by the horizontal dot lines.

The onset temperatures to 5% mass loss were taken as the value corresponding to 95% mass loss as shown in Figure 3.6. TGA of both lidocaine- and procaine-based API-ILs showed signs of decomposition at only slightly higher temperatures, with [Lid][OPr] revealing a steeper mass loss, having lost 5% of its initial mass at $135.4\text{ }^{\circ}\text{C}$, followed by [Pro][OAc] and [Pro][OPr], respectively. These observed mass losses can be explained by a possibly higher water content in IL samples which was determined to be in the range from 0.15% to $0.25\% \pm 0.05$ (w/w) in lidocaine based ILs.

The majority of ILs are thermally stable and only undergo a one-step mass loss process⁵⁰. According to Luo *et al.*⁵⁰, the thermogravimetric curves determined for 16 protic amide based-ILs revealed a two-step mass loss process, which was consistent with the loss of the cation and anion of the ILs, making it easier to absolutely assign a mass loss to the cation and to the anion in an IL. The synthesized API-ILs in this work did also generally underwent a two-step mass loss process as shown in Figure 3.7, where the two mass loss steps were attributed to the anion and cation, respectively.

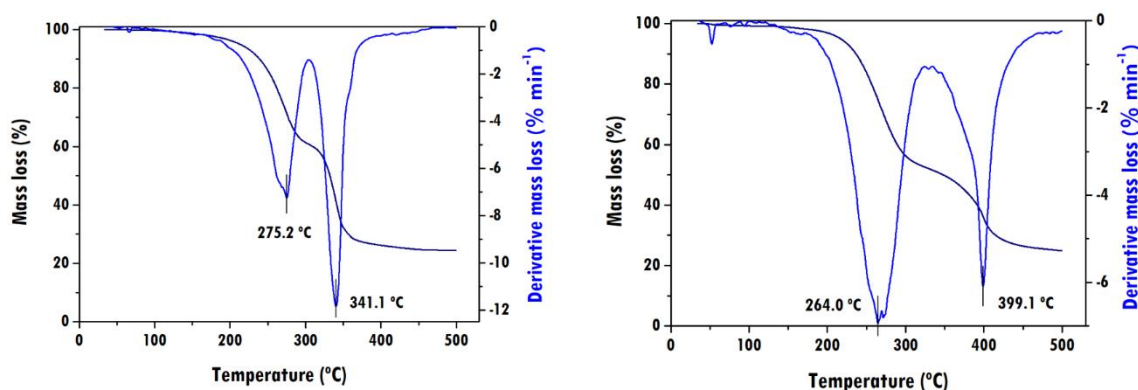


Figure 3.7 Thermogravimetric curves (left Y-axis) and associated derivative curves (right Y-axis) of lidocainium acetate ([Lid][OAc]) (left) and procainium ibuprofenate ([Pro][Ibu]) (right) at 10 °C/min, under argon. Decomposition temperatures associated with the first and second step of the mass loss process (T_{step1} and T_{step2}) were taken as the minimum of the derivative of TG curves as indicated with vertical solid lines.

The rationale behind the separate cation and anion mass loss in the API-ILs studied here can be explained by two synergic reasons: (1) the carboxylic acid moiety is thought to be partially ionized, indicating that the neutral acid and base species are in dynamic equilibrium with ionized species as mentioned above (see section 3.2.2); and (2) the difference in volatility of the neutral acid and base causes the acid to evaporate first, leaving the free base behind. As to the possibly ionized species in the IL, the drastic increase in temperature may disrupt the formed H-bonds between the carboxylic acid moiety of the anion and the counterion, resulting in the neutral acid and base species being present again and thus being more prone to evaporate.

3.2.4. Differential scanning calorimetry

Differential scanning calorimetry (DSC) was used to determine the thermal transitions of the synthesized APIs and API-ILs. DSC experiments were programmed considering the onset temperature, where the sample lost 5% of its initial mass previously determined by TGA. This methodology optimizes DSC experiments by preventing further sample decomposition.

Melting temperatures were taken as the minimum of an endothermic. A glass transition is defined as a step change in molecular mobility in the amorphous phase of the sample that results in a step change in heat flow, hence, glass transition temperatures were taken at the midpoint (inflection point)⁶² between onset and offset of the transition. The thermal transitions of the APIs and synthesized API-ILs are reported in Table 3.5.

Table 3.5 Thermal properties of the synthesized APIs and API-ILs.

| APIs / API-ILs | $T_{g\text{-mid}}^a$ [°C] | T_g^b [°C] | T_m^a [°C] | T_m^b [°C] |
|----------------|---------------------------|---------------------|-------------------|----------------------------|
| Lidocaine | n.d. ^c | -60.0 ⁶³ | 68.9 | 68.0–69.0 ^{52,53} |
| [Lid][OAc] | -43.0 | -43.0 ⁶⁴ | 54.1 | 48.0 ⁶⁴ |
| [Lid][OPr] | -51.5 | | | |
| [Lid][OHex] | -58.1 | -55.9 ⁶⁰ | | |
| [Lid][Ibu] | -28.8 | -27.4 ⁵⁹ | | |
| Procaine | -37.6 | | n.d. ^c | 61.0 ⁵⁴ |
| [Pro][OAc] | -23.6 | -25.0 ⁵¹ | | |
| [Pro][OPr] | -26.2 | | | |
| [Pro][OHex] | -39.1 | | 79.6 ^d | |
| [Pro][Ibu] | -9.8 | -12.7 ⁴⁸ | 49.4 ^d | |
| Ibuprofen | -41.5 | -45.1 ⁶⁵ | 75.1 | 76.0 ⁵⁵ |

^a Glass transition ($T_{g\text{-mid}}$, midpoint-inflection) and melting temperatures (T_m , peak minimum) were acquired at a heating rate of 10 °C min⁻¹ and of 20 °C min⁻¹ in the case of [Lid][OAc], after cooling to -90 °C, under a continuous flux of nitrogen. ^b Glass transition and melting temperatures reported in the literature. ^c Not detected. ^d Melting point was observed only in the first cycle. In general, all samples were heated to 100 °C to ensure total removal of any residual water and consequently, the thermal transitions were determined from the last heating, except where mentioned.

In general, the obtained glass transitions were relatively close to those reported in the literature^{51,59,60,63,64} and decreased as the alkyl chain length of the short-chain carboxylate anions increased. The obtained API melting temperatures were the same as reported in several studies, except for procaine which melting point was not detected.

According to the literature, the melting point of APIs can be significantly lowered through H-bonding formed between the acids and bases^{49,60}. In fact, in the studied lidocaine based ILs, the melting point determined for [Lid][OAc] was lower than the lidocaine free base. In the case of [Lid][OPr], [Lid][OHex], [Pro][OAc] and [Pro][OPr] no melting points were observed and only exhibited glass transitions in the experimental conditions used, indicating that these ILs are glass formers.

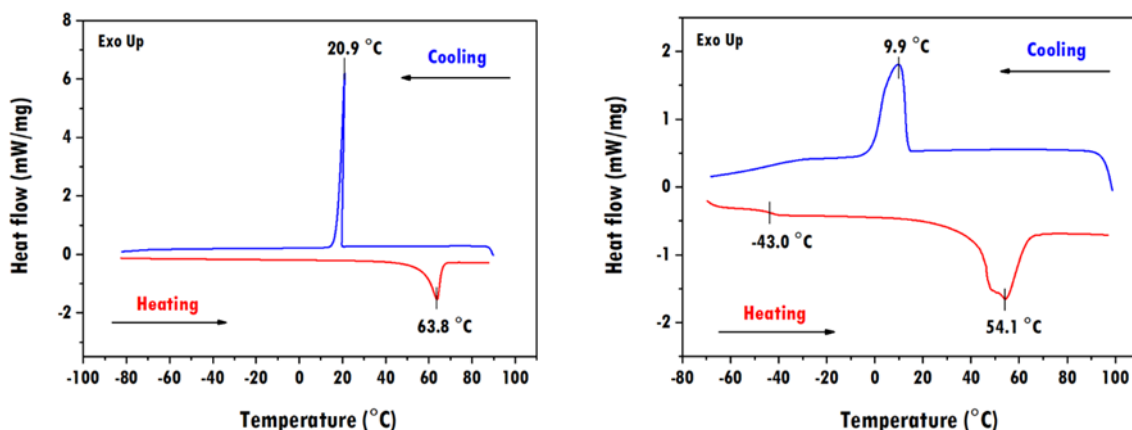


Figure 3.8 Heat flow thermograms for [Lid][OAc] obtained at 10 °C min⁻¹ (left) and at 20 °C min⁻¹ (right) heating (1st cycle) and cooling (2nd cycle) scans. Heat flow signal was conventionally plotted with exotherms up.

A glass transition for [Lid][OAc] was already reported in the literature which was not

possible to be detected at heating and cooling rate of 10 °C min⁻¹ (see Figure 3.8, left). To investigate this, an additional experiment has been performed by increasing the cooling and heating rate to 20 °C min⁻¹ (see Figure 3.8, right). Then, when the [Lid][OAc] sample was heated, a glass transition was successfully detected (-43.0 °C) similar to the reported in the literature⁶⁴. Indeed, this sample exhibited a semicrystalline morphology because it showed a glass transition ($T_{g\text{-mid}} = -43.0$ °C), followed by melting at 54.1 °C. In the subsequent cooling scan, which is showed in Figure 3.8 (right), a crystallization process was observed ($T_c = 9.9$ °C).

Conversely, [Lid][OPr] and [Lid][OHex], which only exhibited T_g , are considered amorphous API-ILs.

3.2.5. Viscosity measurements

Viscosity is an important property for the dissolution studies as it plays a major role in stirring and mixing. The viscosity of a fluid is a measure of its resistance to deformation. If the viscosity is independent of the shear rate and stress, the fluid is classified as Newtonian fluid, once it obeys Newton's law of viscosity,

$$\tau = \dot{\gamma} \eta, \quad \text{Equation 3.1.}$$

where, τ is shear stress (Pa), $\dot{\gamma}$ is shear rate (s⁻¹) and η is viscosity (Pa·s).

To elucidate if the prepared API-ILs showed a Newtonian behavior, they have been submitted to a shear rate sweep at different temperatures, from 20 °C to 100 °C, with a 10 °C interval. From this tests, shear stress was plotted as a function of shear rate and a linear regression was used to assess the viscosity values given as the slope of the linear fitting (Figure 3.9). Shear rate sweep plots at 20 °C are shown in Appendix III.

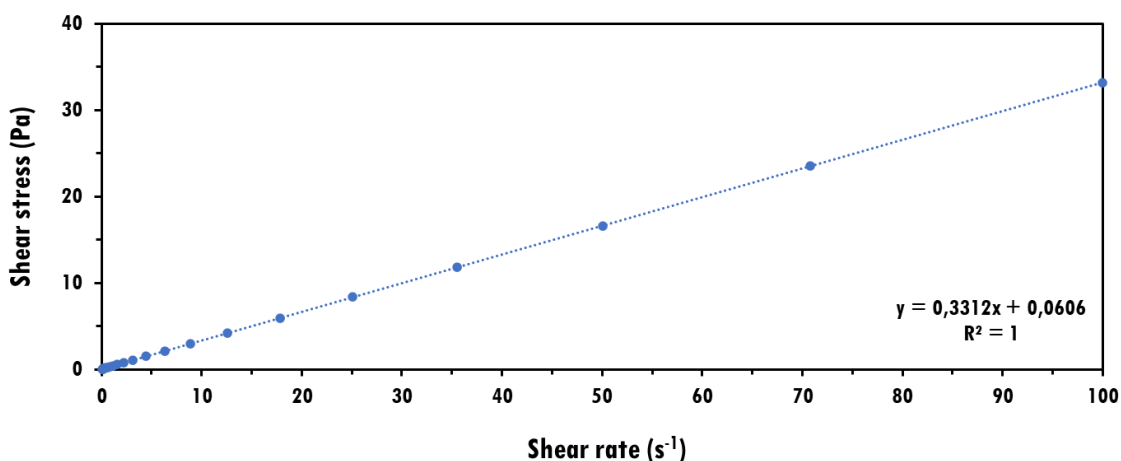


Figure 3.9 Shear stress as a function of shear rate for [Lid][OPr] at 20 °C.

At 20 °C, all ILs exhibited a Newtonian fluid behavior and the respective viscosity values are shown in Table 3.6. To elucidate the effect of the temperature on the viscosity, an additional experiment has been performed, at fixed shear stress (20 Pa). As expected, the viscosity decreased

as the temperature increased (Figure 3.10).

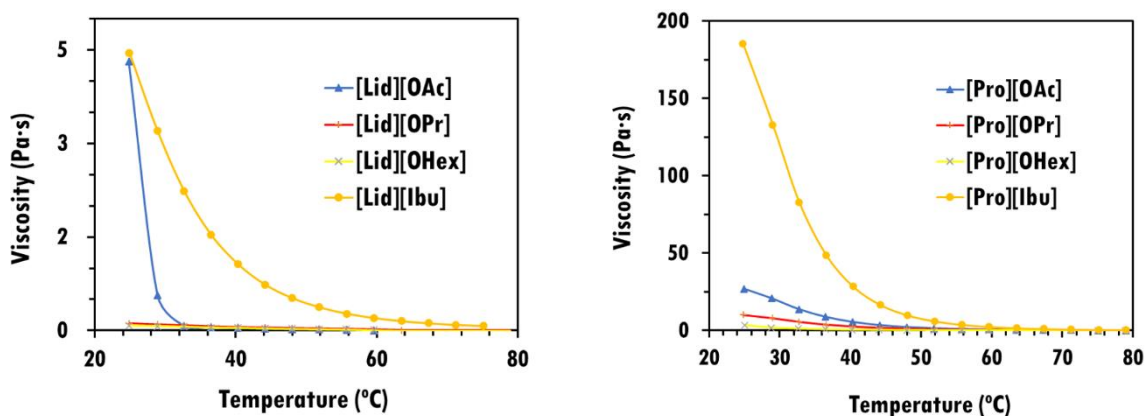


Figure 3.10 Profile of the dependence of viscosity with temperature for lidocaine based-ILs (left) and procaine based-ILs (right) at a heating rate of 5 °C/min.

From the plots showed in Figure 3.10, we can conclude that the synthesized ibuprofen based ILs were far more viscous than the others, as expected. However, all API-ILs show very similar viscosity values above 60 °C, except for [Lid][Ibu].

An Arrhenius-like law was used to describe the temperature dependence of the measured viscosities⁵⁶. Taking the natural logarithm of the Arrhenius equation, yields

$$\ln \eta = \ln A - \frac{E_a}{R} \left(\frac{1}{T} \right), \quad \text{Equation 3.2.}$$

where, η is the viscosity in Pa·s, A is a constant of proportionality, E_a is the activation energy (J mol⁻¹), R is the universal gas constant (J mol⁻¹·K⁻¹) and T is the temperature in K.

The measured viscosities were plotted as an Arrhenius plot which displays the natural logarithm of the measured viscosities plotted against reciprocal of the temperature. Arrhenius plots are shown in Appendix IV.

Using a linear regression, the slope of the line will be equal to E_a/R . Therefore, the activation energies of the synthesized API-ILs are shown in Table 3.6. The value for the coefficient of determination, denoted R^2 , suggested a good fit for the Arrhenius model ($R^2 > 0.98$).

Table 3.6 Viscosities and activation energies of the synthesized API-ILs.

| API-ILs | Viscosity at 20 °C ^a [Pa·s] | Activation energy ^b [kJ/mol] |
|-------------|--|---|
| [Lid][OAc] | 0.74 | 72.89 |
| [Lid][OPr] | 0.33 | 47.23 |
| [Lid][OHex] | 0.27 | 39.68 |
| [Lid][Ibu] | 11.11 | 73.37 |
| [Pro][OAc] | 28.11 | 90.60 |
| [Pro][OPr] | 27.88 | 79.96 |
| [Pro][OHex] | 3.32 | 83.75 |
| [Pro][Ibu] | 522.52 | 104.06 |

^a Viscosity values were determined as the slope of the linear fitting from the shear rate sweep plots. ^b Activation energy values were determined from the slope of the linear fitting multiplied by the gas constant (8.31446 J mol⁻¹·K⁻¹).

The use of equation 3.2 to describe the temperature behavior of viscosity allows the discussion of the energy barrier of a fluid to shear stress, where a higher activation energy means the ions will tend to move past each other at a slow rate⁵⁶. In general, the obtained activation energies were similar to the ones reported by Marrucho *et al.*⁵⁶ for cholinium-based ILs also containing propionate and hexanoate anions.

3.3. Characterization of biopolymers

3.3.1. Fourier-transform infrared spectroscopy

FTIR spectroscopy was used to elucidate the functional groups of the studied biopolymers by analysis of the infrared stretching vibrations. All biopolymers showed a broad band from around 3600 to 3000 cm^{-1} associated with the O–H stretch of the hydroxyl group, present in all polysaccharides. This band overlaps with the symmetric and asymmetric N–H stretches¹⁴.

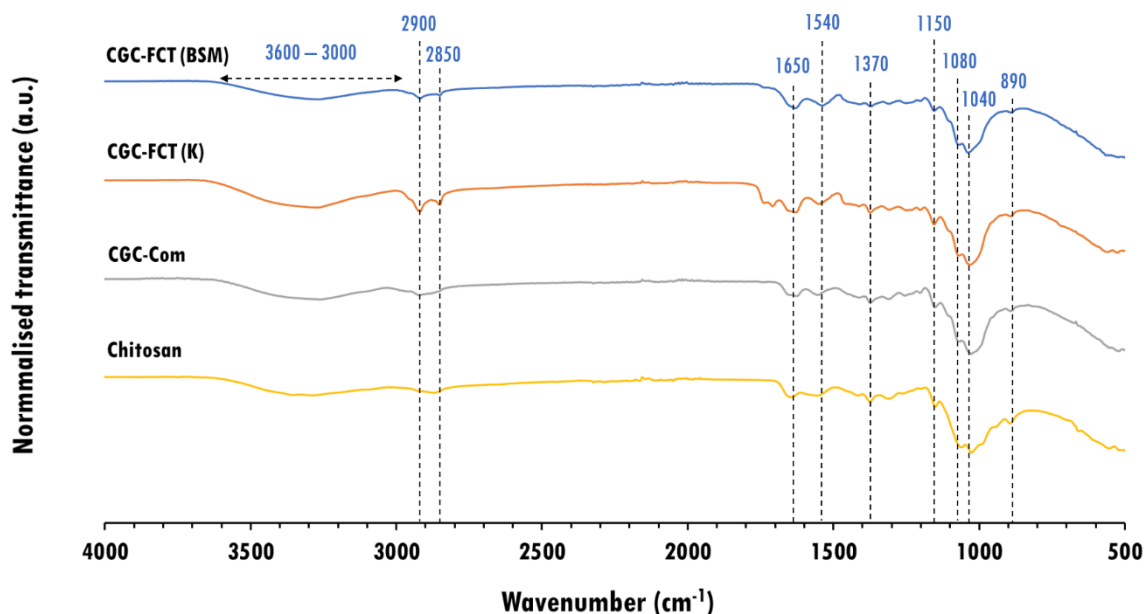


Figure 3.11 FTIR-ATR spectra of the studied biopolymers. Critical wavenumbers in CGC-FCT (medium BSM) are depicted with corresponding colors.

The bands at *ca.* 2900 cm^{-1} assigned to the symmetric CH_2 stretch^{14,57-59} and at *ca.* 2850 cm^{-1} assigned to the asymmetric CH_3 stretch^{14,57,59} only appeared in CGC-FCT (BSM) and CGC-FCT (K) spectra despite their different intensities. The spectrum of CGC-FCT (BSM) showed several bands which were present in the spectra of the other studied biopolymers, including chitosan. These bands are positioned at *ca.* 1650 cm^{-1} (amide I band^{14,57-59}), at *ca.* 1370 cm^{-1} (C–H bending and symmetric CH_3 deformation^{14,57-59}), at *ca.* 1150 cm^{-1} (asymmetric C–O–C stretch^{14,57,59}), at *ca.* 1080 cm^{-1} and at *ca.* 1040 cm^{-1} (C–OH stretch^{14,57,59}) and at *ca.* 890 cm^{-1} (C–H deformation^{14,57,59}).

3.3.2. Thermogravimetric analysis

The thermal stability of the biopolymers was assessed *via* TGA. The values used to indicate the thermal stability were the thermal decomposition values (T_{dec}), which were taken as the minimum of the derivative of thermogravimetric curves. These temperatures are reported in Table 3.7.

Table 3.7 Decomposition temperatures associated with mass loss of the studied biopolymers.

| Biopolymers | T_{dec}^a [°C] |
|---------------|------------------|
| CGC-FCT (BSM) | 329.0 |
| CGC-FCT (K) | 323.4 |
| CGC-Com | 298.4 |
| Chitosan | 296.0 |

^a Decomposition temperatures associated with mass loss (T_{dec} , minimum of the peak of the mass loss derivative) were acquired at a heating rate of 10 °C/min from 25 °C to 600 °C, under continuous argon flow.

The values obtained for thermal decomposition were in the range from 296 to 329 °C, with CGC-FCT (BSM) showing the highest value, hence it exhibits higher thermal stability. Thermogravimetric curves and derivative curves associated with mass loss of the studied biopolymers are shown in Appendix V.

3.4. Dissolution studies

During dissolution studies, biopolymer concentration, stirring rate, oil-bath temperature and operation time were optimized. Oil-bath temperature and operation time were adjusted simultaneously because an increase in temperature generally favors the biopolymers solubility. For this reason, oil-bath temperatures of 100 °C and 70 °C were employed for 1 and 3 days, respectively. The stirring rate was kept constant at 1000 rpm as this frequency of rotation allowed for efficient biopolymer powder interaction with the IL.

Table 3.8 Dissolution results obtained at 70 °C (3-day oil bath) and at 100 °C (1-day oil bath).

| API-ILs | Biopolymers Temperature | CGC _{Com} ^a | | CGC _{BSM} ^b | | CGC _K ^c | | Chitosan ^d | |
|-------------|----------------------------|---------------------------------|--------|---------------------------------|--------|-------------------------------|--------|-----------------------|--------|
| | | 70 °C | 100 °C | 70 °C | 100 °C | 70 °C | 100 °C | 70 °C | 100 °C |
| [Lid][OAc] | | I | I | Sol. | Sol. | I | I | I | I |
| [Lid][OPr] | | I | I | Sol. | Sol. | I | I | I | I |
| [Lid][OHex] | | I | I | I | I | I | I | I | I |
| [Lid][Ibu] | | I | I | I | I | I | I | I | I |
| [Pro][OAc] | | I | I | I | Sol. | I | I | I | I |
| [Pro][OPr] | | I | I | I | Sol. | I | I | I | I |
| [Pro][OHex] | | I | I | I | I | I | I | I | I |
| [Pro][Ibu] | | I | I | I | I | I | I | I | I |

Sol. – Soluble at 1 wt.%. I – Insoluble at 1 wt.%. ^a Commercial (KitoZyme). ^b FCT (medium BSM). ^c FCT (medium K). ^d Practical grade, from shrimp shells.

The obtained dissolution results can be seen in Table 3.8. A solubility of 1 wt% was attained for CGC_{BSM} with ILs containing acetate and propionate anions. These results were expected due to these anions ability to disrupt the H-bonding network⁶⁰ and the previously

mentioned literature reports for acetate based-ILs in chitin dissolution²⁸⁻³⁴ and carboxylate-based ILs in CGC³⁵⁻³⁷ dissolution. In this work, hexanoate based-ILs were not able to dissolve any biopolymer, which can be possibly explained by their higher steric hindrance given by the longer length of the hexanoate alkyl chain.

While chitin content and degree of acetylation (DA) are amongst the most critical factors affecting the dissolution of chitin and chitosan, the β -glucan:chitin molar ratios of the three CGCs studied here were estimated in previous works^{35,36} from elemental analysis (Table 3.9).

Table 3.9 CGCs β -glucan:chitin molar ratio^{38,39}.

| CGCs | β -glucan:chitin molar ratio (mol%) |
|------------------|---|
| Commercial | 50:50 |
| FCT (medium BSM) | 75:25 |
| FCT (medium K) | 63:37 |

As CGC_{BSM} has the lowest chitin content of the studied CGCs, it was expected to be easier to dissolve. In fact, CGC_{BSM} was soluble in the API-ILs ILs containing acetate and propionate anions. However, the mixtures became saturated at 1 wt.%, judged by the fact that the biopolymer particles could not be dissolved further, since they were clearly observed in suspension and/or at the vial bottom.

Ferreira *et al.*³⁷ reported CGC dissolution values above 5 wt.% using choline based-ILs, namely, choline acetate ([Chol][OAc]), choline propionate ([Chol][OPr]) and choline hexanoate ([Chol][OHex]), which were the same carboxylate anions selected here. Even though the dissolution conditions used here were similar (*i.e.*, 24h at *ca.* 100 °C), choline based ILs were able to dissolve CGC to a greater extent since they may perform a better interaction with the polar domains of chitin in CGC because they consist of fully ionized IL (aprotic ILs). In the protic API-ILs studied here, FTIR analysis suggested the acid was partially ionized, resulting in the neutral acid and base species being present, and thus possibly disabling bridging between anions (*e.g.*, AcO⁻) and chitin chains (NH \cdots AcO \cdots HO)³². Besides, recent literature reports also indicate that H-bonding already exists between the carboxyl group of the acid and the base in these ILs.

In the studied procaine based-ILs, dissolution occurred only at 100 °C, while in lidocaine based-ILs dissolution occurred regardless of the operation time and temperature increase from 70 °C to 100 °C. This temperature increase produced a dark brown mixture in all the studied CGCs which suggest that a possible deacetylation reaction has occurred since the shift from light to dark brown is typical in these reactions and the studied API-ILs showed thermal stability at 100 °C in TGA experiments. However, it is recommendable to study the long-term thermal stability of ILs at 100 °C by performing isothermal TGA measurements for 24h (dissolution operation time).

Chitosan was insoluble at 1 wt.% in the studied API-ILs despite having a reported solubility of 10 mg mL⁻¹ in 1.0 M acetic acid and a DA of 6% according to Sigma-Aldrich certificate of

analysis. Although it was expected to be easier to dissolve in acetate based ILs, its dissolution mechanism is thought to be dependent mainly on the acidity of the medium, where chitosan molecules are more or less ionized up to pH 6.0 and the ionization increases as the pH moves to low values^{10,61}. In this way, the synthesized API-ILs are thought to have a basic character making it impossible to dissolve chitosan.

3.5. Development of biopolymeric structures

For the ILs where a successful dissolution of 1 wt.% CGC-FCT (BSM) was visually observed, a biopolymeric structure was developed. After casting the obtained mixture into a metal disk, a phase inversion process in distilled water or water containing 10 % (v/v) of glycerol was performed for 24 h at room temperature. The non-solvent used in the coagulation bath was distilled water because the biopolymer is insoluble, the APIs lidocaine and procaine are slightly water-soluble^{74,75} and, acetic and propionic acids are very water-soluble. After drying at room temperature, the biopolymeric structures were obtained as solids (Figure 3.12 (a) and 3.12 (c)) and liquid (Figure 3.12 (b)).

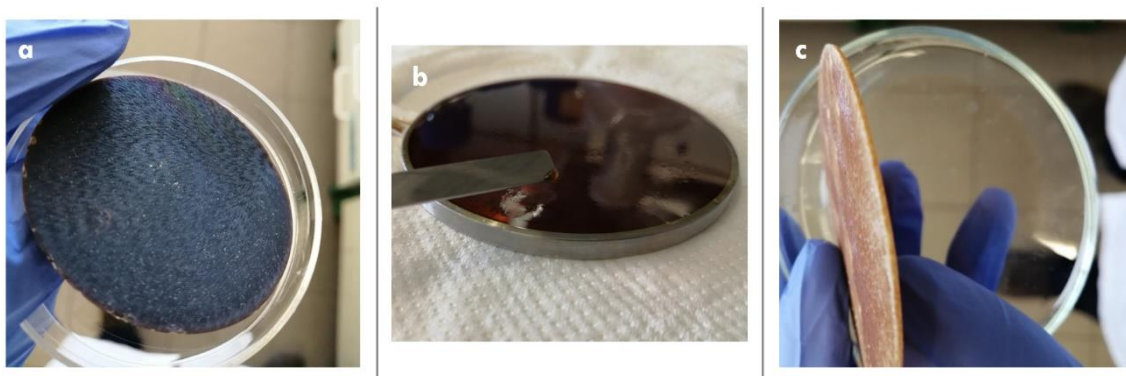


Figure 3.12 Biopolymeric structures based on CGC-FCT (medium BSM). **(a)** [Lid][OPr] based CGC structure obtained from a 1-day oil bath dissolution at 100 °C and prepared using water containing 10% (v/v) of glycerol. **(b)** [Pro][OPr] based CGC structure obtained from a 1-day oil bath dissolution at 100 °C and prepared using water as nonsolvent. **(c)** [Lid][OAc] based CGC structure obtained from a 3-day oil bath dissolution at 70 °C and prepared using water as nonsolvent.

Glycerol is a very hygroscopic molecule commonly added to film-forming solutions to act as plasticizer and avoid film brittleness. The aim of using water containing 10% (v/v) of glycerol as plasticizer in phase inversion was to overcome the fragility and brittleness exhibited by the CGC solid structures obtained using only water.

A total of 8 solid CGC structures (here designed as films) were obtained from lidocaine based ILs ([Lid][OAc] and [Lid][OPr]) using different dissolution conditions, whereas only one liquid (here designed as hydrogel) CGC structure was obtained from procaine based ILs ([Pro][OPr]).

3.6. Characterization of films

3.6.1. Scanning electron microscopy

The cross section and surface morphology of the films was assessed by scanning electron microscopy (SEM) to better understand their morphology. The surface images of [Lid][OAc] based CGC films showed a dense and heterogeneous surface with aggregate formation regardless of the temperature increase from 70 °C to 100 °C (Figure 3.13), which indicate that precipitation of lidocaine possibly occurred during phase inversion since lidocaine is slightly water-soluble⁷⁴. SEM micrographs of the cross section and surface for [Lid][OAc] and [Lid][OPr] based CGC films are shown in Appendix VI.

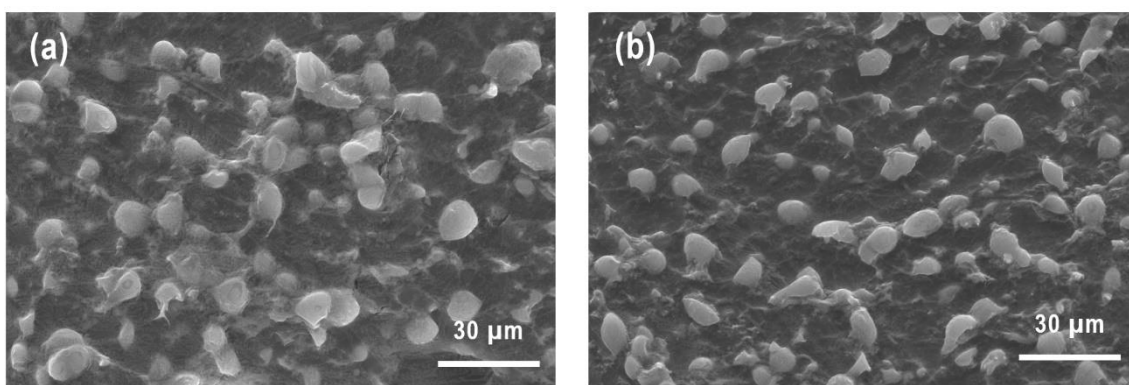


Figure 3.13 Surface images of [Lid][OAc] based CGC films obtained from (a) a 1-day oil bath dissolution at 100 °C and prepared using water as nonsolvent, and (b) a 3-day oil bath dissolution at 70 °C and prepared using water as nonsolvent. Micrographs were obtained at 1000× magnification and acquired using Esprit 1.9 software.

3.6.2. Fourier-transform infrared spectroscopy

FTIR spectroscopy was used to elucidate the functional groups of the obtained films by analysis of the peaks related with the infrared stretching vibrations. Lidocaine free base was used in the synthesis of API-ILs, which were employed as solvents in CGC dissolution for the preparation of the obtained films mentioned in Figure 3.14.

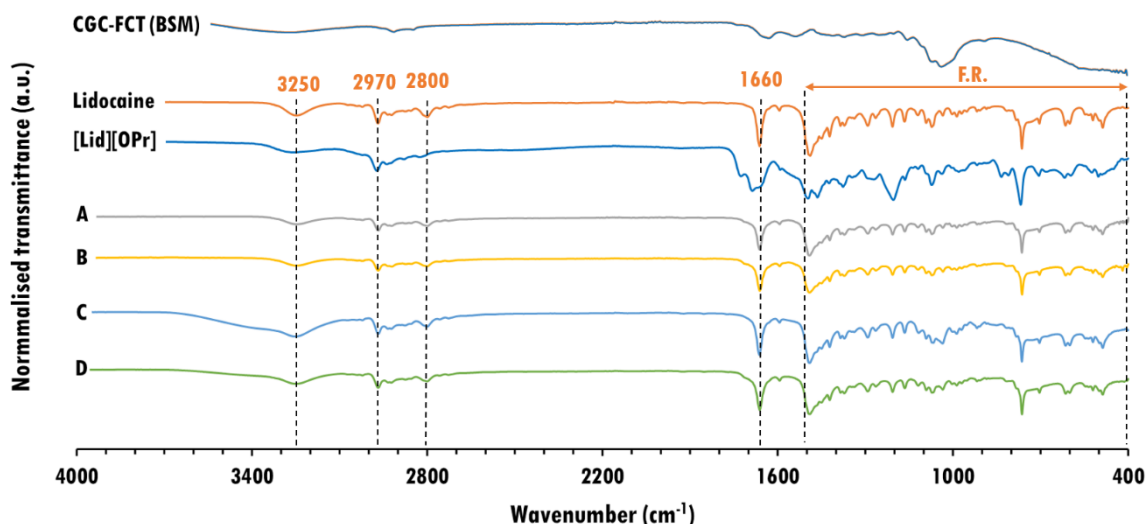


Figure 3.14 FTIR-ATR spectra of CGC-FCT (medium BSM), lidocaine free base, lidocainium propionate ([Lid][OPr]) and respective films (A-D). Critical wavenumbers and fingerprint region (F.R.) in free lidocaine spectrum are depicted with corresponding color. A – 3-day oil bath dissolution at 70 °C and prepared using water as nonsolvent; B – 3-day oil bath dissolution at 70 °C and prepared using water containing 10% (v/v) of glycerol; C – 1-day oil bath dissolution at 100 °C and prepared using water as nonsolvent; D – 1-day oil bath dissolution at 100 °C and prepared using water containing 10% (v/v) of glycerol.

The most critical bands assigned to lidocaine free base showed similar wavenumber values in the spectra of the obtained films (A-D), which indicates the presence of lidocaine upon phase inversion, regardless of the used dissolution conditions. Besides, the fingerprint region of lidocaine free base (between 1500 and 400 cm^{-1}) is very similar to the fingerprint region of all the obtained films which implies they are composed of lidocaine mostly (FTIR-ATR spectra for [Lid][OAc] based CGC films are shown in Appendix VII).

The carbonyl stretch (C=O) is one of the most useful absorptions because its located outside the fingerprint region, found in the range 1750 – 1680 cm^{-1} (see Figure 3.15). Its position varies slightly depending on what sort of functional group it is in (*e.g.*, amide group of lidocaine or carboxyl group of propionic acid).

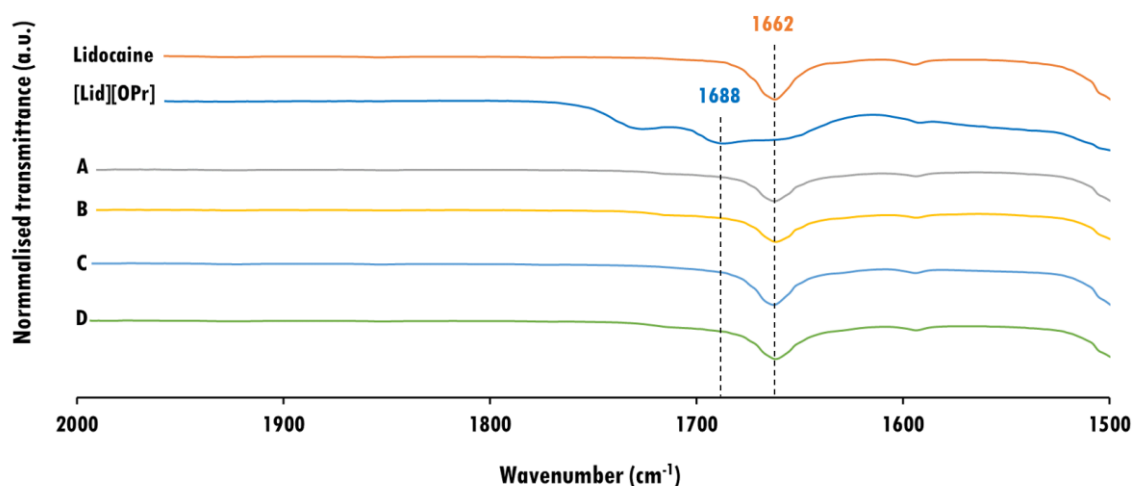


Figure 3.15 Expanded 2000 – 1500 cm^{-1} region of the FTIR-ATR spectra of lidocaine free base, lidocainium propionate ([Lid][OPr]) and respective films (A-D). Critical wavenumbers in lidocaine free base and [Lid][OPr] spectra are depicted with matching colors. A – 3-day oil bath dissolution at 70 °C and prepared using water as nonsolvent; B – 3-day oil bath dissolution at 70 °C and prepared using water containing 10% (v/v) of glycerol; C – 1-day oil bath dissolution at 100 °C and prepared using water as nonsolvent; D – 1-day oil bath dissolution at 100 °C and prepared using water containing 10% (v/v) of glycerol.

The band assigned to the C=O stretch of propionic acid carboxyl group in [Lid][OPr] spectrum at 1688 cm^{-1} is slightly shifted to a higher frequency than in the films and in free lidocaine spectra at 1662 cm^{-1} , suggesting the acid was partially or totally removed upon phase inversion. The rationale behind the acid removal upon phase inversion and not lidocaine free base can be explained by two synergic reasons: (1) as explained in section 3.2.2, the carboxylic acid moiety is thought to be partially ionized, resulting in the neutral acid and base species being present, and (2) free lidocaine is slightly water-soluble⁶³, whereas propionic and acetic acids are very water-soluble^{66,67}.

The most intense and characteristic bands present in CGC-FCT (BSM) spectrum discussed in section 3.3.1 did not appear in the films' spectra (A-D) because the films' FTIR analysis infers that they are composed mainly of lidocaine free base as explained above. This result was expected given that the biopolymer concentration used in dissolution studies was 1 wt%, which translates in 0.01 g of biopolymer per 10 g of API-IL, for example.

3.6.3. Differential scanning calorimetry

DSC was used to determine the thermal transitions of the obtained films. As mentioned earlier, lidocaine free base was used in the synthesis of API-ILs, which were employed as solvents in CGC dissolution for the preparation of the 8 obtained films mentioned in Figure 3.16 from A1 to D1, where 1 stands for [Lid][OAc] based CGC films, and from A2 to D2 where 2 stands for [Lid][OPr] based CGC films.

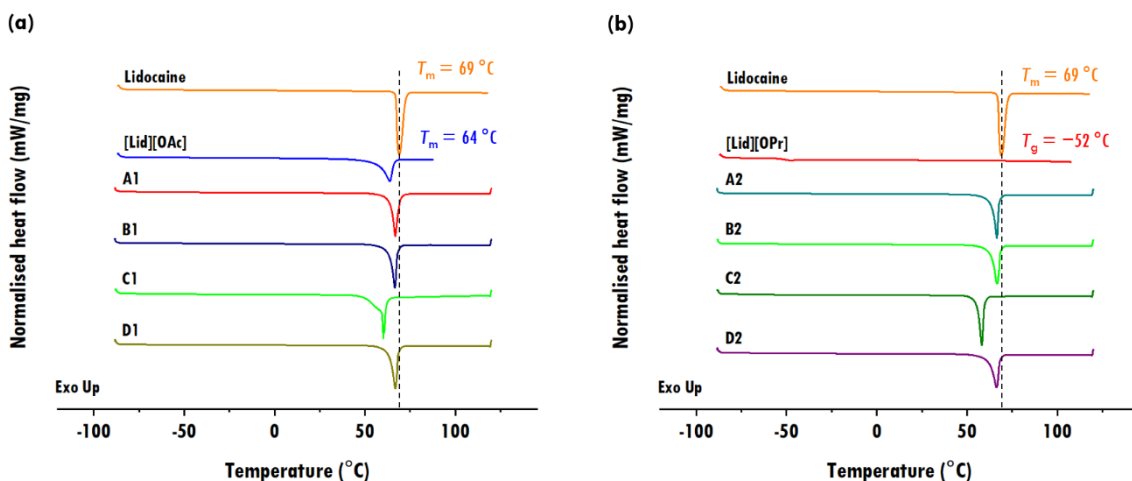


Figure 3.16 (a) Heat flow thermograms for lidocaine free base (Lidocaine, $T_m = 69\text{ }^\circ\text{C}$), lidocainium acetate ([Lid][OAc], $T_m = 64\text{ }^\circ\text{C}$), and respective films (A1-D1). (b) Heat flow thermograms for free lidocaine (Lidocaine, $T_m = 69\text{ }^\circ\text{C}$), lidocainium propionate ([Lid][OPr], $T_g = -52\text{ }^\circ\text{C}$), and respective films (A2-D2). Thermal transitions in free lidocaine and API-ILs thermograms are depicted with matching colors. A – 3-day oil bath dissolution at $70\text{ }^\circ\text{C}$ and prepared using water as nonsolvent; B – 3-day oil bath dissolution at $70\text{ }^\circ\text{C}$ and prepared using water containing 10% (v/v) of glycerol as nonsolvent; C – 1-day oil bath dissolution at $100\text{ }^\circ\text{C}$ and prepared using water as nonsolvent; D – 1-day oil bath dissolution at $100\text{ }^\circ\text{C}$ and prepared using water containing 10% (v/v) of glycerol. Melting temperatures (T_m , peak minimum) and glass transition (T_g , midpoint-inflection) were acquired at a heating rate of $10\text{ }^\circ\text{C}/\text{min}$, after cooling to $-90\text{ }^\circ\text{C}$, under nitrogen.

Lidocaine free base melted within the range reported in the literature ($68\text{--}69\text{ }^\circ\text{C}$ ^{52,53}). As it can be seen in Figure 3.16, the obtained films showed melting points at *ca.* $69\text{ }^\circ\text{C}$, similar to lidocaine free base. Besides, the endothermic peaks exhibited by the films were sharp as in lidocaine free base heat flow thermogram. These results are in line and support the conclusions from the previously discussed FTIR studies, which implied the films were composed of lidocaine mostly.

According to the literature, the melting point of APIs can be significantly lowered through H-bonding between only partially ionized mixtures of acids and bases^{26,49}. In general, the films showed lower melting temperatures than lidocaine free base, which can be explained by the presence of residual amounts of acetic or propionic acids. According to the previously discussed FTIR studies, these components are present in lower amounts when compared to lidocaine free base, however they may cause defects in the crystalline lattice of lidocaine free base, making it easier to overcome the intermolecular forces and consequently, lowering the melting temperature.

3.6.4. Thermogravimetric analysis

The thermal stability of the obtained films was assessed *via* TGA. The values used to indicate the thermal stability were the thermal decomposition values in terms of the onset temperature to 5% mass loss ($T_{5\%}$). These temperatures are reported in Table 3.10.

Table 3.10 Decomposition temperatures associated with mass loss of the obtained films.

| Films | Temperature | Coagulation medium | Abbreviation | $T_{5\%}^a$ [°C] |
|----------------|-------------|--------------------|--------------|------------------|
| [Lid][OAc]-CGC | 70 °C | Water | A1 | 201.1 |
| | | Glycerol 10% (v/v) | B1 | 177.5 |
| | 100 °C | Water | C1 | 195.5 |
| | | Glycerol 10% (v/v) | D1 | 194.1 |
| [Lid][OPr]-CGC | 70 °C | Water | A2 | 202.7 |
| | | Glycerol 10% (v/v) | B2 | 177.2 |
| | 100 °C | Water | C2 | 187.6 |
| | | Glycerol 10% (v/v) | D2 | 204.8 |

^a Onset temperatures where occurs loss of 5% of its initial mass ($T_{5\%, \text{onset}}$) of the obtained films were acquired at a heating rate of 10 °C min⁻¹ from 25 °C to 500 °C, under continuous argon flow.

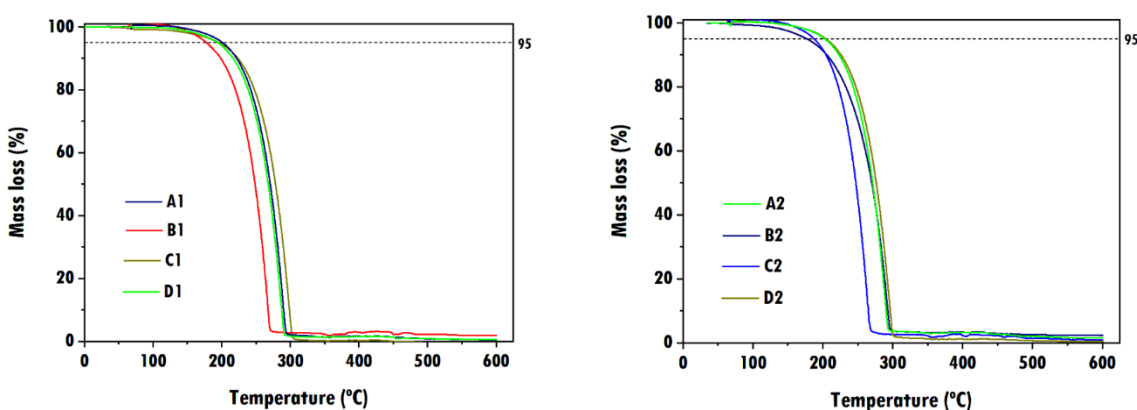


Figure 3.17 Thermogravimetric curves for [Lid][OAc] based CGC films (left) and for [Lid][OPr] based CGC films (right) at 10 °C/min. The onset temperatures, where occurs loss of 5 % of its initial mass, were taken as the value corresponding to 95% mass loss represented by horizontal dashed lines.

TGA traces of both [Lid][OAc] and [Lid][OPr] based CGC films were similar and showed signs of decomposition at only slightly elevated temperatures. Films A1, A2 and D2 revealed a less steep mass loss, having lost 5% of its mass at *ca.* 200 °C. On the other hand, films B1 and C2 exhibited a steeper mass loss above the onset temperature to 5% mass loss, having lost around 95% of their mass slightly above *ca.* 250 °C, whereas the other films showed around 95% mass loss at *ca.* 300 °C. As mentioned in section 3.2.2, CGC-FCT (BSM) showed thermal decomposition at 329.0 °C, hence by the time the films have lost almost all their mass, the CGC will still be present.

3.6.5. Contact angle analysis

Contact angle measurements were performed to evaluate the hydrophilicity of the obtained films. In other words, a drop of distilled water was placed at the film surface to measure its wettability. Wettability refers to how a liquid deposited on a solid (film) substrate spreads out or the ability of liquids to form limit surfaces with solid states⁶⁸. When a film forms a contact angle with the water droplet smaller than 90°, it can be considered as a hydrophilic film. Higher hydrophilicity enables the film to have better cell attachment and enhanced biological behavior, in the case of a potential dermal application⁶⁹.

Table 3.11 Contact angles of the obtained films.

| Films | Temperature | Coagulation medium | Contact angle ^a (°) |
|-----------------|-------------|--------------------|--------------------------------|
| [Lid][OAc]-CGC | 70 °C | Water | 36.23 ± 3.03 |
| | | Glycerol 10% (v/v) | 41.87 ± 3.93 |
| | 100 °C | Water | 63.07 ± 7.35 |
| | | Glycerol 10% (v/v) | 75.55 ± 4.06 |
| [Lid][OPr]- CGC | 70 °C | Water | 35.05 ± 6.74 |
| | | Glycerol 10% (v/v) | 60.90 ± 8.12 |
| | 100 °C | Water | 48.99 ± 3.26 |
| | | Glycerol 10% (v/v) | 90.76 ± 2.77 |

^a Determined by placing a drop of distilled water at the film sample surface using a syringe (sessile drop method).

In general, all films showed contact angles lower than 90° exhibiting a hydrophilic behavior, where the water has spread over a large area at the surface of the film. The films obtained using water containing 10% (v/v) of glycerol as plasticizer showed to be significantly less hydrophilic than without any plasticizer, which can be possibly explained by the presence of glycerol molecules at the film surface which is less polar than water.

Ferreira *et al.*³⁷ also obtained hydrophilic CGC films using choline based-ILs composed by the same anions studied here. The reported contact angles were similar to the higher ones obtained here, namely 70.0 ± 3.4° using [Chol][OAc] and 79.2 ± 6.2° using [Chol][OPr].

3.6.6. Mechanical properties

Puncture tests were performed to assess the mechanical properties of the films. The maximum force at break was estimated from these tests as the force needed to break the film using a needle probe. From the obtained forces and knowing the diameter of the needle probe, the tensile strength of the films was determined as the ratio between the maximum force at break and the needle probe cross-sectional area, using Equation 3.3.

$$\sigma = \frac{F}{\pi R^2}, \quad \text{Equation 3.3.}$$

where, σ is tensile strength (Pa), F is the maximum force at break (N) and R is the needle probe radius (m).

Since the obtained films had different thicknesses, a normalised tensile strength was determined as the ratio between the tensile strength and the respective film mean thickness to enable a viable comparison between the films' tensile strength. Herein, the tensile strength was assessed as the maximum load that the film can hold until rupture. A higher tensile strength enables the film to resist external stress, maintain its integrity and act as a barrier³⁶.

Table 3.12 Mechanical properties of the obtained films.

| Films | Temperature | Coagulation medium | Thickness ^a (mm) | Tensile strength (MPa) | Normalised tensile strength (MPa/mm) |
|--------------------------|-------------|--------------------|-----------------------------|------------------------|--------------------------------------|
| [Lid][OAc]-CGC-FCT (BSM) | 70 °C | Water | 1.88 ± 0.02 | 0.74 ± 0.20 | 0.39 ± 0.11 |
| | | Glycerol 10% (v/v) | 2.10 ± 0.19 | 1.02 ± 0.56 | 0.48 ± 0.26 |
| | 100 °C | Water | 2.04 ± 0.03 | 1.66 ± 0.52 | 0.81 ± 0.25 |
| | | Glycerol 10% (v/v) | 2.05 ± 0.02 | 1.14 ± 0.24 | 0.56 ± 0.12 |
| [Lid][OPr]-CGC-FCT (BSM) | 70 °C | Water | 1.95 ± 0.13 | 0.96 ± 0.35 | 0.49 ± 0.18 |
| | | Glycerol 10% (v/v) | 2.85 ± 0.05 | 1.52 ± 0.07 | 0.53 ± 0.03 |
| | 100 °C | Water | 1.68 ± 0.12 | 1.36 ± 0.46 | 0.81 ± 0.28 |
| | | Glycerol 10% (v/v) | 1.95 ± 0.10 | 0.87 ± 0.32 | 0.45 ± 0.16 |

^a Thickness measurements were performed at three random positions avoiding the edges of the film to calculate the mean thickness.

The highest value of tensile strength was achieved for the films obtained at 100 °C using water as nonsolvent. The effect of the anion in the IL ([OAc] or [OPr]) did not seem to be significant, which can be explained by the fact that the acid has been partially removed as indicated by FTIR studies. Also, the increase of dissolution temperature from 70 °C to 100 °C led to higher tensile strength values using the IL [Lid][OAc], suggesting that the mechanical properties of the prepared films were better.

The aim of using water containing 10% (v/v) of glycerol as plasticizer in phase inversion was to overcome the fragility and brittleness exhibited by the films obtained using only water. On the one hand, the use of the plasticizer increased the tensile strength of the films obtained at 70 °C. On the other hand, the use of water as nonsolvent produced films considerably more resistant, invalidating the use of glycerol 10% (v/v) to overcome the brittleness in the obtained films.

Many studies have evaluated chitin films for having high strength, flexibility, and conformability in the dry state without the aid of chemical modifications or plasticizers⁷⁰. Ferreira *et al.*³⁷ obtained flexible CGC films with good mechanical properties using choline based-ILs composed by the same anions studied here. The reported tensile strengths were far higher than the ones obtained here, namely 3.39 ± 0.53 MPa/mm using [Chol][OAc] and 1.91 ± 0.26 MPa/mm using [Chol][OPr].

In general, the obtained CGC films were brittle and fragile which limits their potential for application. The brittleness exhibited by the films could be attributed to free lidocaine that tends to crystallize once the acid has been removed upon phase inversion.

3.7. Characterization of hydrogel

3.7.1. Fourier-transform infrared spectroscopy

FTIR spectroscopy was used to elucidate the functional groups of the obtained hydrogel by analysis of the peaks related with the infrared stretching vibrations. Procaine free base was used in the synthesis of API-ILs, which were employed as solvents in CGC dissolution for the preparation of the obtained hydrogel.

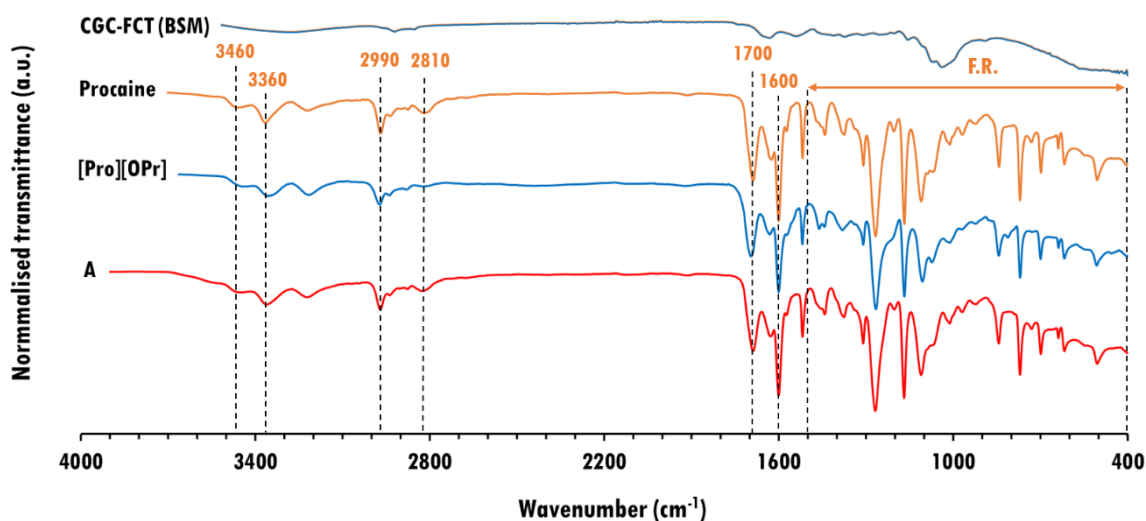


Figure 3.18 FTIR-ATR spectra of CGC-FCT (medium BSM), procaine free base, procainium propionate ([Pro][OPr]), and respective hydrogel (A) obtained from a 1-day oil bath dissolution at 100 °C and prepared using water as nonsolvent. Critical wavenumbers and fingerprint region (F.R.) in free procaine spectrum are depicted with corresponding color.

In Figure 3.18, the most critical bands assigned to procaine free base showed similar wavenumber values in the hydrogel spectrum (A), which indicates the presence of procaine upon phase inversion. Besides, the fingerprint region of procaine free base is very similar to the fingerprint region of the obtained hydrogel which implies it is composed of procaine mostly since each compound produces its unique pattern of peaks in this region.

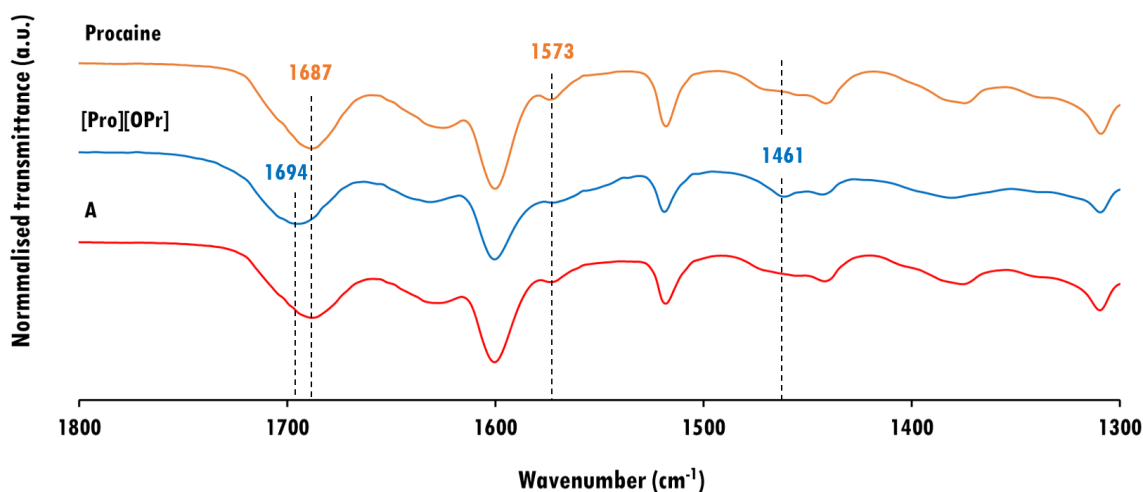


Figure 3.19 Expanded 1800 – 1300 cm^{-1} region of the FTIR-ATR spectra of procaine free base, procainium propionate ([Pro][OPr]), and respective hydrogel (A) obtained from a 1-day oil bath dissolution at 100 °C and prepared using water as nonsolvent.

In Figure 3.19, the position of the C=O stretch varies slightly depending on what sort of functional group it is in (*e.g.*, ester group of procaine or carboxyl group of propionic acid). The band assigned to the C=O stretch of propionic acid carboxyl group in [Pro][OPr] spectrum at 1694 cm^{-1} is slightly shifted to a higher frequency than in the hydrogel and free procaine spectra at 1687 cm^{-1} , suggesting the acid was partially removed upon phase inversion. Besides, the peak located at 1573 cm^{-1} in procaine free base spectrum appears in the hydrogel spectrum, whereas the band located at 1461 cm^{-1} in [Pro][OPr] spectrum did not appear in the hydrogel and procaine free base spectra. The rationale behind the acid removal upon phase inversion and not procaine free base can be explained by two synergic reasons: (1) as explained in section 3.2.2, the carboxylic acid moiety is thought to be partially ionized, resulting in the neutral acid and base species being present, and (2) procaine is slightly water-soluble⁶⁴, whereas propionic acid is soluble in water⁶⁷.

As mentioned in the films' FTIR studies, the most intense and characteristic bands present in CGC-FCT (BSM) spectrum discussed in section 3.3.1 did not appear in the hydrogel spectrum because the hydrogel FTIR analysis implies that it is composed mainly of free procaine as explained above. This result was expected given that the biopolymer concentration used in dissolution studies was 1 wt%, which translates in 0.01 g of biopolymer per 10 g of API-IL, for example.

3.7.2. Differential scanning calorimetry

DSC was used to determine the thermal transitions of the obtained films. As mentioned earlier, procaine free base was used in the synthesis of API-ILs, which were employed as solvents in CGC dissolution for the preparation of the obtained hydrogel.

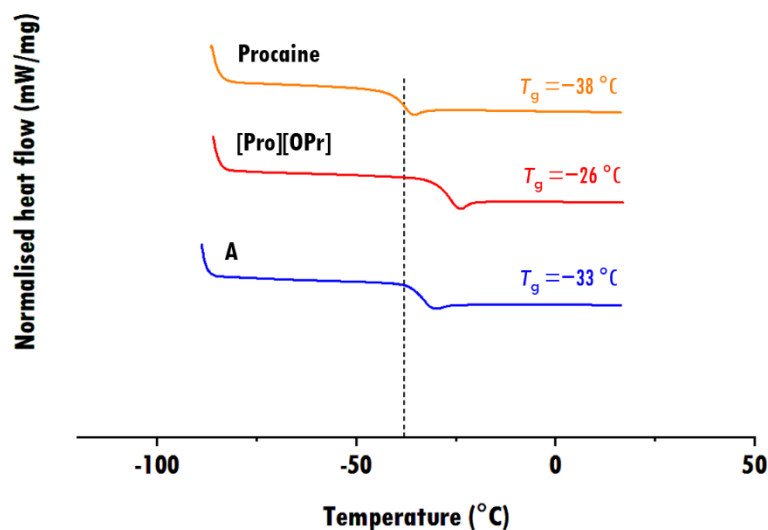


Figure 3.20 Heat flow thermograms for procaine free base (Procaine, $T_g = -38\text{ °C}$), procainium propionate ([Pro][OPr], $T_g = -26\text{ °C}$), and respective hydrogel (A, $T_g = -33\text{ °C}$) obtained from a 1-day oil bath dissolution at 100 °C and prepared using water as nonsolvent. Thermal transitions in free procaine, procainium propionate, and respective hydrogel thermograms are depicted with matching colors. Glass transitions (T_g , midpoint-inflection) were acquired at a heating rate of 10 °C min^{-1} , after cooling to -90 °C , under nitrogen. The drying procedure employed to remove any residual water from the samples consisted of the first heating scan, where the sample was heated to 120 °C followed by a 1-minute isotherm. For this reason, the thermal transitions were determined from the last heating and cooling scans.

As it can be seen in Figure 3.20, procaine free base, [Pro][OPr] and the obtained hydrogel showed similar glass transitions. However, the T_g of the hydrogel (-33 °C) was closer to the T_g of procaine (-38 °C). These results are in line and support the conclusions from the previously discussed FTIR studies, which implied the films were composed of procaine mostly and propionic acid was partially removed upon phase inversion.

3.7.3. Thermogravimetric analysis

The thermal stability of the obtained hydrogel was assessed *via* TGA. The values used to indicate the thermal stability were the onset temperatures where occurs loss of 5% of its initial mass ($T_{5\%, \text{onset}}$), and the thermal decomposition value (T_{dec}) which was taken as the minimum of the derivative of the thermogravimetric curve.

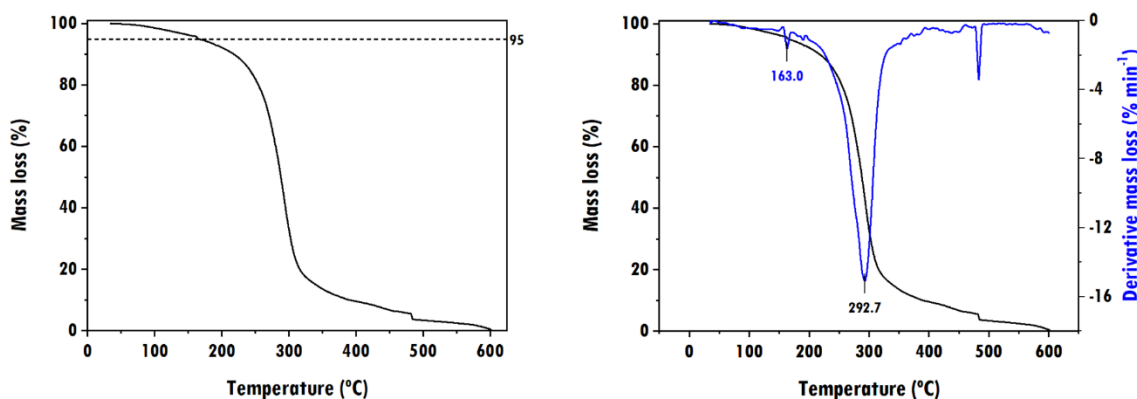


Figure 3.21 Thermogravimetric curve (left) and derivative curve (right) associated with mass loss of the obtained hydrogel. The onset temperatures where occurs loss of 5 % of its initial mass was taken as the value corresponding to 95% mass loss represented by the horizontal dashed line and was acquired at a heating rate of 10 °C/min from 25 °C to 500 °C, under continuous argon flow.

The endothermic peak observed at 163.0 °C (Figure 3.21, right) can be related to the evaporation of the solvent used in free procaine synthesis (water) since the hydrogel sample had lost 5% of its mass until 165.5 °C (Figure 3.21, left). As mentioned in section 3.2.2, CGC-FCT (BSM) showed thermal decomposition at 329.0 °C, hence by the time the hydrogel has lost *ca.* 80% of its mass, the CGC will still be present.

3.7.4. Rheological studies

Rheological studies were performed to assess the viscoelastic properties of the obtained hydrogel. A stress sweep was performed in the range of 0.1 to 1000 Pa at a constant frequency of 1 Hz. The linear viscoelastic region did not appear in the stress sweep test because this region occurred before the minimum tension value chosen in the test (0.1 Pa). However, we selected a tension of 0.5 Pa to perform the frequency sweep test because we considered it a minimum value so that enough energy was exerted on the sample and to obtain data related to the storage and loss moduli, G' and G'' , respectively. The relation between these moduli will enable to assess the viscoelastic properties of the sample, even though the mechanical spectrum obtained is indicative since a tension value outside the linear viscoelastic region was chosen to perform the frequency sweep.

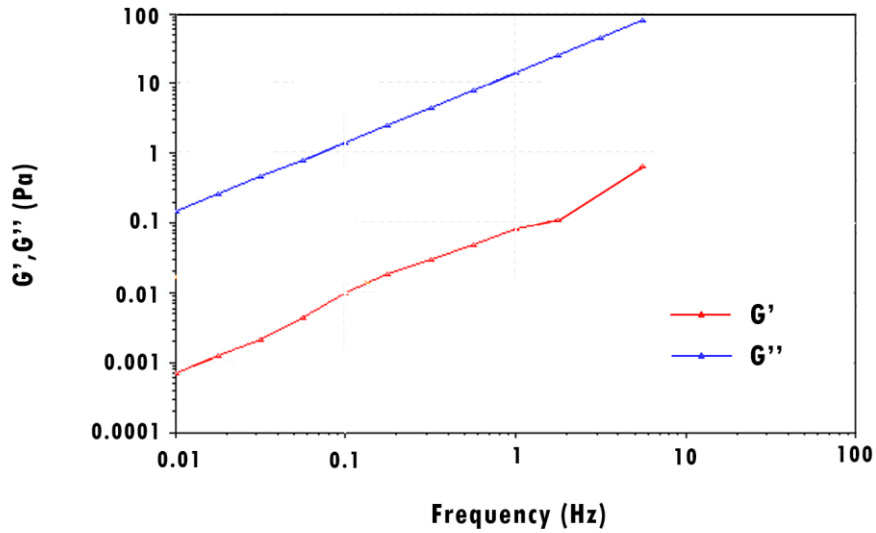


Figure 3.22 Mechanical spectrum of the hydrogel obtained from a 1-day oil bath dissolution at 100 °C and prepared using water as nonsolvent.

Since G'' is proportionally superior to G' in two orders of magnitude we can conclude that the sample has a viscous behavior and very little elastic, that is, close to the liquid as one would expect for its appearance.

4. Conclusions

The synthesized API-ILs were considered protic ILs because FTIR studies suggested the acid was partially ionized, resulting in the neutral acid and base species being present in a dynamic equilibrium with ionized species. Besides, recent literature reports on the same ILs also indicated that hydrogen-bonding occurs between the carboxyl group of the acid and the base.

After the preparation of the polymeric structures in the form of films and hydrogels, they were fully characterized using different techniques. FTIR results suggested that the films were mainly composed by lidocaine free base, and the hydrogel by procaine free base. The band assigned to the C=O stretch of propionic acid in the API-ILs spectra was slightly shifted to a higher frequency when compared to the films/hydrogel and to the lidocaine/procaine free bases spectra, suggesting that the acid was partially removed upon phase inversion. The rationale behind the acid removal upon phase inversion and not lidocaine/procaine free bases can be explained by two synergic reasons: (1) the carboxylic acid moiety is thought to be partially ionized, resulting in the neutral acid and base species being present, and (2) lidocaine and procaine free bases are slightly water-soluble, whereas propionic and acetic acids are very water-soluble.

DSC results of the polymeric structures obtained were in accordance and support the conclusions from the previously discussed FTIR studies, since the films presented melting points similar to lidocaine free base, and the hydrogel presented a glass transition similar to procaine free base.

CGC-FCT (BSM) showed thermal decomposition at 329 °C *via* TGA, hence by the time the films and hydrogel have lost a large amount of their mass, the biopolymer will still be present.

The obtained hydrogel exhibited a viscous behavior, whereas the 8 films exhibited hydrophilic surface and, poor mechanical properties which limits their potential for application.

5. Future work

The synthesized ILs were composed mostly by the base in terms of mass, which may explain the insolubility of chitosan, for example. For this reason, eutectic mixtures containing the APIs and carboxylic acids may be performed in the acid-base molar ratio of 2:1, instead of 1:1.

In order to optimize the phase inversion method and thus the development of polymeric structures, IL solubility studies with solvents of different polarity should be performed to screen a suitable non-solvent capable to remove the IL upon phase inversion method to a greater extent than performed here. During phase inversion method, the non-solvent volume, time of operation, temperature and drying conditions (environment) are parameters that should be considered.

After obtaining polymeric structures, elemental analysis for glucosamine quantification should be performed to assess the glucosamine content and degree of acetylation since the interaction with ILs under high temperatures may cause reduction of the DA and a reduction of their β -glucan moiety³⁷.

Lastly, to further evaluate the potential application of the obtained polymeric structures and API-ILs in topical drug delivery, drug release tests may be performed.

References

1. Edebali, S. *Advanced Sorption Process Applications*, IntechOpen **2019**.
2. Meyers, M.A. Biological Materials: Structure & Mechanical Properties, *Progress in Materials Science* **2008**, *53*, 1.
3. D'Ayala, G., Malinconico, M., & Laurienzo, P. Marine, Derived Polysaccharides for Biomedical Applications: Chemical Modification Approaches. *Molecules* **2008**, *13*, 2069–2106.
4. Klemm, D., Heublein, B., Fink, H., and Bohn, A. Cellulose: Fascinating Biopolymer / Sustainable Raw Material, *Angewandte Chemie* **2004**, *44*, 3358.
5. Xiong, R. Naturally-derived biopolymer nanocomposites: Interfacial design, properties and emerging applications *Materials Science and Engineering* **2018**, *125*, 1–41.
6. B. Rufato, K., P. Galdino, J., S. Ody, K., G.B. Pereira, A., Corradini, E., F. Martins, A., C. Muniz, E. Hydrogels Based on Chitosan and Chitosan Derivatives for Biomedical Applications. *Chapter 4: Hydrogels - Smart Materials for Biomedical Applications* **2019**.
7. Maghchiche Abdelhak. A Review: Application of Biopolymers in the Pharmaceutical Formulation. *Journal of Advances in Bio- Pharmaceutics and Pharmacovigilance* **2019**, *1*(1), 15–25.
8. Silva, S. S., Mano, J. F., & Reis, R. L. Ionic liquids in the processing and chemical modification of chitin and chitosan for biomedical applications. *Green Chemistry* **2017**, *19*(5), 1208–1220.
9. Rinaudo, M. Chitin and chitosan: Properties and applications. *Progress in Polymer Science* **2006**, *31*(7), 603–632.
10. Pardo-Castaño, C., & Bolaños, G. Solubility of chitosan in aqueous acetic acid and pressurized carbon dioxide-water: experimental equilibrium and solubilization kinetics. *The Journal of Supercritical Fluids* **2019**, *151*, 63–74.
11. Silva, S. S., Mano, J. F., & Reis, R. L. Ionic liquids in the processing and chemical modification of chitin and chitosan for biomedical applications. *Green Chemistry* **2017**, *19*(5), 1208–1220.
12. Roy, J. C., Salaün, F., Giraud, S., Ferri, A., Chen, G., & Guan, J. *Solubility of Chitin: Solvents, Solution Behaviors and Their Related Mechanisms*, IntechOpen **2017**.
13. Roca, C., Chagas, B., Farinha, I., Freitas, F., Mafra, L., Aguiar, F., Reis, M. A. M. Production of yeast chitin–glucan complex from biodiesel industry byproduct. *Process Biochemistry* **2012**, *47*(11), 1670–1675.
14. Farinha, I., Duarte, P., Pimentel, A., Plotnikova, E., Chagas, B., Mafra, L., Reis, M. A. M. Chitin–glucan complex production by *Komagataella pastoris*: Downstream optimization and product characterization. *Carbohydrate Polymers* **2015**, *130*, 455–464.
15. Farinha, I., Araújo, D., & Freitas, F. Optimization of medium composition for production of chitin–glucan complex and mannose-containing polysaccharides by the yeast *Komagataella pastoris*. *Journal of Biotechnology* **2019**, *303*, 30–36.
16. Chagas, B., Farinha, I., Galinha, C.F., Freitas, F., Reis, M.A.M. Chitin–glucan complex production by *Komagataella (Pichia) pastoris*: impact of cultivation pH and temperature on polymer content and composition. *New Biotechnology* **2014**, *31*, 468–474.

17. EFSA Panel on Dietetic Products, Nutrition and Allergies (NDA); Scientific Opinion on the safety of “Chitin-Glucan” as a Novel Food ingredient. *European Food Safety Authority Journal* **2010**, 8(7), 1687.
18. P. Wasserscheid, T. Welton, *Ionic Liquids in Synthesis* Wiley-VCH, **2003**.
19. Hough, W. L., & Rogers, R. D. Ionic Liquids Then and Now: From Solvents to Materials to Active Pharmaceutical Ingredients. *Bulletin of the Chemical Society of Japan* **2007**, 80(12), 2262–2269.
20. M. Deetlefs, K. R. Seddon and M. Shara, Predicting physical properties of ionic liquids, *Physical Chemistry Chemical Physics* **2006**, 8, 642–649.
21. Ionic Liquids IIIB: Fundamentals, Progress, Challenges, and Opportunities—Transformations and Processes, ed. R. D. Rogers and K. R. Seddon, ACS Symposium Series 902, *American Chemical Society*, Washington, DC, **2005**.
22. Hough, W. L., Smiglak, M., Rodríguez, H., Swatloski, R. P., Spear, S. K., Daly, D. T., Rogers, R. D. The third evolution of ionic liquids: active pharmaceutical ingredients. *New Journal of Chemistry* **2007**, 31(8), 1429.
23. Welton, T. Room-Temperature Ionic Liquids. Solvents for Synthesis and Catalysis. *Chemical Reviews* **1999**, 99(8), 2071–2084.
24. Hough, W.L. *Functional Ionic Liquids for Use in Pharmaceutical Applications* **2010**, University of Alabama Libraries.
25. Ohno H., Yoshizawa M. Ion conductive characteristics of ionic liquids prepared by neutralization of alkylimidazoles. *Solid State Ionics* **2002**, 154, 303–309.
26. Kelley, S. P.; Narita, A.; Holbrey, J. D.; Green, K. D.; Reichert, W. M.; Rogers, R. D. Understanding the Effects of Ionicity in Salts, Solvates, Co-Crystals, Ionic Co-Crystals, and Ionic Liquids, Rather than Nomenclature, Is Critical to Understanding Their Behavior. *Crystal Growth & Design* **2013**, 13, 965–975.
27. Berton, P., Di Bona, K. R., Yancey, D., Rizvi, S. A. A., Gray, M., Gurau, G., Rogers, R. D. Transdermal Bioavailability in Rats of Lidocaine in the Forms of Ionic Liquids, Salts, and Deep Eutectic. *ACS Medicinal Chemistry Letters* **2017**, 8(5), 498–503.
28. Hadad, C., Husson, E., & Van Nhien, A. N. *Conversion of Chitin in Ionic Liquids*. Encyclopedia of Ionic Liquids **2019**, 1–6.
29. Swatloski, R. P., Spear, S. K., Holbrey, J. D., & Rogers, R. D. Dissolution of Cellulose with Ionic Liquids. *Journal of the American Chemical Society* **2002**, 124(18), 4974–4975.
30. H. Xie, S. Zhang and S. Li, *Green Chemistry* **2006**, 8, 630–633.
31. Qin, Y., Lu, X., Sun, N., & Rogers, R. D. Dissolution or extraction of crustacean shells using ionic liquids to obtain high molecular weight purified chitin and direct production of chitin films and fibers. *Green Chemistry* **2010**, 12(6), 968.
32. Uto, T., Idenoue, S., Yamamoto, K., & Kadokawa, J. Understanding dissolution process of chitin crystal in ionic liquids: theoretical study. *Physical Chemistry Chemical Physics* **2018**, 20(31), 20669–20677.
33. Shamshina, J. Chitin in Ionic Liquids: Historical Insights on the Polymer’s Dissolution and Isolation. A Review. *Green Chemistry* **2019**, 21, 3974–3993.
34. Chen, Q., Xu, A., Li, Z., Wang, J., & Zhang, S. Influence of anionic structure on the dissolution of chitosan in 1-butyl-3-methylimidazolium-based ionic liquids. *Green Chemistry* **2011**, 13(12), 3446.
35. Ardiyanti, R. Design and Characterization of Chitin–Glucan Polymeric Structures for Wound Dressing Materials. Master’s thesis **2014**.

36. Oliveira, A. Development of Chitin–Glucan Polymeric Structures Using Biocompatible Ionic Liquids. Master's thesis **2016**.
37. Ferreira, I. C., Araújo, D., Voisin, P., Alves, V. D., Rosatella, A. A., Afonso, C. A. M., Neves, L. A. Chitin-Glucan Complex – Based Biopolymeric Structures Using Biocompatible Ionic Liquids. *Carbohydrate Polymers* **2020**, 116–679.
38. Doug MacFarlane, Mega Kar and Jennifer M Pringle. *Fundamentals of Ionic Liquids: From Chemistry to Applications*, Wiley-VCH Verlag GmbH & Co. KGaA. **2017**.
39. Cojocar, O. A., Kelley, S. P., Gurau, G., & Rogers, R. D. Procainium Acetate Versus Procainium Acetate Dihydrate: Irreversible Crystallization of a Room-Temperature Active Pharmaceutical-Ingredient Ionic Liquid upon Hydration. *Crystal Growth & Design* **2013**, 13(8), 3290–3293.
40. Claridge, Timothy D.W. *High-Resolution NMR Techniques in Organic Chemistry*, Elsevier **2016**.
41. Fitzpatrick, Daniel E.; Maujean, Timothé; Evans, Amanda C.; Ley, Steven V. Across-the-World Automated Optimization and Continuous-Flow Synthesis of Pharmaceutical Agents Operating Through a Cloud-Based Server. *Angewandte Chemie - International Edition*, **2018**, 57(46), 15128–15132.
42. Choquesillo-Lazarte, Duane; Nemeč, Vinko; Cinčić, Dominik, Halogen bonded cocrystals of active pharmaceutical ingredients: pyrazinamide, lidocaine and pentoxifylline in combination with haloperfluorinated compounds *Crystal engineering communications*, **2017**, 19(35), 5293–5299.
43. Lide, D.R. *Handbook of Chemistry and Physics*. 79th ed. Boca Raton, FL: CRC Press Inc., **1998**, 3-69.
44. Stott, P. Transdermal delivery from eutectic systems: enhanced permeation of a model drug, ibuprofen. *Journal of Controlled Release* **1998**, 50(1-3), 297–308.
45. Powell, M. F. Lidocaine and Lidocaine Hydrochloride. *Analytical Profiles of Drug Substances* **1986**, 761–779.
46. Trovatti, E., Silva, N. H. C. S., Duarte, I. F., Rosado, C. F., Almeida, I. F., Costa, P., Neto, C. P. Biocellulose Membranes as Supports for Dermal Release of Lidocaine. *Biomacromolecules* **2011**, 12(11), 4162–4168.
47. Anacleto S.D.S., Borges M.M.C., de Oliveira H.L. Evaluation of physicochemical properties as supporting information on quality control of raw materials and veterinary pharmaceutical formulations. *Journal of Pharmaceutical Analysis* **2018**, 8(3), 168-175.
48. Wu, H., Deng, Z., Zhou, B., Qi, M., Hong, M., & Ren, G. Improved transdermal permeability of ibuprofen by ionic liquid technology: Correlation between counterion structure and the physicochemical and biological properties. *Journal of Molecular Liquids* **2019**, 283, 399–409.
49. Bica, K., Shamshina, J., Hough, W. L., MacFarlane, D. R., & Rogers, R. D. Liquid forms of pharmaceutical co-crystals: exploring the boundaries of salt formation. *Chemical Communications*. **2011**, 47(8), 2267–2269.
50. Luo, H., Huang, J.-F., & Dai, S. Studies on Thermal Properties of Selected Aprotic and Protic Ionic Liquids. *Separation Science and Technology* **2008**, 43(9-10), 2473–2488.
51. Kumar, L., Papat, D., & Bansal, A. K. Investigation of the Atypical Glass Transition and Recrystallization Behavior of Amorphous Prazosin Salts. *Pharmaceutics* **2011**, 3(3), 525–537.

52. Liu, X., Ma, X., Kun, E., Guo, X., Yu, Z., & Zhang, F. Influence of lidocaine forms (salt vs. freebase) on properties of drug–eudragit® L100-55 extrudates prepared by reactive melt extrusion. *International Journal of Pharmaceutics* **2018**, 547(1-2), 291–302.
53. Wojnarowska, Z., Paluch, K. J., Shoifet, E., Schick, C., Tajber, L., Knapik, J., Paluch, M. Molecular Origin of Enhanced Proton Conductivity in Anhydrous Ionic Systems. *Journal of the American Chemical Society* **2015**, 137(3), 1157–1164.
54. Dudognon, E., Danède, F., Descamps, M., & Correia, N. T. Evidence for a New Crystalline Phase of Racemic Ibuprofen. *Pharmaceutical Research* **2008**, 25(12), 2853–2858.
55. Jacquemin, J., Husson, P., Padua, A. A. H., & Majer, V. Density and viscosity of several pure and water-saturated ionic liquids. *Green Chemistry*. **2006**, 8(2), 172–180.
56. Patinha, D. J. S., Tomé, L. C., Garcia, H., Ferreira, R., Pereira, C. S., Rebelo, L. P. N., Marrucho, I. M. The role of water in cholinium carboxylate ionic liquid’s aqueous solutions. *The Journal of Chemical Thermodynamics* **2015**, 84, 93–100.
57. Cardenas, G., Cabrera, G., Taboada, E., & Miranda, S. P. Chitin characterization by SEM, FTIR, XRD, and ¹³C cross polarization/mass angle spinning NMR. *Journal of Applied Polymer Science* **2004**, 93(4), 1876–1885.
58. Jalal, A. F., Risheed, C. M., & Ibrahim, B. M. Optimization of chitin extraction from chicken feet. *Journal of Analytical and Bioanalytical Techniques* **2012**, 3, 145.
59. Lu, Y., Sun, Q. F., She, X. L., Xia, Y. Z., Liu, Y. X., Li, J. Fabrication and characterisation of -chitin nanofibers and highly transparent chitin films by pulsed ultrasonication. *Carbohydrate Polymers* **2013**, 98(2), 1497–1504.
60. Shamshina, J. Chitin in Ionic Liquids: Historical Insights on the Polymer’s Dissolution and Isolation. A Review. *Green Chemistry* **2019**, 21, 3974–3993.
61. Mathaba, M., & Daramola, M. O. Effect of Chitosan’s Degree of Deacetylation on the Performance of PES Membrane Infused with Chitosan during AMD Treatment. *Membranes* **2020**, 10(3), 52.
62. Xie, H., Zhang, S., & Li, S. Chitin and chitosan dissolved in ionic liquids as reversible sorbents of CO₂. *Green Chemistry* **2006**, 8(7), 630.
63. <https://www.scbt.com/p/lidocaine-137-58-6>. Last accessed 13/12/2020.
64. <https://www.scbt.com/pt/p/procaine-59-46-1?requestFrom=search>. Last accessed 13/12/2020.
65. Vieira, M. G. A., da Silva, M. A., dos Santos, L. O., Beppu, M. M. Natural-based plasticizers and biopolymer films: A review. *European Polymer Journal* **2011**, 47(3), 254–263.
66. <https://foodb.ca/compounds/FDB008299> Last accessed 13/12/2020.
67. <https://echa.europa.eu/registration-dossier/-/registered-dossier/24094/4/9> Last accessed 13/12/2020.
68. Dwivedi, C., Pandey, I., Pandey, H., Ramteke, P. W., Pandey, A. C., Mishra, S. B., & Patil, S. Electrospun Nanofibrous Scaffold as a Potential Carrier of Antimicrobial Therapeutics for Diabetic Wound Healing and Tissue Regeneration. *Nano- and Microscale Drug Delivery Systems* **2017**, 147–164.
69. Wang, W., Caetano, G., Ambler, W. S., Blaker, J. J., Frade, M. A., Mandal, P., Diver, C., & Bártolo, P. Enhancing the Hydrophilicity and Cell Attachment of 3D Printed PCL/Graphene Scaffolds for Bone Tissue Engineering. *Materials* **2016**, 9(12), 992.
70. Yusof, N. L. B. M., Wee, A., Lim, L. Y., & Khor, E. Flexible chitin films as potential wound-dressing materials: Wound model studies. *Journal of Biomedical Materials Research* **2003**, 66(2), 224–232.

Appendices

Appendix I – Synthesis of API-ILs

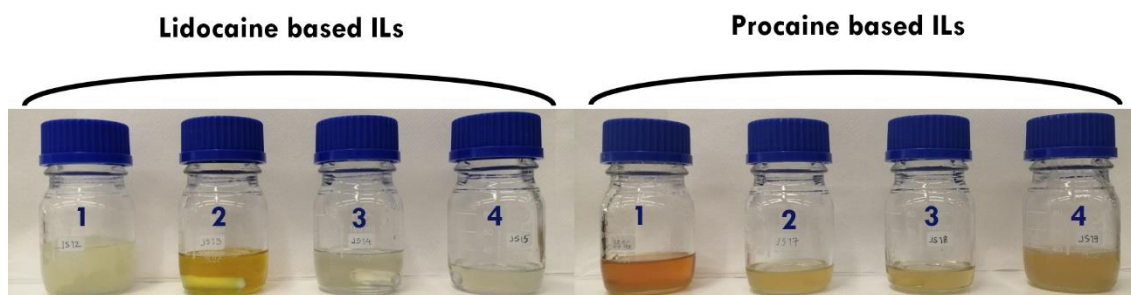


Figure A1. Synthesized API-ILs at room temperature. The same counterions were labeled with the same number. 1 - Acetate; 2 - Propionate; 3 - Hexanoate; 4 - Ibuprofenate.

Appendix II – Proton nuclear magnetic resonance spectroscopy

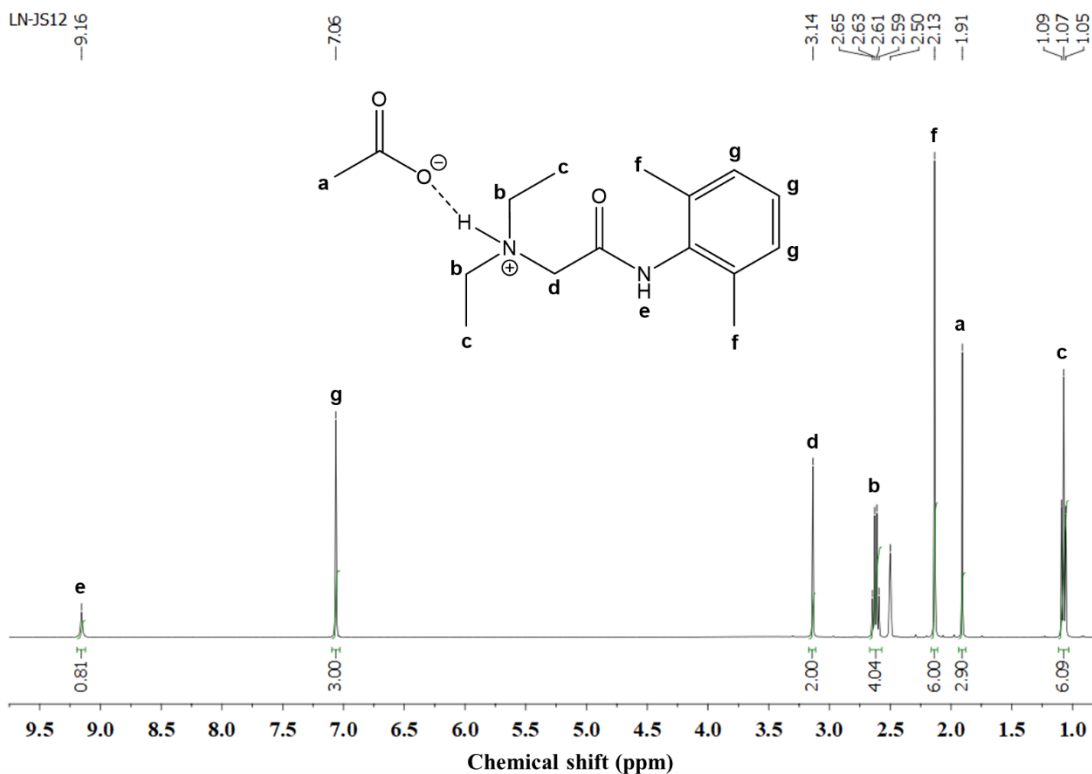


Figure A2.1 ^1H NMR spectrum of [Lid][OAc] in $\text{DMSO-}d_6$ solution and assignment of the proton signals to hydrogen-labeled chemical structure of [Lid][OAc].

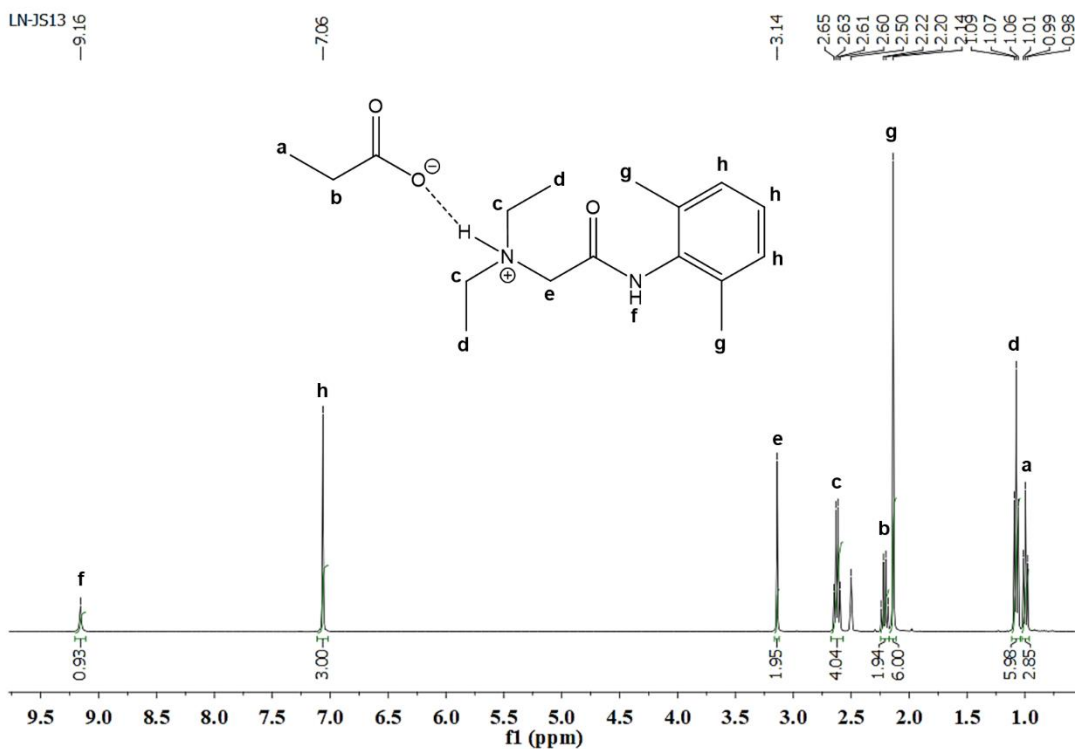


Figure A2.2 ^1H NMR spectrum of [Lid][OPr] in $\text{DMSO-}d_6$ solution and assignment of the proton signals to hydrogen-labeled chemical structure of [Lid][OPr].

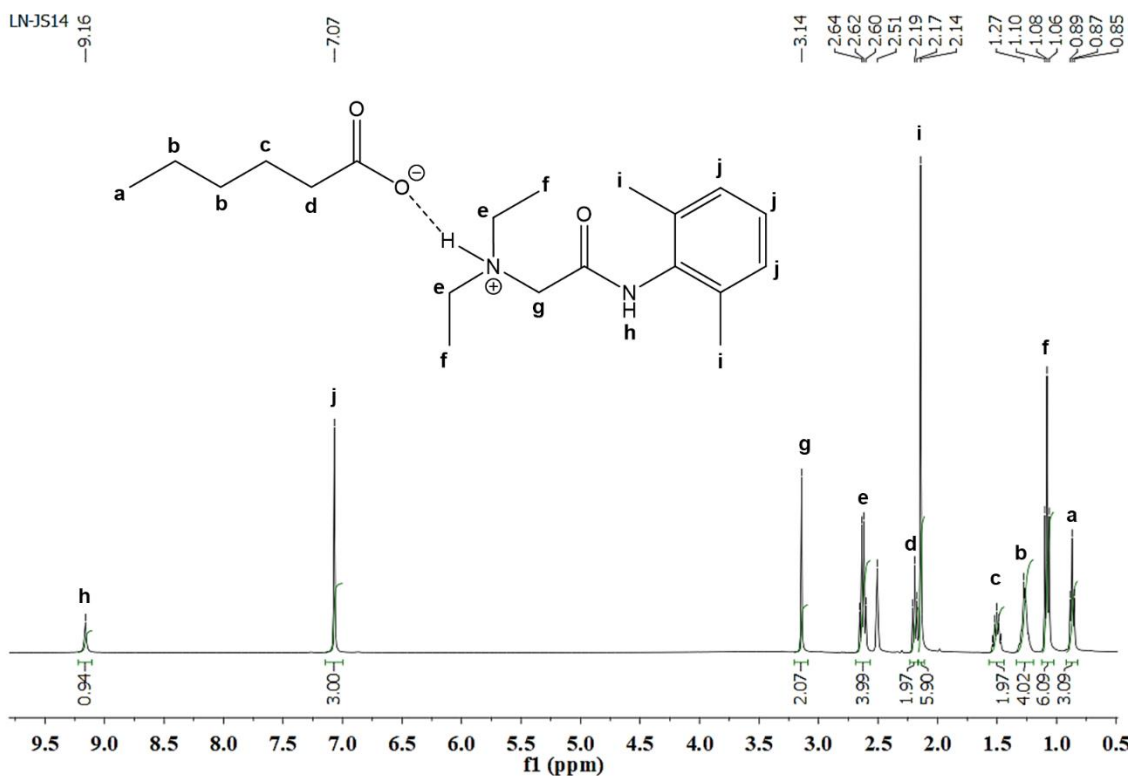


Figure A2.3 ^1H NMR spectrum of [Lid][OHex] in $\text{DMSO-}d_6$ solution and assignment of the proton signals to hydrogen-labeled chemical structure of [Lid][OHex].

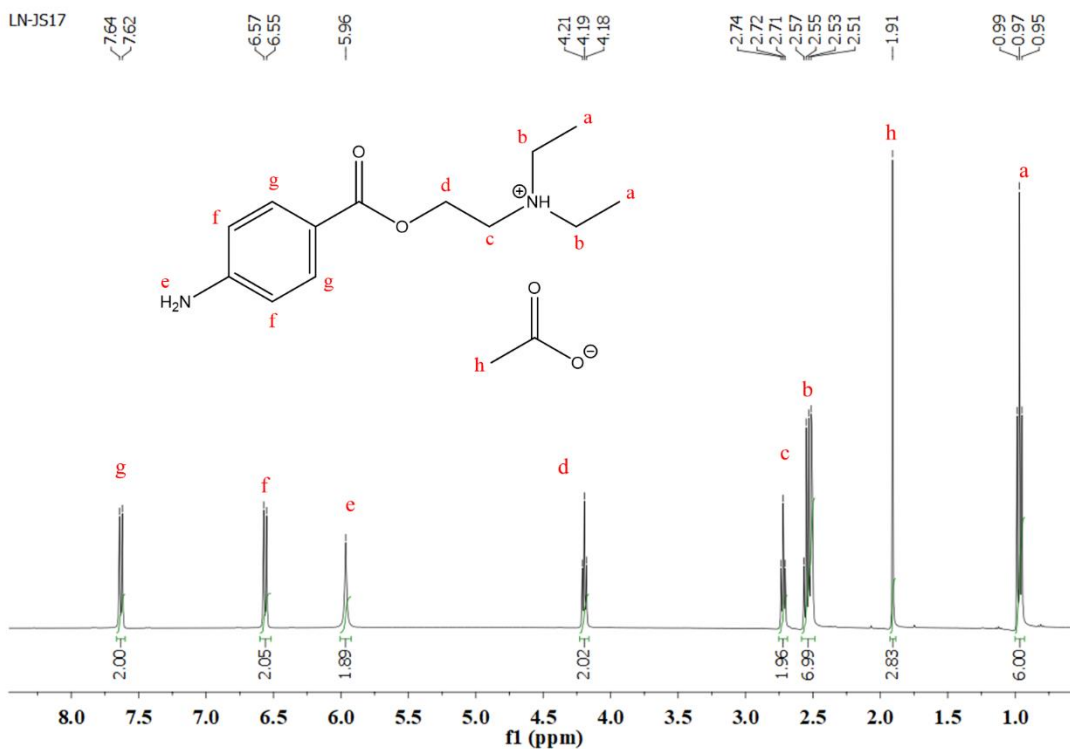


Figure A2.4 ^1H NMR spectrum of [Pro][OAc] in $\text{DMSO-}d_6$ solution and assignment of the proton signals

to hydrogen-labeled chemical structure of [Lid][OAc].

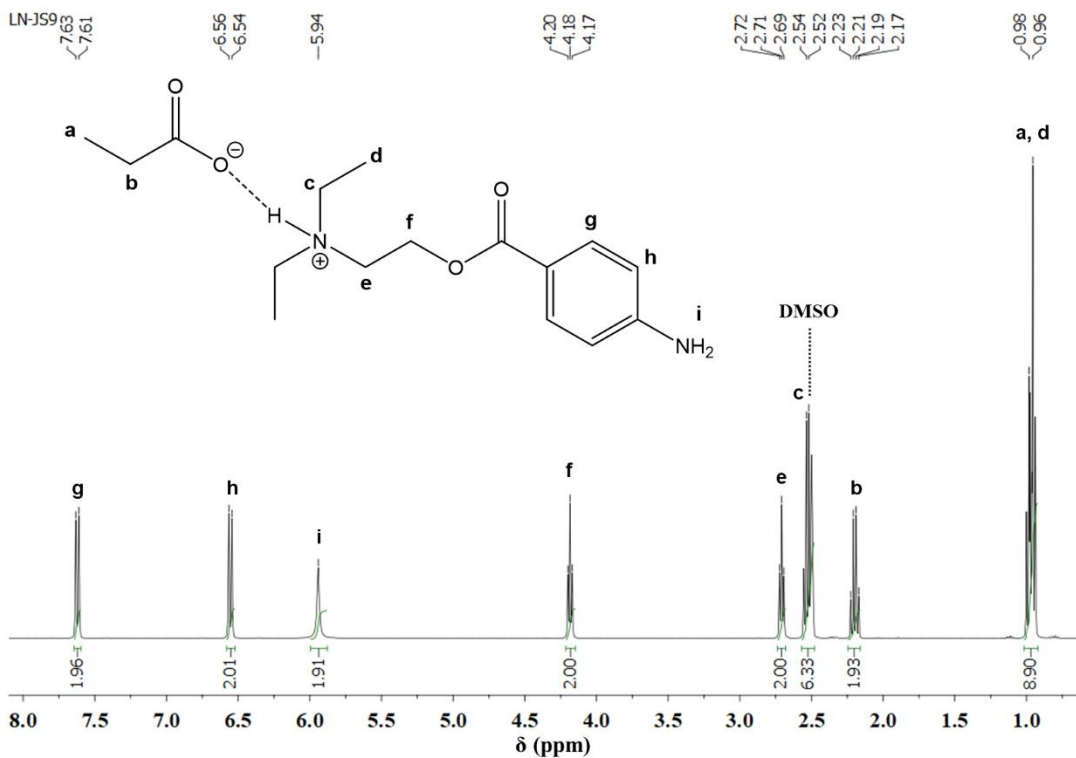


Figure A2.5 ¹H NMR spectrum of [Pro][OPr] in DMSO-*d*₆ solution and assignment of the proton signals to hydrogen-labeled chemical structure of [Pro][OPr].

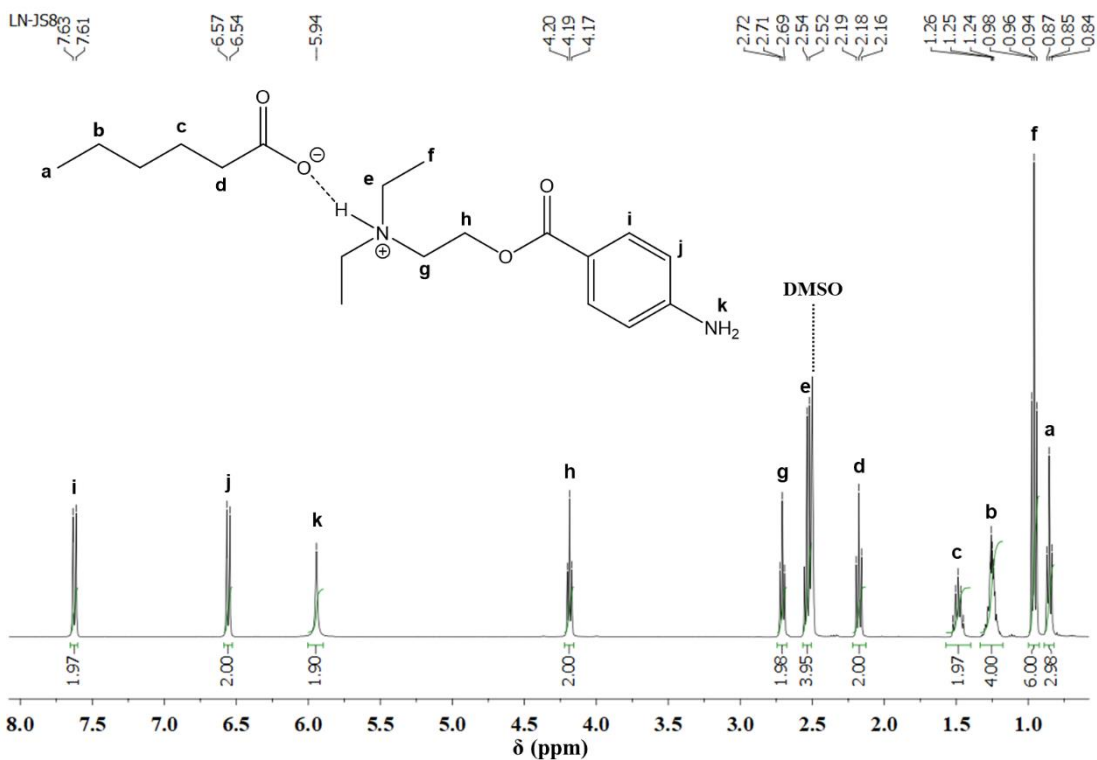


Figure A2.3 ^1H NMR spectrum of [Pro][OHex] in $\text{DMSO-}d_6$ solution and assignment of the proton signals to hydrogen-labeled chemical structure of [Pro][OHex].

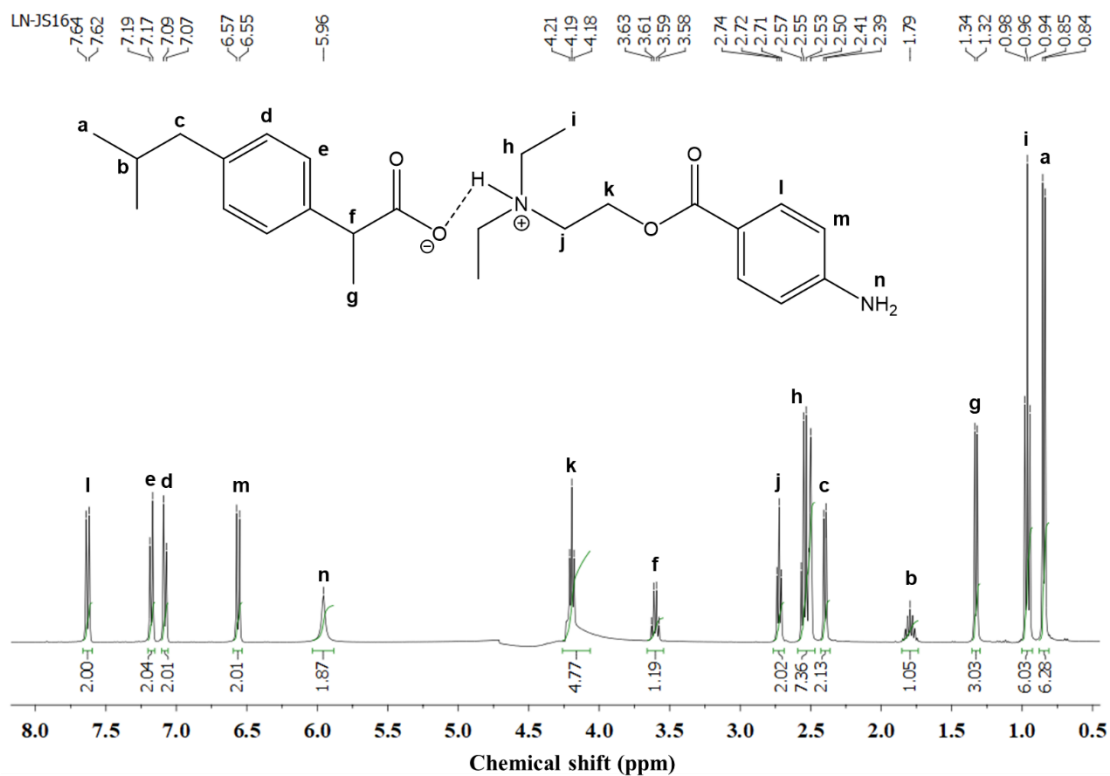


Figure A2.7 ^1H NMR spectrum of [Pro][Ibu] in $\text{DMSO-}d_6$ solution and assignment of the proton signals to hydrogen-labeled chemical structure of [Pro][Ibu].

Appendix III – Viscosity measurements (shear rate sweeps)

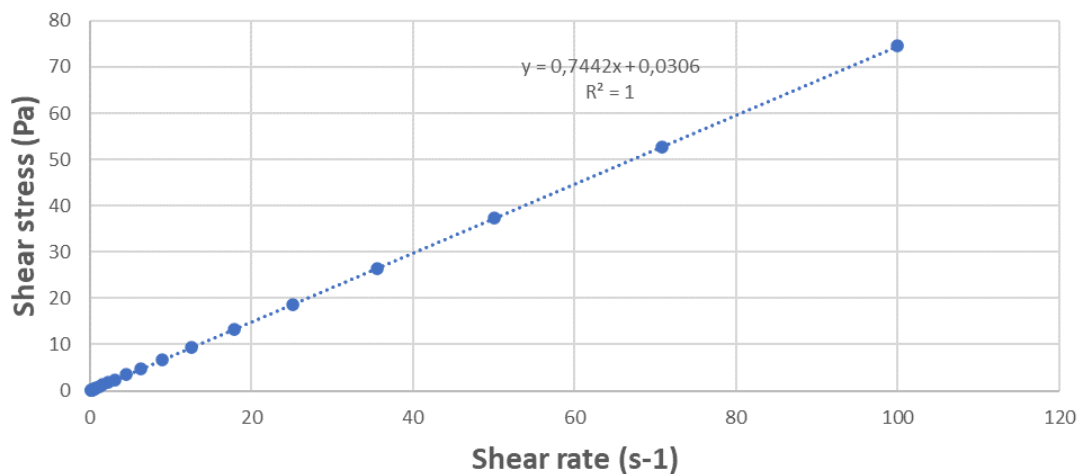


Figure A3.1 Shear stress as a function of shear rate for [Lid][OAc] at 20 °C.

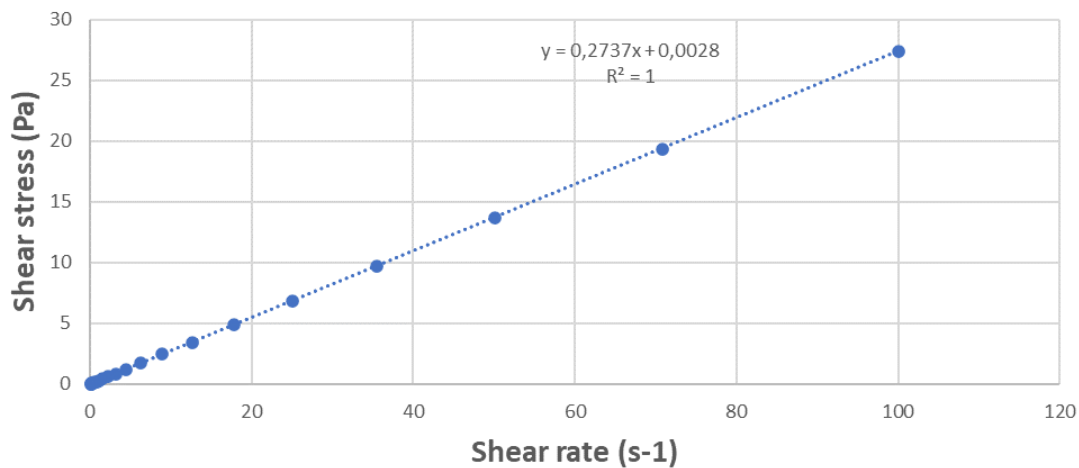


Figure A3.2 Shear stress as a function of shear rate for [Lid][OHex] at 20 °C.

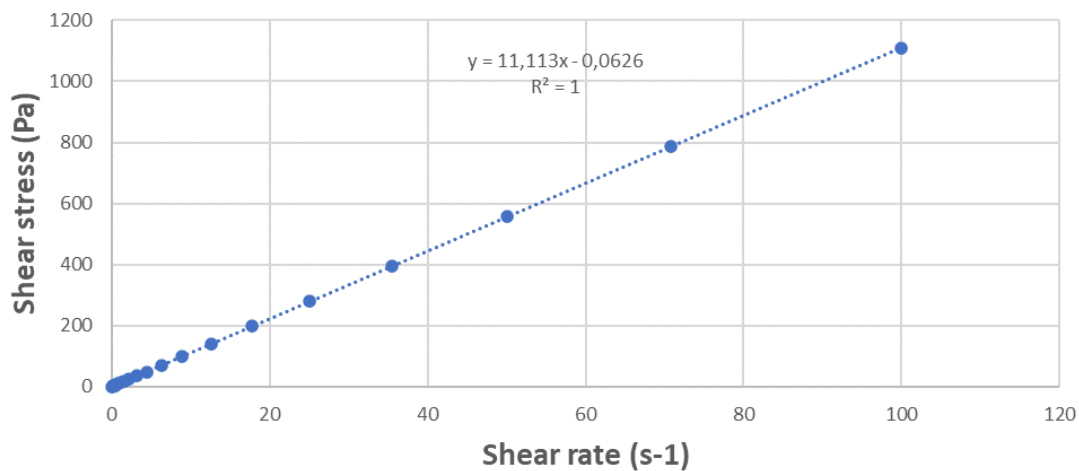


Figure A3.3 Shear stress as a function of shear rate for [Lid][Ibu] at 20 °C.

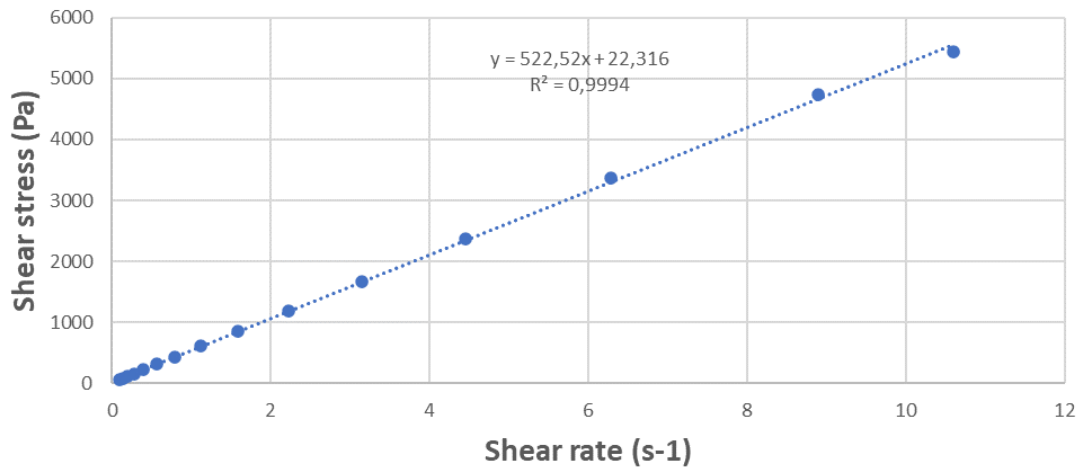


Figure A3.4 Shear stress as a function of shear rate for [Pro][Ibu] at 20 °C.

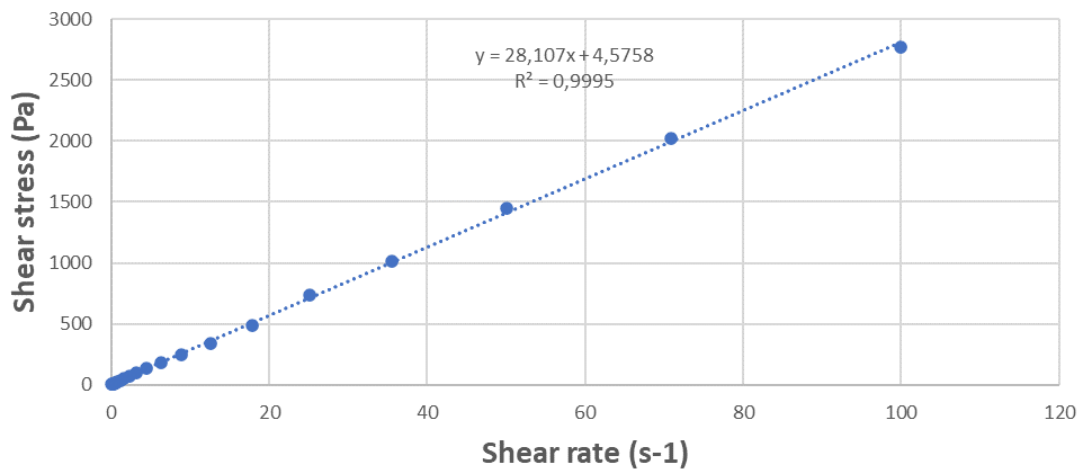


Figure A3.5 Shear stress as a function of shear rate for [Pro][OAc] at 20 °C.

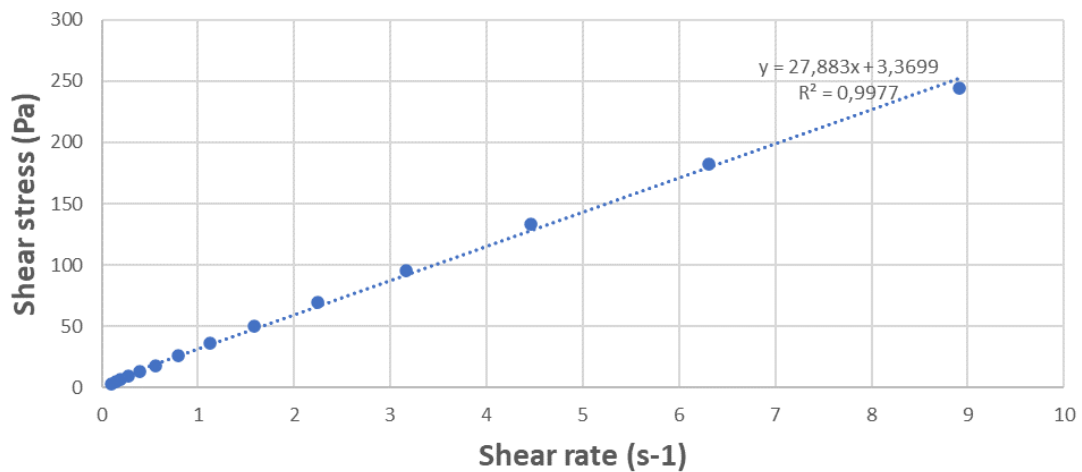


Figure A3.6 Shear stress as a function of shear rate for [Pro][OPr] at 20 °C.

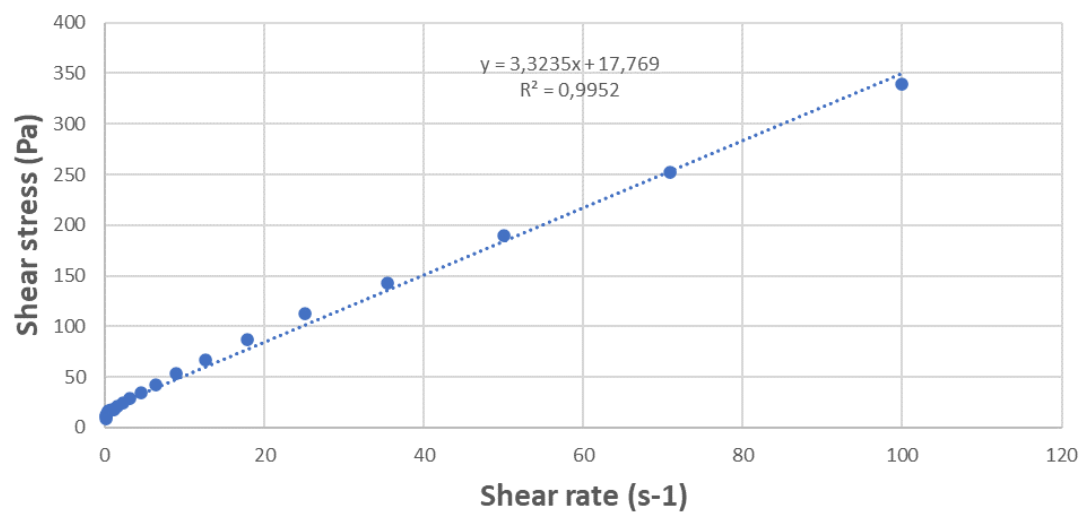


Figure A3.7 Shear stress as a function of shear rate for [Pro][OHex] at 20 °C.

Appendix IV – Viscosity measurements (temperature sweeps)

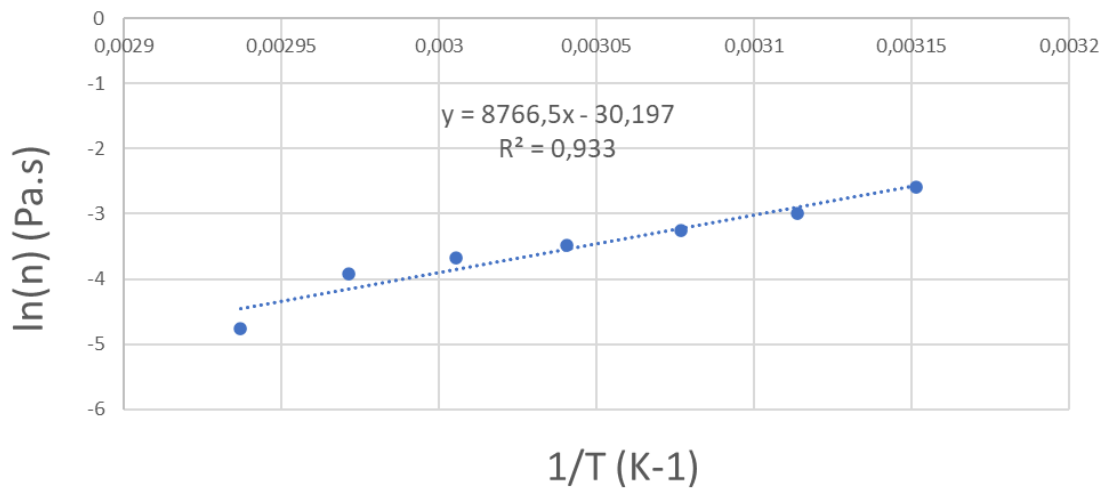


Figure A4.1 Arrhenius plot for [Lid][OAc].

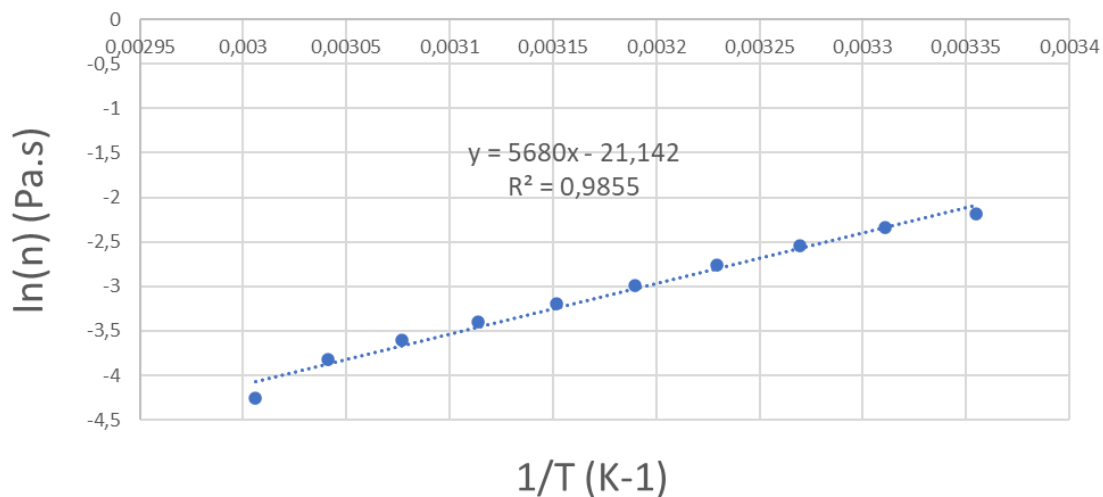


Figure A4.2 Arrhenius plot for [Lid][OPr].

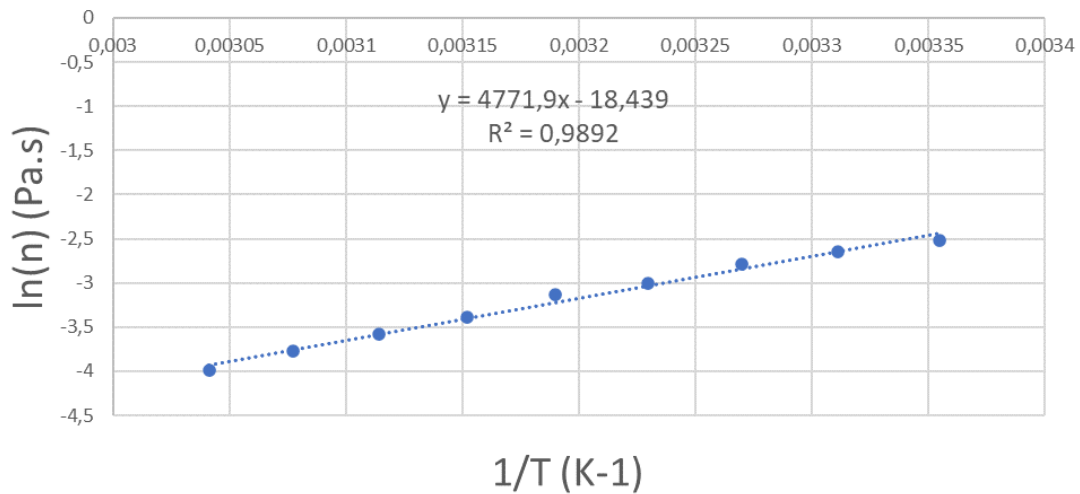


Figure A4.3 Arrhenius plot for [Lid][OHex].

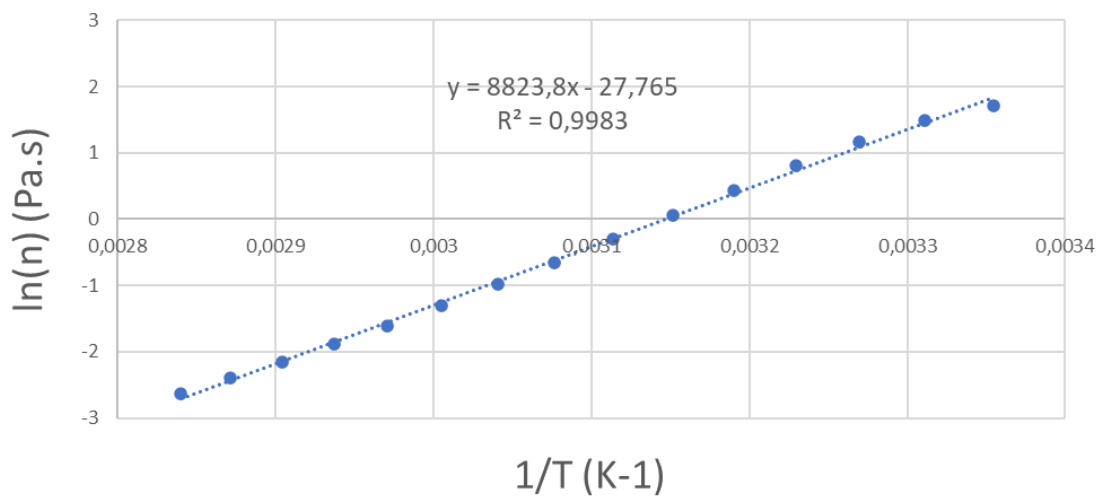


Figure A4.5 Arrhenius plot for [Lid][Ibu].

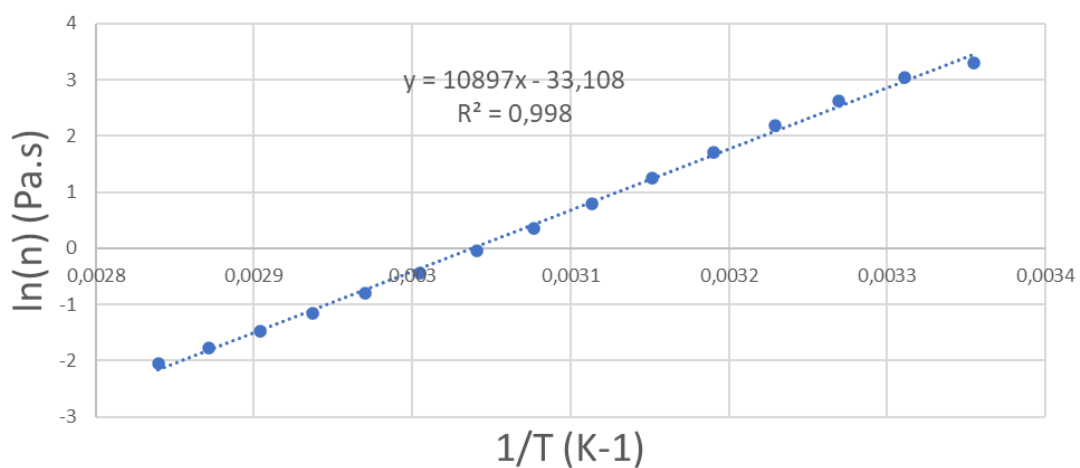


Figure A4.6 Arrhenius plot for [Pro][OAc].

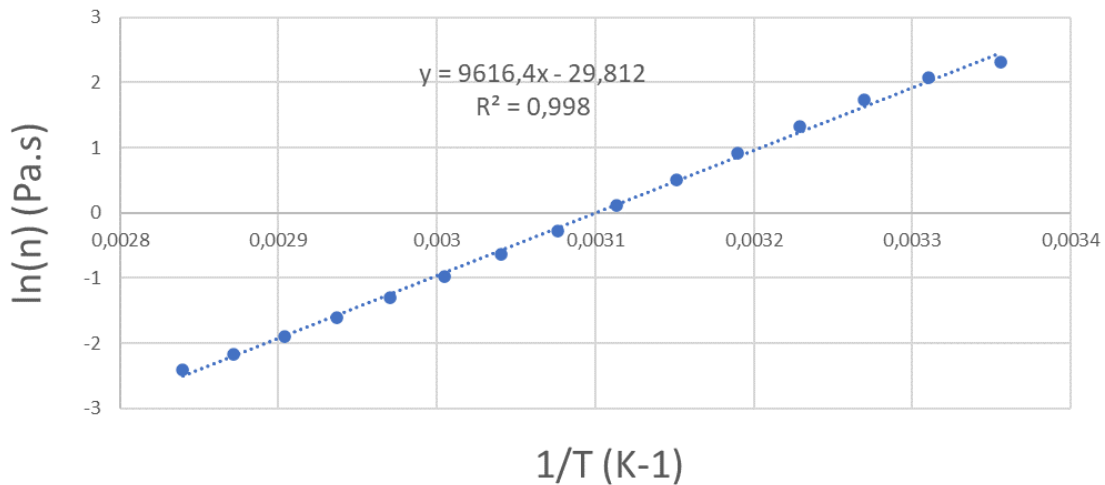


Figure A4.6 Arrhenius plot for [Pro][OPr].

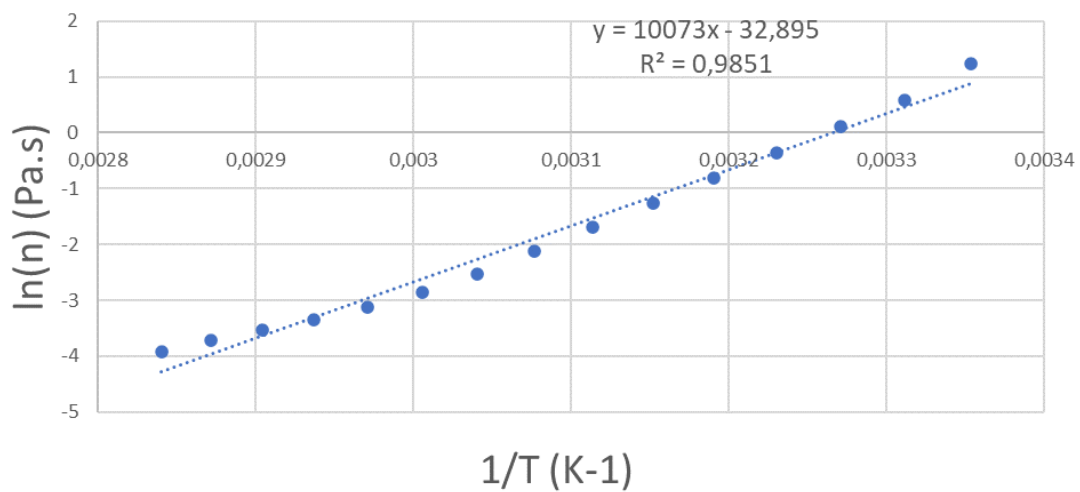


Figure A4.7 Arrhenius plot for [Pro][OHex].

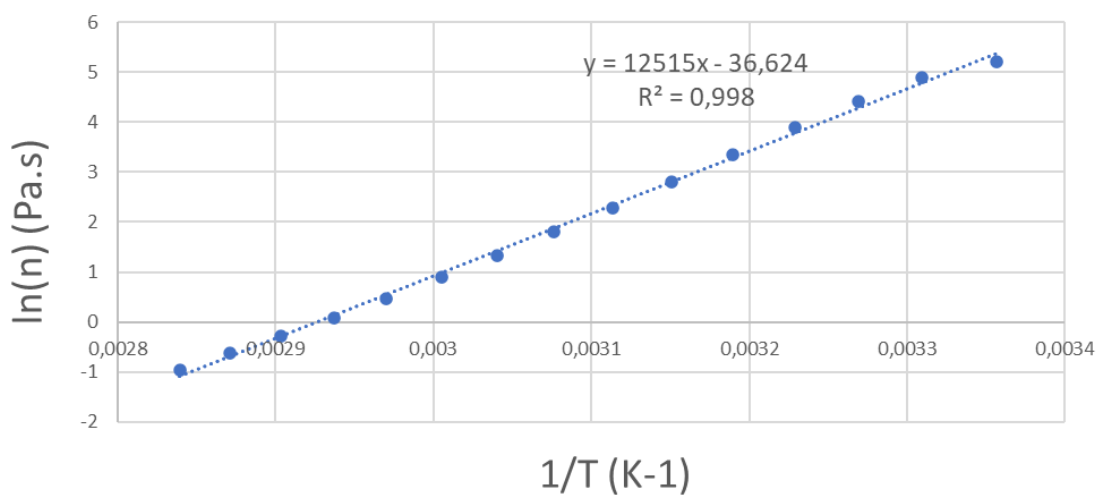


Figure A4.8 Arrhenius plot for [Pro][Ibu].

Appendix V – Thermogravimetric analysis

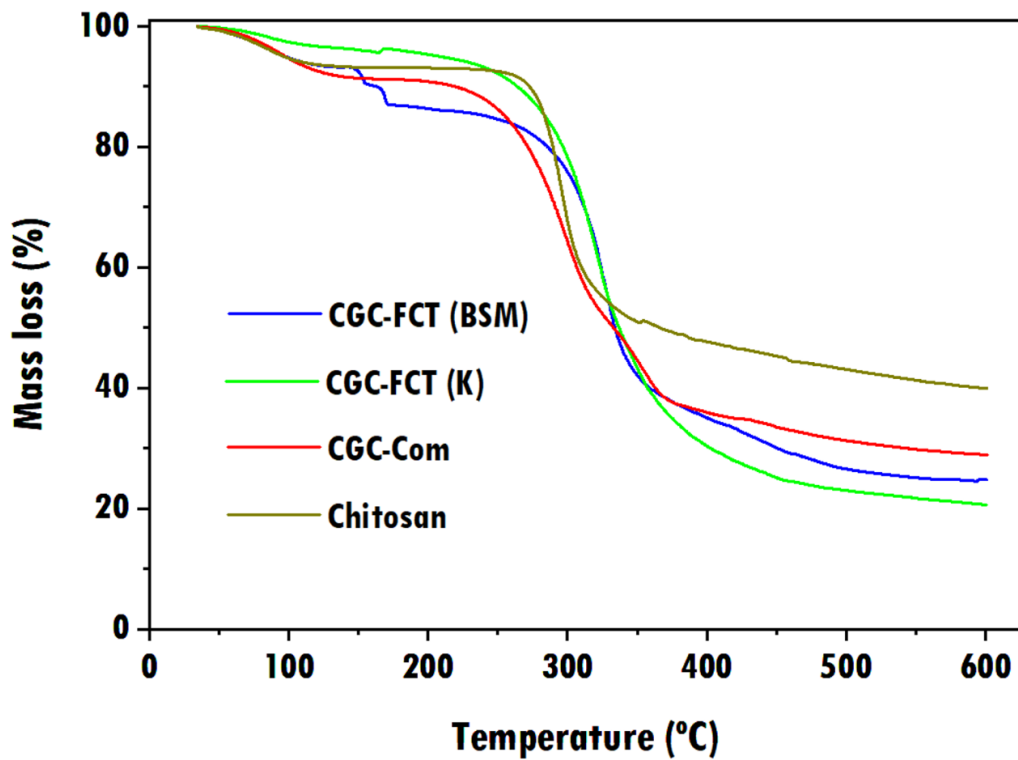


Figure A5.1 Thermogravimetric curves associated with mass loss of the studied biopolymers.

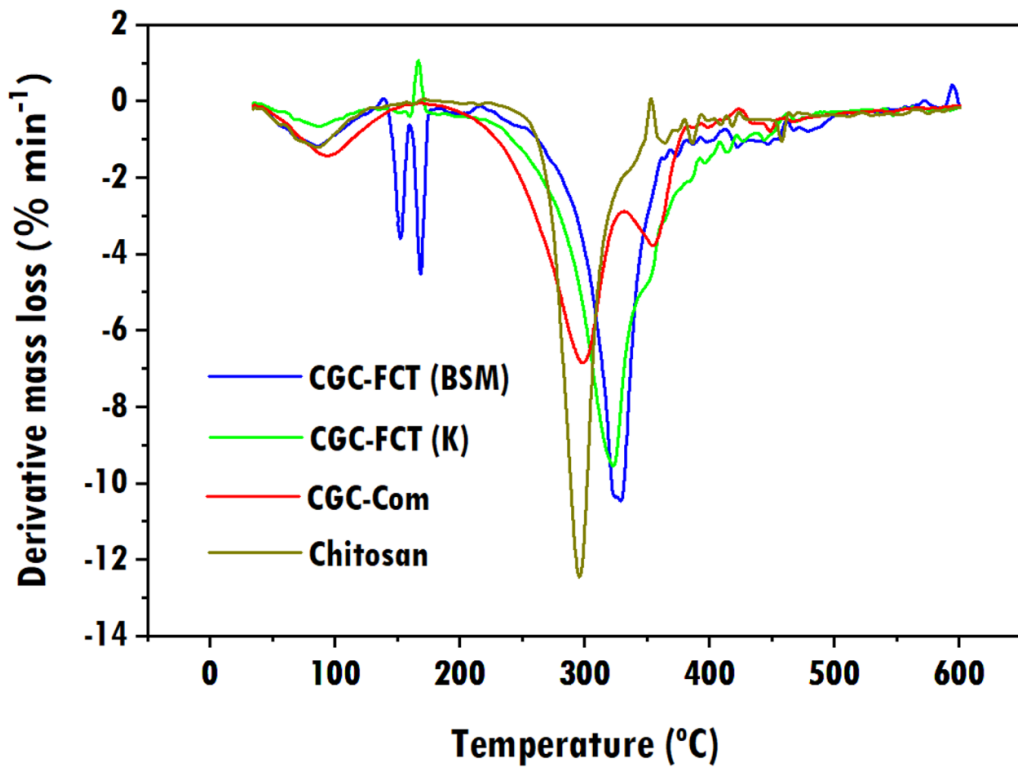
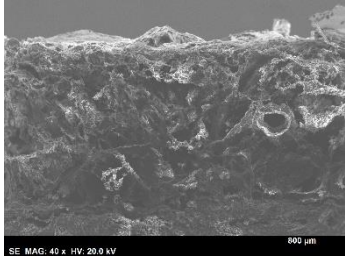
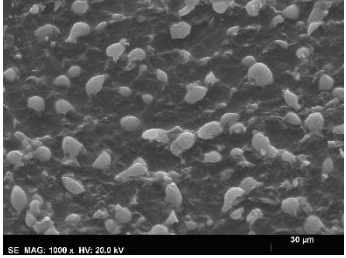
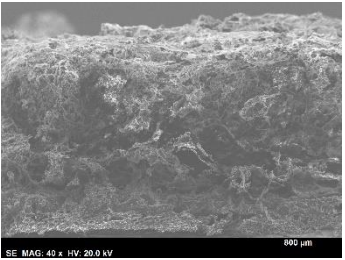

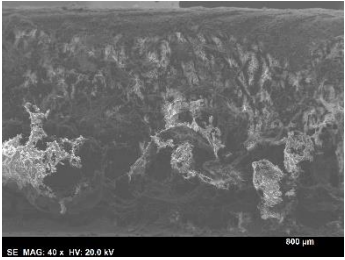
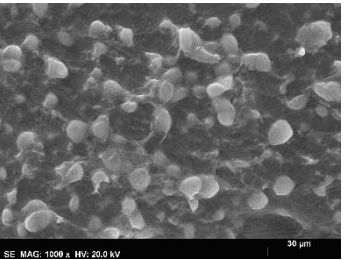
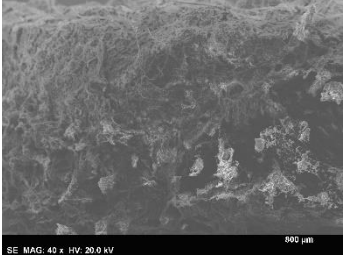
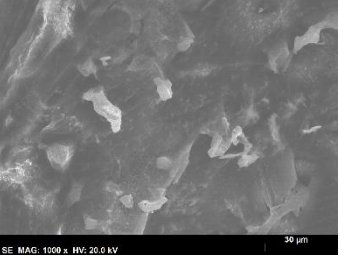


Figure A5.2 Thermogravimetric derivative curves associated with mass loss of the studied biopolymers.

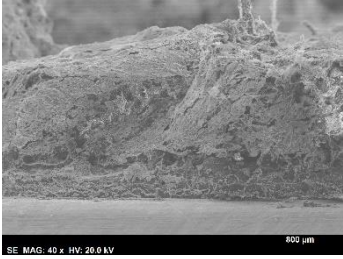
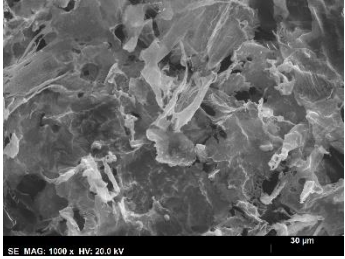
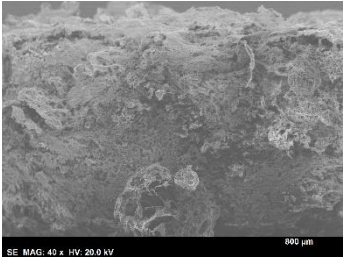
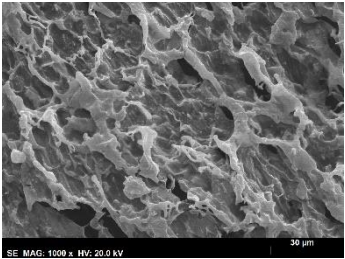
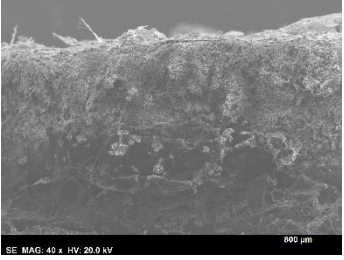
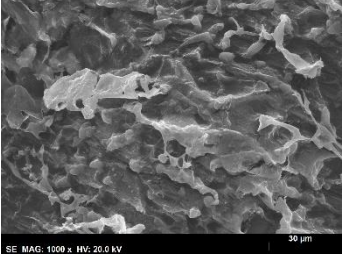
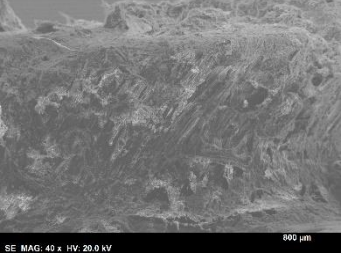
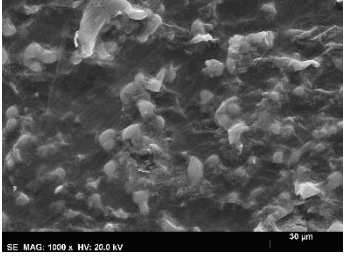
Appendix VI – Scanning electron microscopy

Table A6.1 SEM micrographs of the cross section and surface for [Lid][OAc] based CGC films obtained at 70 °C and 100 °C (oil bath dissolution temperature).

| Temperature | Coagulation medium | Cross section ^a | Surface ^b |
|-------------|---------------------|---|--|
| 70 °C | Water |  |  |
| | Glycerol, 10% (v/v) |  |  |
| 100 °C | Water |  |  |
| | Glycerol, 10% (v/v) |  |  |

^a Film cross section (magnification 40×). ^b Film surface (magnification 1000×).

Table A6.2 SEM micrographs of the cross section and surface for [Lid][OPr] based CGC films obtained at 70 °C and 100 °C (oil bath dissolution temperature).

| Temperature | Coagulation medium | Cross section ^a | Surface ^b |
|-------------|---------------------|---|--|
| 70 °C | Water |  |  |
| | Glycerol, 10% (v/v) |  |  |
| 100 °C | Water |  |  |
| | Glycerol, 10% (v/v) |  |  |

^aFilm cross section (magnification 40×). ^bFilm surface (magnification 1000×).

Appendix VII – Fourier-transform infrared spectroscopy

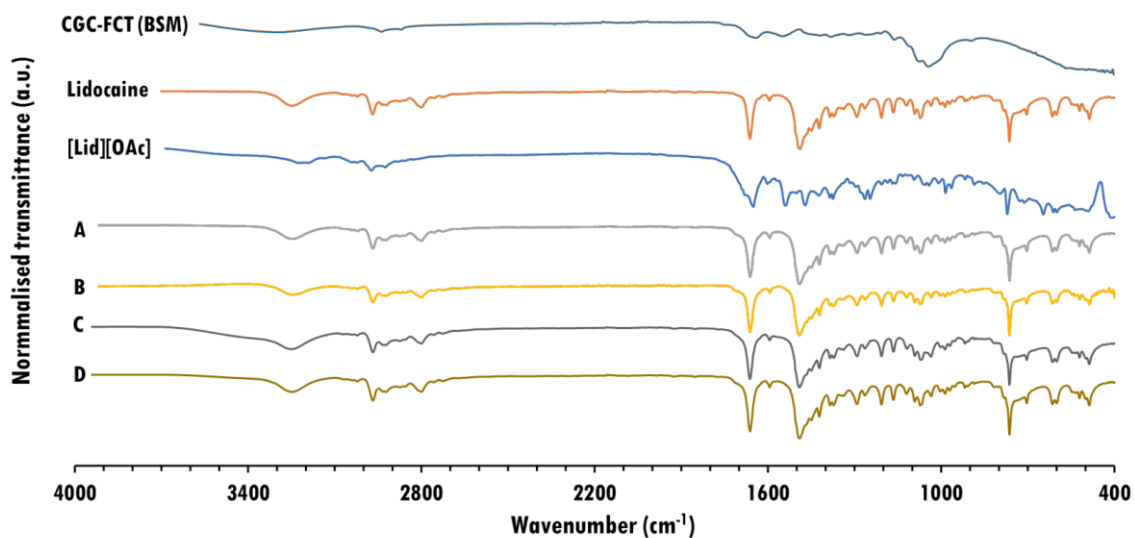


Figure A7.1 FTIR-ATR spectra of CGC-FCT (medium BSM), lidocaine free base, lidocainium acetate and respective films (A-D). A – 3-day oil bath dissolution at 70 °C and prepared using water as nonsolvent; B – 3-day oil bath dissolution at 70 °C and prepared using water containing 10% (v/v) of glycerol; C – 1-day oil bath dissolution at 100 °C and prepared using water as nonsolvent; D – 1-day oil bath dissolution at 100 °C and prepared using water containing 10% (v/v) of glycerol.